

UCLA

UCLA Electronic Theses and Dissertations

Title

Theory of gated hemicarcerands and Diels-Alder reactions of tetrazines

Permalink

<https://escholarship.org/uc/item/6028d3n8>

Author

LIU, FANG

Publication Date

2014

Peer reviewed|Thesis/dissertation

UNIVERSITY OF CALIFORNIA

Los Angeles

Theory of Gated Hemicarcerands and
Diels-Alder Reactions of Tetrazines

A dissertation submitted in partial satisfaction of the
requirements for the degree Doctor of Philosophy
in Chemistry

by

Fang Liu

2014

ABSTRACT OF THE DISSERTATION

Theory of Gated Hemicarcerands and
Diels-Alder Reactions of Tetrazines

by

Fang Liu

Doctor of Philosophy in Chemistry

University of California, Los Angeles, 2014

Professor Kendall N. Houk, Chair

The concept of gating was introduced into host-guest chemistry by our group in the 1990s, as a result of computational studies on Cram's hemicarcerands. Since that time, a variety of gated host systems have been developed by our group and others. The gated hemicarcerands presented in this dissertation are examples of hosts with controllable gates that function upon external stimuli, which we refer to as redox reaction gated hemicarcerands and photochemically

gated hemicarcerands. In both cases, a chemically modifiable moiety was installed on the host molecule so that it undergoes chemical change in response to external stimuli. In particular, we took advantage of disulfide-dithiol interchange (redox reaction control) and anthracene dimerization (photochemical control) to achieve gating in these hemicarcerands. Molecular mechanics computations were employed to understand the experimental observations during the complexation and decomplexation processes.

The second part of this dissertation focuses on understanding Diels-Alder reactivities of a wide range of organic molecules with the tools of computational chemistry. Among these extensively studied molecules, tetrazine is the most outstanding one, in the sense that its cycloaddition reactions with strained alkenes are extremely rapid, with second order rate constants up to $2000 \text{ M}^{-1}\text{s}^{-1}$. Such reactions take place at a decent rate even at micromolar concentration, suggesting their application in live cell imaging. The emerging use of tetrazines as labeling reagents has added an extra dimension to bioorthogonal cycloadditions. Our computational studies have provided a thorough understanding of the cycloaddition reactivities and a guideline for developing new reagents.

The dissertation of Fang Liu is approved.

Anastassia N. Alexandrova

Jing Huang

Kendall N. Houk, Committee Chair

University of California, Los Angeles

2014

DEDICATION

*This dissertation is dedicated to my beloved husband, Xing Jiang,
for his endless support along the way.*

TABLE OF CONTENTS

List of Figures, Schemes, and Tables.....	ix
Acknowledgment.....	xv
VITA.....	xviii
Chapter 1. Gating in Host-Guest Chemistry.....	1
1.1 Overview of Host-Guest Chemistry.....	1
1.2 Gated Container Molecules.....	2
1.3 Gating Mechanisms.....	4
1.4 References.....	11
Chapter 2. Redox Reaction-Gated Hemicarcerands.....	15
2.1 Water-Soluble Redox Reaction-Gated Hemicarcerands.....	15
2.2 Computational Explorations.....	15
2.3 Attempted Synthesis of Gated Hemicarcerand 5	19
2.4 References.....	21
Chapter 3. Photochemically Gated Hemicarcerands.....	22
3.1 Photochemically Gated Hemicarcerands.....	22
3.2 Computational Exploration.....	24

3.3 References.....	28
Chapter 4. Bioorthogonal Cycloaddition.....	30
4.1 Introduction to Bioorthogonal Chemistry.....	30
4.2 Reactivity and Orthogonality.....	31
4.3 Developing New Bioorthogonal Reagents.....	38
4.4 Tetrazines in Bioorthogonal Cycloaddition.....	41
4.5 References.....	42
Chapter 5. Diels-Alder Reactivity of Tetrazines.....	46
5.1 Introduction to Tetrazine Diels-Alder Reactions.....	46
5.2 Computational Methods.....	52
5.3 Strain Effects.....	53
5.4 Substituent Effects.....	61
5.5 Correlation between Activation Energies, Distortion Energies, and HOMO-LUMO Gaps.....	69
5.6 References.....	73
Chapter 6. Diels-Alder Reactivities of Cycloalkenes.....	79
6.1 Introduction to Cycloalkene Diels-Alder Reactions.....	79

6.2 Computational Methods.....	83
6.3 Comparison of Reactivities.....	84
6.4 References.....	99

LIST OF FIGURES, SCHEMES, AND TABLES

List of Figures

Figure 1.1 Complexes of crown ether, spherand, and cryptand with alkali metal cations.....	1
Figure 1.2 Ribbon structure of pancreatic lipase and HIV-1 protease.....	2
Figure 1.3 Structures of a cylindrical capsule and a molecular basket.....	3
Figure 1.4 Energy definitions for host-guest complexation by a carcerand or hemicarcerand.....	4
Figure 1.5 Stimulated gating converts a carceplex to a hemicarceplex.....	5
Figure 1.6 Structure of thermally-gated hemicarcerand 1	6
Figure 1.7 Energy profiles for the escape of acetonitrile from 1b through gating.....	8
Figure 1.8 French door cartoon and sliding door cartoon.....	9
Figure 1.9 Structures of hosts with large portals and small portals.....	10
Figure 2.1 Redox reaction-gated hemicarcerand 4 and water-soluble redox reaction-gated hemicarcerand 5	16
Figure 2.2 Optimized structures of isolated host 5 in water.....	17
Figure 2.3 Optimized structures of complexes formed between 5 and guests i	18
Figure 2.4 Optimized structures of complexes formed between 5 and guests ii-vii	18
Figure 3.1 Photo-induced release of a guest molecule G from a photoactive hemicarceplex.....	22

Figure 3.2 Organic molecules i-xv tested in complexation study.....	24
Figure 3.3 Optimized structures of isolated host and complexes between host and chloroform solvent.....	25
Figure 3.4 Optimized structures of complexes formed between i and 6b	26
Figure 3.5 Optimized structures of complexes formed between 6b and guests ii-xv	27
Figure 4.1 Bioorthogonal reactions.....	30
Figure 4.2 Optimized transition structures for cycloadditions with methyl azide and dimethyltetrazine.....	33
Figure 4.3 Distortion/interaction model.....	35
Figure 4.4 Graph of distortion, interaction, and activation energies for reactions of <i>trans</i> -cyclooctene 1 and dibenzocyclooctyne 2 with methyl azide 3 and dimethyltetrazine 4	35
Figure 4.5 FMO diagram for the cycloadditions of <i>trans</i> -cyclooctene and dibenzocyclooctyne with methyl azide and dimethyltetrazine.....	36
Figure 4.6 Space-filling models of, methyl azide, dibenzocyclooctyne, dimethyltetrazine, and transition states TS3_2 and TS4_2	37
Figure 4.7 Schematic of mutual orthogonality to label two different biomolecules.....	38
Figure 4.8 Color-coded matrix of rate constants (in $M^{-1} s^{-1}$) for 120 cycloadditions in water....	39
Figure 5.1 Bioorthogonal cycloaddition.....	46

Figure 5.2 The π orbitals of acetylene, parent tetrazine, and ethylene.....	50
Figure 5.3 Low-lying vacant orbitals involved in the Diels-Alder reactions of tetrazine 1-7	51
Figure 5.4 Tetrazines and dienophiles investigated in this report.....	51
Figure 5.5 M06-2X/6-31G(d)-optimized transition structures for reactions of 3,6-dimethyl-tetrazine 2 with 2-butyne 8 , <i>trans</i> -2-butene 9 , cyclooctyne 10 , and <i>trans</i> -cyclooctene 11	53
Figure 5.6 Distortion/interaction model.....	56
Figure 5.7 Plot of $\Delta E_{act}^{\ddagger}$, $\Delta E_{dist}^{\ddagger}$, and $\Delta E_{int}^{\ddagger}$ for tetrazines 1-7	57
Figure 5.8 Plot of distortion energy of angle versus distortion angle and geometries of ground-state <i>trans</i> -cyclooctene and cyclooctyne.....	59
Figure 5.9 Graph of distortion, interaction, and activation energies for transition states of reactions of tetrazines 2 and dienophiles 8-11	60
Figure 5.10 M06-2X/6-31G(d)-optimized transition structures for reactions of <i>trans</i> -2-butene.....	62
Figure 5.11 Graph of distortion, interaction, and activation energies for transition states of reaction of tetrazines 1-7 and <i>trans</i> -2-butene 9	63
Figure 5.12 Total energy, distortion energy, and interaction energy along the reaction coordinate (forming bond distance in Å) for reactions of tetrazines 1-7 with <i>trans</i> -2-butene.....	64
Figure 5.13 Transition structures involving 1 and 7 and corresponding IRC points with similar forming bond distances.....	66
Figure 5.14 Plot of distortion energy of angle versus distortion angle for tetrazines 1-7	67

Figure 5.15 Correlation between angular distortion energies at fixed distortion angles and the reaction enthalpies of the corresponding isodesmic reactions.....	69
Figure 5.16 Plots of activation energy vs total distortion energy and reaction energy.....	70
Figure 5.17 Plots of interaction energy vs inverse of the FMO energy gap.....	72
Figure 6.1 Dienes and dienophiles investigated.....	83
Figure 6.2 Optimized <i>endo</i> transition structures for reactions of cyclopentadiene and 1,3-dimethoxybutadiene.....	85
Figure 6.3 Optimized <i>exo</i> transition structures for reactions of cyclopentadiene and 1,3-dimethoxybutadiene.....	87
Figure 6.4 Graph of distortion, interaction, and activation energies for <i>endo</i> reactions of dienes 1 and 2 with dienophiles 5-9	89
Figure 6.5 Graph of distortion, interaction, and activation energies for <i>exo</i> reactions of dienes 1 and 2 with dienophiles 5-9	89
Figure 6.6 Plots of activation energy versus distortion energy of dienophile, total distortion energy, and reaction energy.....	90
Figure 6.7 Optimized transition structures for reactions of dienes 3 and 4	92
Figure 6.8 Graph of distortion, interaction, and activation energies for reactions of dienes 3 and 4 with dienophiles 5-9	93

Figure 6.9 Plots of activation energy versus distortion energy of dienophile, total distortion energy, and reaction energy.....	94
Figure 6.10 FMO energies for alkenes and dienes.....	95
Figure 6.11 Important frontier molecular orbitals involved in the Diels-Alder reactions of dienes 1-4.....	96
Figure 6.12 Plot of distortion energy versus out-of-plane distortion angle for dienophiles 5-9...97	
List of Schemes	
Scheme 2.1 Synthesis of water soluble gated hemicarcerand 5	20
Scheme 3.1 Synthesis of photochemically gated hemicarcerand 6a	23
Scheme 4.1 Azide-cyclooctyne cycloaddition and tetrazine- <i>trans</i> -cyclooctene cycloaddition...31	
Scheme 4.2 Mutual orthogonality.....	32
Scheme 4.3 Cycloadditions of tetrazines with strained alkenes.....	41
Scheme 5.1 Rate constants of Diels-Alder cycloadditions of tetrazines with strained and unstrained alkenes and alkynes.....	47
Scheme 5.2 Diels-Alder reactions of substituted tetrazines.....	49
Scheme 6.1 Reactions of cyclopentadiene with cycloalkenes in Diels-Alder reactions.....	80
Scheme 6.2 Reactivities of cycloalkenes in Diels-Alder reactions with 3,6-bis(trifluoromethyl) tetrazine.....	81

List of Tables

Table 2.1 Computed binding energies for complexes between 5 and guests i-vii	19
Table 3.1 Computed binding energies for complexes between 6b and guests i-xv	28
Table 5.1 Activation energies for Diels-Alder reactions between tetrazines 1-7 and dienophiles 8-11	54
Table 6.1 Strain Energies of cycloalkenes and cycloalkanes.....	81
Table 6.2 Calculated activation free energies and rate constants in comparison with experimental data.....	92

ACKNOWLEDGMENT

My study here at UCLA has a significant impact on my life and I am grateful to everyone who has given me a hand along the way.

I would like to acknowledge my advisor, Professor Kendall N. Houk, for his generosity in taking me into the group and his encouragement and guidance over the years. All the achievements and accomplishments presented in this dissertation and beyond are under his supervision.

Chapter 1

This chapter is a version of:

Liu, F.; Helgeson, R. C.; Houk, K. N. "Building on Cram's legacy: stimulated gating in hemicarcerands." *Acc. Chem. Res.* **2014**, *in press*.

Permission was given for use of this work in this thesis.

Chapter 2

I would like to thank Dr. Roger C. Helgeson for his help in the wet lab. Roger has taught me a lot of lab techniques and background of Cram's host-guest chemistry, which benefit me a lot. More importantly, he inspired me with his passion for chemistry.

Chapter 3

This chapter is a version of:

Wang, H.; Liu, F.; Helgeson, R. C.; Houk, K. N. “Reversible photochemically gated transformation of a hemicarcerand to a carcerand.” *Angew. Chem. Int. Ed.* **2013**, *52*, 655-659.

Permission was given for use of this work in this thesis.

I would like to thank Dr. Hao Wang, who did all the experimental work in this project.

Chapter 4

This chapter is based in part on:

Liang, Y.; Mackey, J. L.; Lopez, S. A.; Liu, F.; Houk, K. N. “Control and design of mutual orthogonality in bioorthogonal cycloadditions.” *J. Am. Chem. Soc.* **2012**, *134*, 17904-17907.

This project involved other group members: Yong Liang, Steven A. Lopez, Joel L. Mackey, and Melika Pourati.

I would like to thank my teammates for their help and cooperation.

Chapter 5

This chapter is a version of:

Liu, F.; Liang, Y.; Houk, K. N. “Theoretical elucidation of the origins of substituent and strain effects on the rates of Diels-Alder reactions of substituted tetrazines.” *manuscript in preparation*.

Permission was given for use of this work in this thesis.

I would like to thank Dr. Yong Liang for his helpful discussion from time to time.

Chapter 6

This chapter is a version of:

Liu, F.; Paton, R. S.; Kim, S.; Liang, Y.; Houk, K. N. “Diels-Alder reactivities of strained and unstrained cycloalkenes with normal and inverse-electron-demand dienes: activation barriers and distortion/interaction analysis.” *J. Am. Chem. Soc.* **2013**, *135*, 15642-15649.

Permission was given for use of this work in this thesis.

Funding

National Institute of General Medical Sciences, National Institutes of Health (GM 52705)

National Science Foundation (CHE-1059084)

Computations were performed on the Extreme Science and Engineering Discovery Environment (XSEDE) and the UCLA IDRE Hoffman2 cluster.

VITA

EDUCATION

2009 Nankai University, B. S. in Chemistry

AWARDS

2008 Nankai University, National Fellowship

2007 Nankai University, Shi-Xian Yang Scholarship

PUBLICATIONS

1. Liu, F.; Liang, Y.; Houk, K. N. "Theoretical elucidation of the origins of substituent and strain effects on the rates of Diels-Alder reactions of substituted tetrazines." *manuscript in preparation*.
2. Tork, L.; Jimenez-Oses, G.; Doubleday, C.; Liu, F.; Houk, K. N. "Molecular dynamics of the cycloaddition of tetrazines to alkenes: stereoelectronic and dynamic effects on N₂ extrusion." *manuscript in preparation*.
3. Liu, F.; Helgeson, R. C.; Houk, K. N. "Building on Cram's legacy: stimulated gating in hemicarcerands." DOI: 10.1021/ar5001296.
4. de Loera, D.; Liu, F.; Houk, K. N.; Garcia-Garibay, M. A. "Aziridine nitrogen inversion by dynamic NMR: activation parameters in a fused bicyclic structure." *J. Org. Chem.* **2013**, *78*, 11623-11626.

5. Liu, F.; Paton, R. S.; Kim, S.; Liang, Y.; Houk, K. N. "Diels-Alder reactivities of strained and unstrained cycloalkenes with normal and inverse-electron-demand dienes: activation barriers and distortion/interaction analysis." *J. Am. Chem. Soc.* **2013**, *135*, 15642-15649.
6. Edwards, N. Y.; Liu, F.; Chen, G. "Experimental and computational studies of anion recognition by pyridine-functionalised calixarenes." *Supramol. Chem.* **2013**, *25*, 481-489.
7. Wang, H.; Liu, F.; Helgeson, R. C.; Houk, K. N. "Reversible photochemically gated transformation of a hemicarcerand to a carcerand." *Angew. Chem. Int. Ed.* **2013**, *52*, 655-659.
8. Liu, F.; Wang, H.; Houk, K. N. "Gating in host-guest chemistry." *Curr. Org. Chem.* **2013**, *17*, 1470-1480.
9. Liang, Y.; Mackey, J. L.; Lopez, S. A.; Liu, F.; Houk, K. N. "Control and design of mutual orthogonality in bioorthogonal cycloadditions." *J. Am. Chem. Soc.* **2012**, *134*, 17904-17907.
10. Liu, F.; Wang, H.; Houk, K. N. "Gated container molecules." *Sci. China. Chem.* **2011**, *54*, 2038-2044.

TEACHING EXPERIENCE

2009-2010 General and Organic Chemistry (discussion and laboratory)

2013 Theoretical and Computational Organic Chemistry

2013 General Chemistry (as an instructor at UCLA Extension)

2014 Advanced Organic Chemistry

CHAPTER 1: GATING IN HOST-GUEST CHEMISTRY

1.1 Overview of Host-Guest Chemistry

Host-guest chemistry originated from an exploration of evolutionary biological molecules and their substrates. The active sites of these receptors have concave surfaces which bind specifically with substrates with convex surfaces. To mimic and better understand the complexation processes in natural systems, chemists came up with a variety of host molecules with concave surfaces. Among them, Pedersen's crown ethers,^[1] Cram's spherands,^[2] and Lehn's cryptands^[3] exhibit good selectivity in binding organic and metal cations, and are milestones in the development of synthetic hosts (Figure 1.1). The Nobel Prize in Chemistry was awarded to these chemists in 1987. Further efforts have been devoted to achieve chiral recognition and controllable binding in more sophisticated systems.

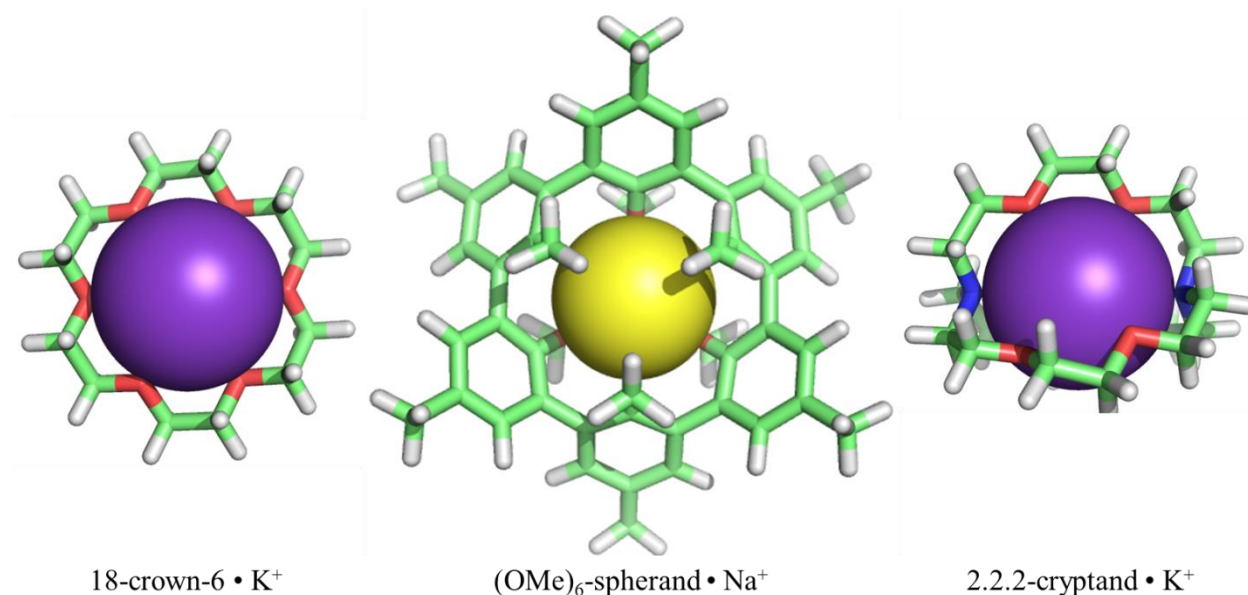


Figure 1.1 Complexes of crown ether, spherand, and cryptand with alkali metal cations.

1.2 Gated Container Molecules

The development of container molecules with gates was inspired by the observations of controllable access of substrates to the active sites in many natural enzymes. The conformational changes of the peptide loops were found to be a common gating mechanism.^[4] For example, pancreatic lipase, an enzyme that hydrolyzes dietary fat in the digestive system, has a lid over its active site when not activated (Figure 1.2a). The lid opens when the protein is activated upon contact with a lipid surface.^[5] Some gating processes require conformational change of the entire subunits.

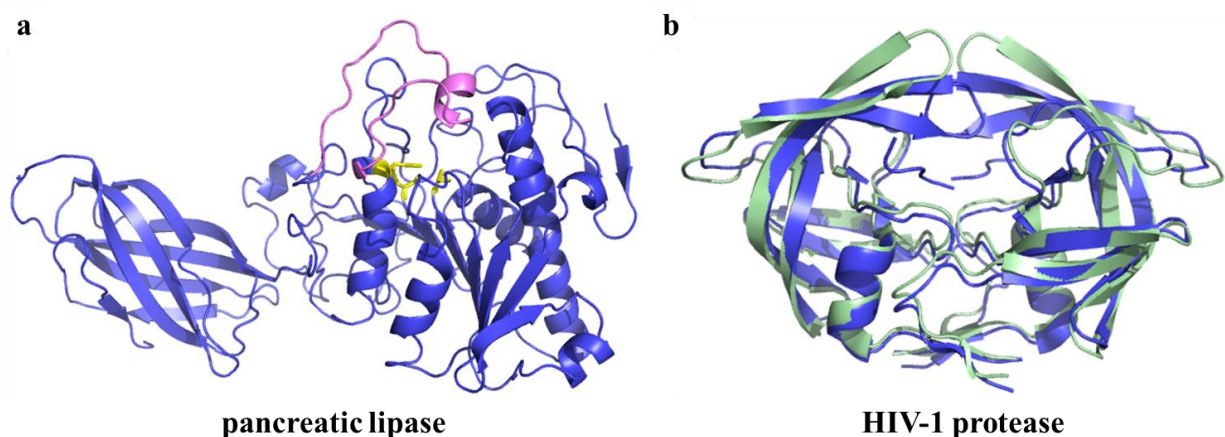


Figure 1.2 a) Ribbon structure of pancreatic lipase (PDB entry 1HPL) with the active site (shown in yellow) covered by the lid (shown in purple). b) Ribbon structures of HIV-1 protease in both closed (PDB entry 1TW7) and semi-open (PDB entry 2NPH) states (shown in blue and green, respectively).

One example is HIV-1 protease. Both crystal structure analysis and molecular dynamics simulations have shown that HIV-1 protease switches from a *closed* conformation (Figure 1.2, blue) to a *semi-open* (Figure 1.2, green) and further into an *open* conformation to expose its

active site to the environment.^[6] In the *closed* conformation, the two flaps are packed onto each other closely, restricting access to the active site. In the *semi-open* conformation, the two flaps slide away from each other to expose the active site.

Numerous gated container molecules have been developed based on the concept of “gating”. Some of these hosts are characterized by dimerization and dissociation gating, where two cavitands are held together by intermolecular forces such as hydrogen bonds and ionic forces and can dissociate into isolated cavitands when the forces are interrupted, resulting in release of guest molecules.^[7] One example is Rebek’s cylindrical capsule (Figure 1.3a), the cavity of which is measured to be 420 Å³ and can encapsulate benzene, toluene, and *p*-xylene under certain conditions.^[7b] Gating in some other container molecules involves conformational changes of flexible moieties.^[8] Badjić’s molecular baskets are prime examples. Figure 1.3b shows one gated molecular basket in its open and closed forms.^[8c]

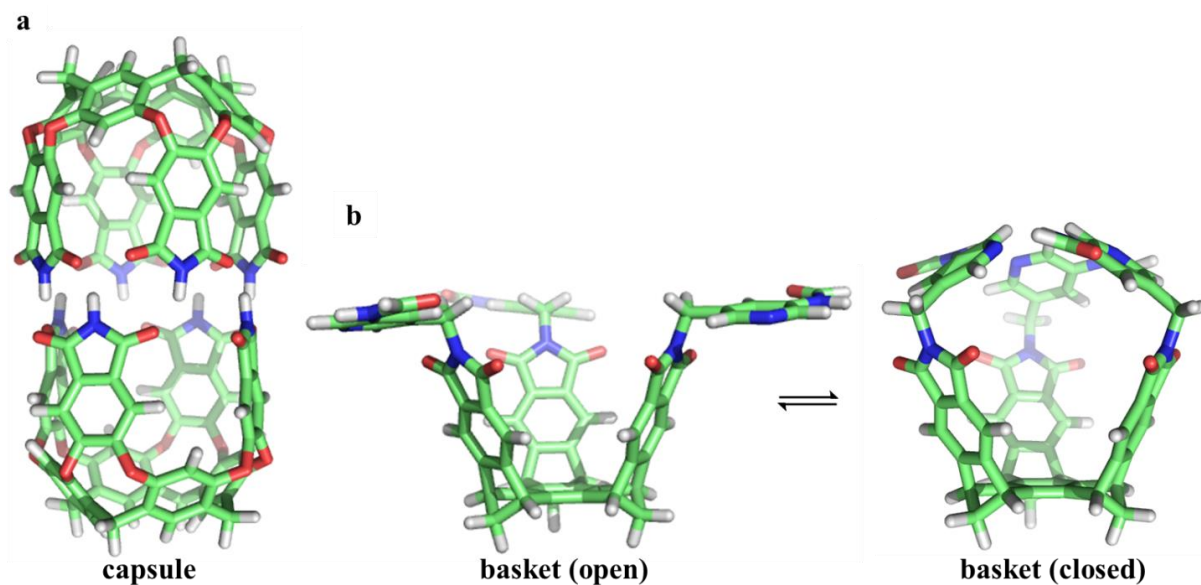


Figure 1.3 a) Structure of a cylindrical capsule. b) Gate-opening and closing in a molecular basket.

1.3 Gating Mechanisms

I would like to highlight the fact that gating in synthetic hosts was first discovered in our lab as a result of computational investigations.^[9] The following section will focus on computational exploration on gating mechanisms, in the context of Cram's hemicarcerands.

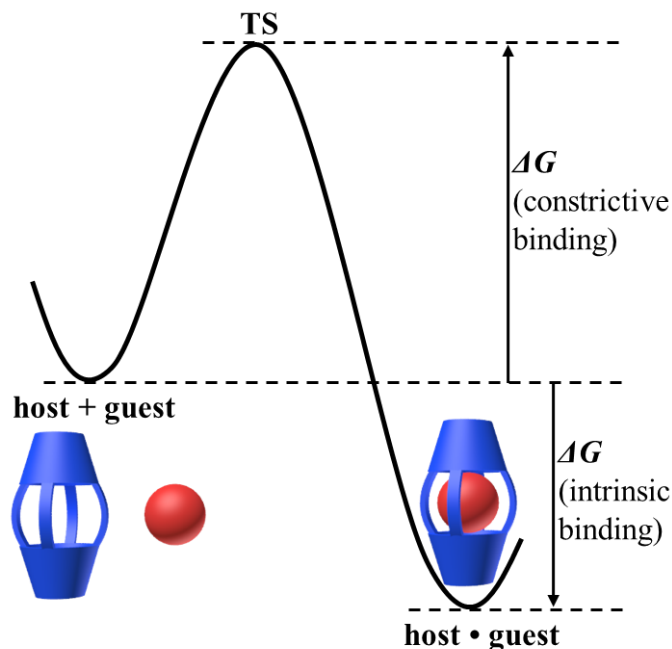


Figure 1.4 Energy definitions for host-guest complexation by a carcerand or hemicarcerand.

Before going into calculations, a few key words, defined by Donald J. Cram at UCLA, should be defined. *Carcerands* refer to host molecules that form stable complexes with small organic molecules during their synthesis. The incarcerated guests cannot escape without breaking covalent bonds in the carcerands. The complexes formed in such cases are called *carceplexes*. *Hemicarcerands* can release the encapsulated guests when heated to a higher temperature without breaking any covalent bonds. The complexes formed between hemicarcerands and small molecules are *hemicarceplexes*.^[10] To better describe the binding properties in these host-guest

systems, *intrinsic binding* (the free energy difference between the complex and the free host and guest) and *constrictive binding* (the additional activation free energy for decomplexation, arising from the physical barrier for egress of guest) are defined as shown in Figure 1.4.^[11]

How to interpret these energies? A more negative intrinsic binding energy indicates a more stable complex and, therefore, a larger decomplexation barrier. Constrictive binding free energy does not affect intrinsic binding but does influence rates of complexation and guest release. If constrictive binding is higher than ~ 25 kcal/mol, the host-guest complexation will take many days to occur under ambient conditions. With a closed gate, a hemicarceplex behaves like a carceplex, presenting a high decomplexation barrier, such that the imprisoned guest cannot escape. However, once the gate is opened, the decomplexation barrier of the hemicarceplex is significantly lowered to allow the release of the guest (Figure 1.5).

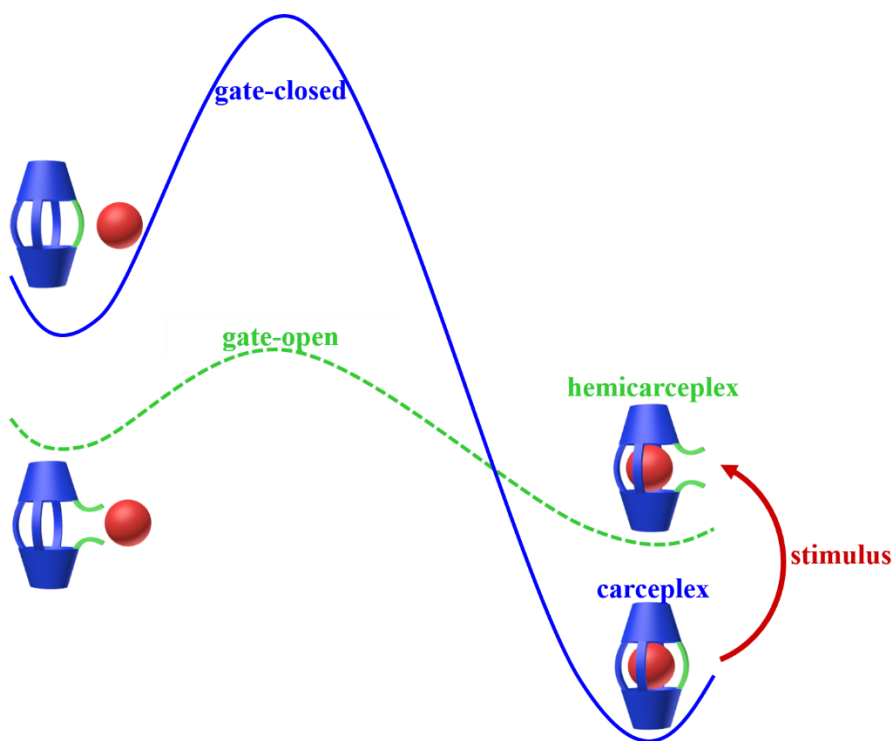


Figure 1.5 Stimulated gating converts a carceplex to a hemicarceplex.

With all these crucial concepts clarified, we are now ready for the tour through computational investigations of gating. The mechanism of the controlled binding and release of guests in hemicarcerands was elucidated through computational studies by Nakamura in our group in the 1990s on host **1a** shown in Figure 1.6a.^[9] This host was found to form complexes with one or two acetonitriles molecules during its synthesis. The complex with two acetonitriles loses one upon heating at 110°C for 3 days, but the escape of a second acetonitrile was not observed.^[12] From its structure, it is clear that **1a** has four side portals (one of them is highlighted in blue in Figure 1.6a) and two polar portals (one of them is highlighted in red in Figure 1.6a). Based on CPK space-filling models, Cram proposed that the acetonitrile could only escape through the polar portal, since it is larger than the side portal as shown in Figure 1.6b. Based on CPK space-filling models, Cram proposed that the acetonitrile could only escape through the polar portal, since it is larger than the side portal as shown in Figure 1.6b.

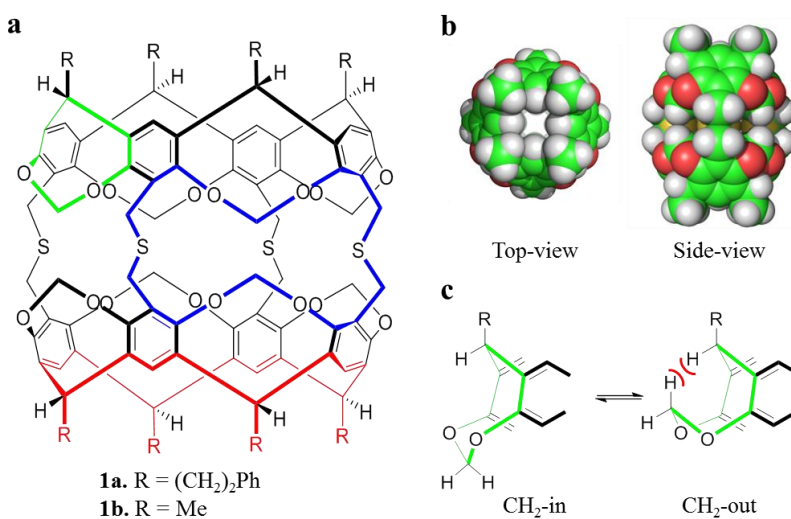


Figure 1.6 a) Structure of thermally-gated hemicarcerand **1** with one side portal colored in blue, one polar portal colored in red and one eight-membered ring colored in green. b) CPK model of **1b** showing the polar portal is slightly larger than the side portals. c) The CH₂-in and CH₂-out conformational change in an eight membered ring in **1** (colored in green) that leads to the closing and opening of the thermal gate.

However, CPK models failed to explain why the escape of a second acetonitrile is not favored, nor can these models provide any information about the activation energy for the decomplexation. With force-field computations, Nakamura in our group was able to reveal some structural and dynamic properties not available from the space-filling model or experiments. To reduce the computational effort, calculations were carried out on **1b** instead of the actual host **1a**, since preliminary studies showed that the “feet” (R groups) have little effect on the portal sizes. All possible structures of **1b** were optimized with AMBER* force field in the Macromodel program.^[13] It was found that each eight-membered ring in **1** (Figure 1.6a, one unit is highlighted in green) has two conformations: CH₂-in and CH₂-out (Figure 1.6c). The CH₂-out conformation is calculated to be about 7 kcal/mol higher in energy than the CH₂-in conformation, due to the steric repulsion between the two clashing hydrogens in the CH₂-out conformation (Figure 1.6c). At room temperature, the equilibrium between CH₂-in and CH₂-out is greater than 10⁵ to 1 (CH₂-out less than 0.001%). When the temperature is raised to 110°C, the proportion of CH₂-out increases by about two orders of magnitude.

Both equatorial and polar escape pathways were studied by constrained optimizations, where the distance between one acetonitrile molecule and one of the phenyl carbons on **1b** was taken as the reaction coordinate. Optimizations were carried out at fixed distance along each pathway. The activation energies for equatorial and polar escape pathways were high in the CH₂-in conformation, 52 and 46 kcal/mol, respectively. This result suggested that the trapped acetonitriles are not able to escape the cavity with the host in its CH₂-in (closed) form.

However, the conformational change of the eight-membered ring from CH₂-in to CH₂-out dramatically lowers the barrier of equatorial-escape, as shown in Figure 1.7. The ground state

hemiacarceplex (Figure 1.7, left) has to overcome the barriers for sequential conformational flips of two $-\text{OCH}_2\text{O}-$ moieties (22 and 26 kcal/mol, respectively) to achieve an intermediate (Figure 1.7, middle) with its side portal widely open. Then the escape of an acetonitrile through the open portal requires only 22 kcal/mol in terms of activation energy (Figure 1.7, right). The overall barrier for decomplexation through gating is 26 kcal/mol, which corresponds to a half-life of 15 days at ambient temperature, but one minute at 110°C. This result agrees well with the experimental observation. Molecular dynamics simulations also showed that the escape of the first acetonitrile is exergonic by 11 kcal/mol, while the escape of a second acetonitrile is endergonic by 3 kcal/mol, which provided an explanation of the fact that the second acetonitrile does not exit the cavity.

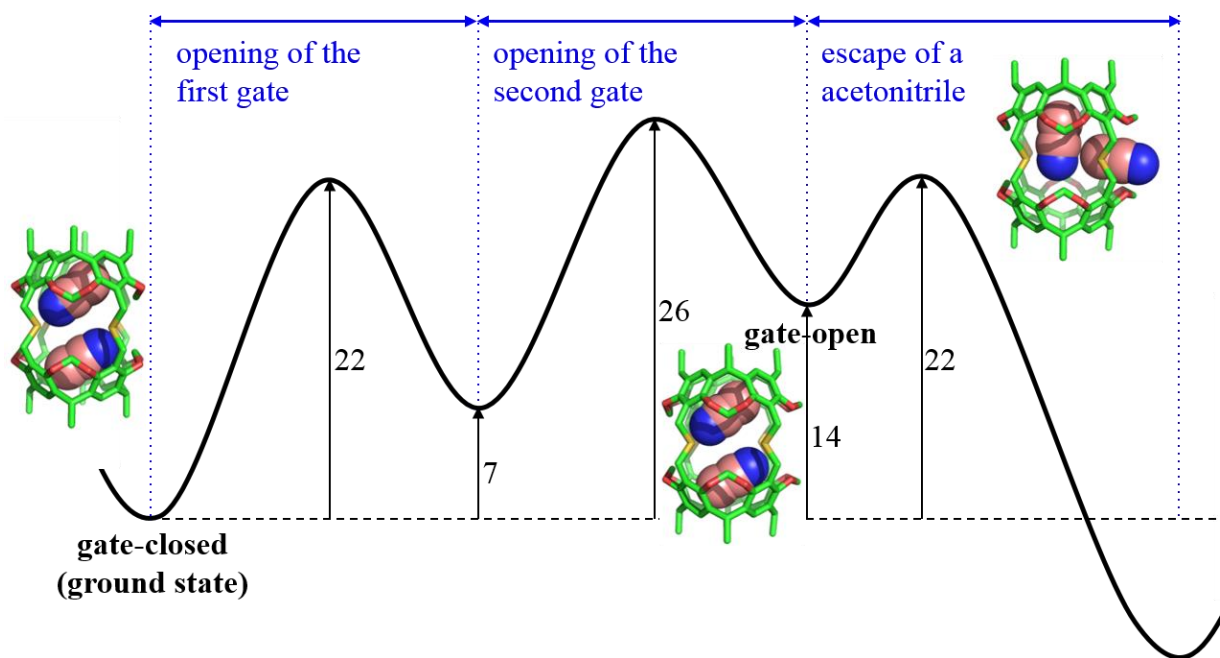


Figure 1.7 Energy profiles for the escape of acetonitrile from **1b** through gating.

The term “gating” was introduced at that time to describe a conformational process that controls the entrance and egress of a guest in synthetic host molecules. Two types of gating exist

in hemicarceplexes, and we named these French door and sliding door. The types of doors that inspire these names are shown in Figure 1.8. French door gating describes two edge-to-edge door openings, here the sequential flips of two $\text{-OCH}_2\text{O-}$ moieties that lead to the opening of a portal. The sliding door often involves the conformational change of the whole molecular skeleton, resulting in the enlargement of the side portal, without any pronounced outward motion of the doors, as shown schematically at the bottom right of Figure 1.8.

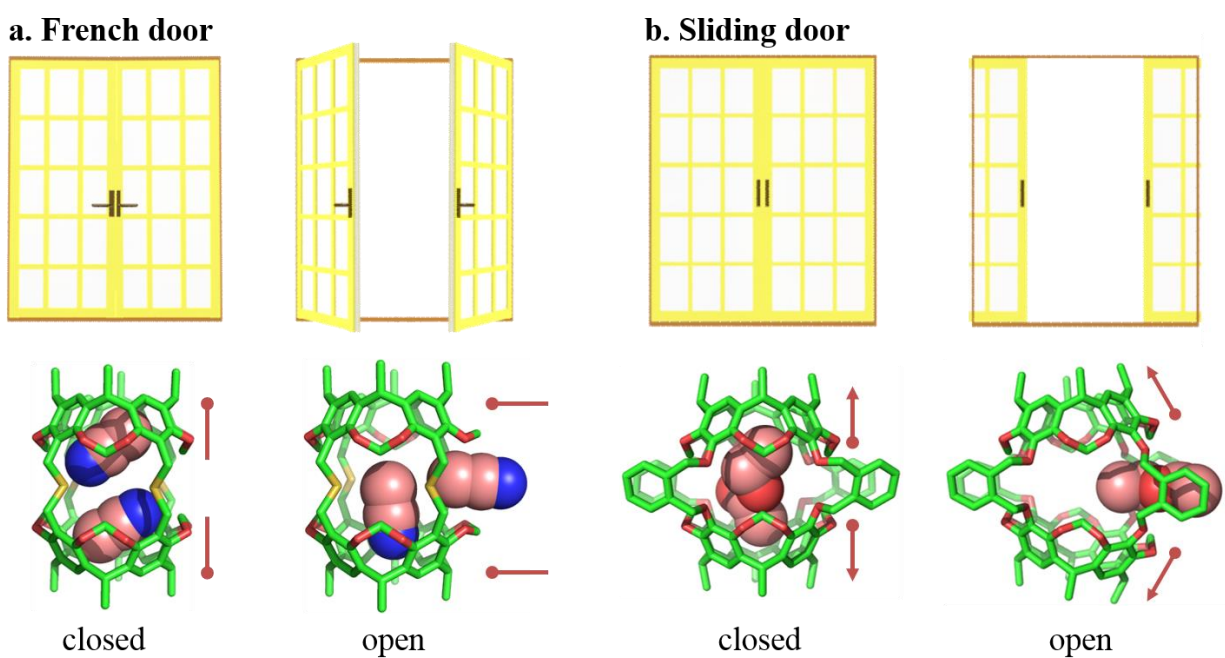


Figure 1.8 a) French door cartoon and analogous gating in **1b**. b) Sliding door cartoon and analogous gating in a four *o*-xylyl bridged hemicarcerand.

From the analysis of gating processes in four different hemicarcerands, we found that the importance of gating in the complexation and decomplexation processes varies, depending on the nature of guests and the size of the hemicarcerand portals.^[14] Some hosts have portals so large that the guests readily pass into and out of the cavity with almost no barriers. In such cases,

gating does not influence the entry and exit of guests. An example is the complexation of hemicarcerand **2** (Figure 1.9, left) with benzene. Calculations with the AMBER* force field showed that there is no barrier to complexation, and the decomplexation barrier is only about 8 kcal/mol after solvation corrections, which suggests rapid entry and exit of the benzene without gating.

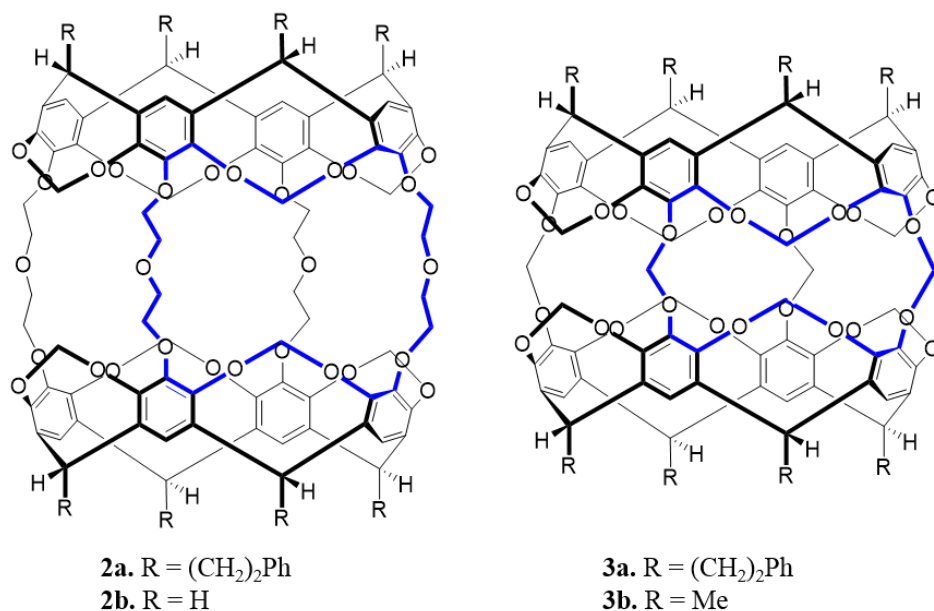


Figure 1.9 Structures of hosts with large portals (left) and small portals (right); one of the four side portals in each structure is highlighted in blue.

In contrast, some hosts have portals too small to allow the passage of guest molecules even with an open gate. The barrier to loss of dimethyl sulfoxide from **3** (Figure 1.9, right) is calculated to be greater than the energy to break a C-C bond (~90 kcal/mol). Some hosts have portals small enough to incorporate guests, but still big enough for the exit of the guests upon a conformational change, as the release of acetonitrile from hemicarcerand **1**. Gating becomes a

crucial factor in forming stable, and yet reversible, complexes of such hosts with appropriate guests.

The involvement of gating in complexation was explored in detail in a study of the complexation of hemicarcerand **2b** with 40 aromatic and bicyclic guests.^[15] The structural optimization and molecular dynamics simulations with the MM3* force field showed that thermal gating is not required for the entry of smaller aromatic guests such as toluene and p-xylene; gating is a crucial factor only in the complexation and decomplexation of hemicarcerand **2b** with larger bicyclic guests such as norbornene. These results are in accord with the experimental fact that simple aromatics either fail to complex with hemicarcerand **2a** or escape the host cavity upon attempted isolation, while larger bicyclics form isolable complexes with **2a**.^[16]

Intrigued and stimulated by these experimental and theoretical observations, we set out to go beyond thermal gating and to build container molecules with gates that could be controlled by chemical and photochemical stimuli, which will be described in detail in the follow two chapters.

1.4 References

[1] Pedersen, C. J. Cyclic polyethers and their complexes with metal salts. *J. Am. Chem. Soc.* **1967**, *89*, 7017-7036.

[2] (a) Kyba, E. P.; Helgeson, R. C.; Madan, K.; Gokel, G. W.; Tarnowski, T. L.; Moore, S. S.; Cram, D. J. Host-guest complexation. 1. Concept and illustration. *J. Am. Chem. Soc.* **1977**, *99*, 2564-2571. (b) Cram, D. J.; Kaneda, T.; Helgeson, R. C.; Brown, S. B.; Knobler, C. B.;

Maverick, E. F.; Trueblood, K. N. Host-guest complexation. 35. Spherands, the first completely preorganized ligand systems. *J. Am. Chem. Soc.* **1985**, *107*, 3645-3657.

[3] Jazwinski, J.; Lehn, J.-M.; Lilienbaum, D.; Ziessel, R.; Guilhem, J. Pascard, C. Polyaza macrobicyclic cryptands: synthesis, crystal structures of a cyclophane type macrobicyclic cryptand and of its dinuclear copper (I) cryptate, and anion binding features. *J. Chem. Soc., Chem. Commun.* **1987**, *22*, 1691-1694.

[4] (a) Jiang, Y.; Lee, A.; Chen, J.; Cadene, M.; Chait, B. T.; MacKinnon, R. The open pore conformation of potassium channels. *Nature* **2002**, *417*, 523-526. (b) Perozo, E.; Cortes, D. M.; Sompornpisut, P.; Kloda, A.; Martinac, B. Open channel structure of MscL and the gating mechanism of mechanosensitive channels. *Nature* **2002**, *418*, 942-948.

[5] Belle, V.; Fournel, A.; Woudstra, M.; Ranaldi, S.; Prieri, F.; Thome, V.; Currault, J.; Verger, R.; Guigliarelli, B.; Carriere, F. Probing the opening of the pancreatic lipase lid using site-directed spin labeling and EPR spectroscopy. *Biochemistry-US.* **2007**, *46*, 2205-2214.

[6] (a) Toth, G.; Borics, A. Flap opening mechanism of HIV-1 protease. *J. Mol. Graph. Model.* **2006**, *24*, 465-474. (b) Yedidi, R. S.; Protease, G.; Martinez, J. L.; Vickrey, J. F.; Martin, P. D.; Wawrzak, Z.; Liu, Z.; Kovari, I. A.; Kovari, L. C. Contribution of the 80s loop of HIV-1 protease to the multidrug-resistance mechanism: crystallographic study of MDR769 HIV-1 protease variants. *Acta. Cryst.* **2011**, *67*, 524-532.

[7] (a) Branda, N.; Grotzfeld, R. M.; Valdes, C.; Rebek, J. Jr. Control of self-assembly and reversible encapsulation of Xenon in a self-assembling dimer by acid-base chemistry. *J. Am. Chem. Soc.* **1995**, *117*, 85-88. (b) Heinz, T.; Rudkevich, D. M.; Rebek, J. Jr. Pairwise selection

of guests in a cylindrical molecular capsule of nanometer dimensions. *Nature*, **1995**, *394*, 764-766. (c) Koblenz, T. S.; Dekker, H. L.; de Koster, C G.; van Leeuwen, P. W. N. M.; Reek, J. N. H. Bisphosphine based hetero-capsules for the encapsulation of transition metals. *Chem. Commun.* **2006**, 1700-1702. (d) Scarso, A.; Pellizzaro, L.; de Lucchi, O.; Linden, A.; Fabris, F. Gas hosting in enantiopure self-assembled oximes. *Angew. Chem. Int. Ed.* **2007**, *46*, 4972-4975. (e) Kulasekharan, R.; Jayaraj, N.; Porel, M.; Choudhury, R.; Sundaresan, A. K.; Parthasarathy, A.; Ottaviani, M. F.; Jockusch, S.; Turro, N. J.; Ramamurthy, V. Guest rotation within a capsuleplex probed by NMR and EPR techniques. *Langmuir*, **2010**, *26*, 6943-6953.

[8] (a) Moran, J. R.; Ericson, J. L.; Dalcanale, E.; Bryant, J. A.; Knobler, C. B.; Cram, D. J. Vases and kites as cavitands. *J. Am. Chem. Soc.* **1991**, *113*, 5707-5714. (b) Roncucci, P.; Pirondini, L.; Paderni, G.; Massera, C.; Dalcanale, E.; Azov, V. A.; Diederich, F. Conformational behavior of pyrazine-bridged and mixed-bridged cavitands: a general model for solvent effects on thermal "vase-kite" switching. *Chem. Eur. J.* **2006**, *12*, 4775-4784. (c) Wang, B.; Bao, X.; Stojanovic, S.; Hadad, C. M.; Badjic, J. D. Encapsulation of guests within a gated molecular basket: thermodynamics and selectivity. *Org. Lett.* **2008**, *10*, 5361-5364. (d) Durola, F.; Dube, H.; Ajami, D.; Rebek, J. Jr. Control of nanospaces with molecular devices. *Supramol. Chem.* **2011**, *23*, 37-41.

[9] Nakamura, K.; Houk, K. N. Mechanism and thermodynamics of guest escape from a carcerand. *J. Am. Chem. Soc.* **1995**, *117*, 1853-1854.

[10] Cram, D. J.; Tanner, M. E.; Knobler, C. B. Host-guest complexation. 58. Guest release and capture by hemicarcerands introduces the phenomenon of constrictive binding. *J. Am. Chem. Soc.* **1991**, *113*, 7717-7727.

- [11] Cram, D. J.; Blanda, M. T.; Paek, K.; Knobler, C. B. Constrictive and intrinsic binding in a hemicarcerand containing four portals. *J. Am. Chem. Soc.* **1992**, *114*, 7765-7773.
- [12] Bryant, J. A.; Blanda, M. T.; Vincenti, M.; Cram, D. J. Shell closures of tetrabenzyl chloride cavitands with tetrabenzylthiol cavitands provide carceplexes in which one or two guest molecules are incarcerated. *J. Chem. Soc., Chem. Commun.* **1990**, *20*, 1403-1405.
- [13] Macromodel, version 9.1, Schrödinger, LLC, New York, NY, 2006.
- [14] Houk, K. N.; Nakamura, K. Sheu, C.; Keating, A. E. Gating as a control element in constrictive binding and guest release by hemicarcerands. *Science* **1996**, *273*, 627-629.
- [15] Sheu, C.; Houk, K. N. Molecular mechanics and statistical thermodynamics studies of complexes of a flexible hemicarcerands with neutral guests. *J. Am. Chem. Soc.* **1996**, *118*, 8056-8070.
- [16] Byun, Y.; Vadhat, O.; Blanda, M. T.; Knobler, C. B.; Cram, D. J. Binding properties and crystal structures of a hemicarcerand containing four diethylene glycol units connecting two bowls. *J. Chem. Soc., Chem. Commun.* **1995**, *17*, 1825-1827.

CHAPTER 2: REDOX REACTION-GATED HEMICARCERANDS

2.1 Water-Soluble Redox Reaction-Gated Hemicarcerands

In 2009, Helgeson in our group synthesized the redox reaction-gated hemicarcerand **4**, which undergoes disulfide-dithiol interchange in the presence of base and thiol compounds (Figure 2.1a).^[1] The gate-opening process was proved to be thiol-concentration dependent; the disulfide gate opens more rapidly in a higher concentration of thiol. Hayden's calculations helped the understanding of the relationship between guest size and the ability to control guest encapsulation and release by gating in this hemicarcerand.

Since the glutathione (GSH) concentration in human cancerous cells is found to be two to five times higher than in normal cells,^[2] the gate-opening of hemicarcerand **4** in cancerous cells should be more rapid than that in normal cells, which indicates the potential application of disulfide-gated hemicarcerands as anticancer-drug delivery vehicles that release drug in cancer cells selectively. However, water solubility should be enhanced before such hemicarcerands can be used in biological systems. My initial project involved the design and attempted synthesis of a new redox-gated hemicarcerand **4** by shortening the "feet" (R groups, colored in red in Figure 2.1) and introducing carboxyl groups to the bridges (colored in blue in Figure 2.1). I carried out extensive computational studies and undertook the synthesis of the proposed water soluble gated hemicarcerand.

2.2 Computational Explorations

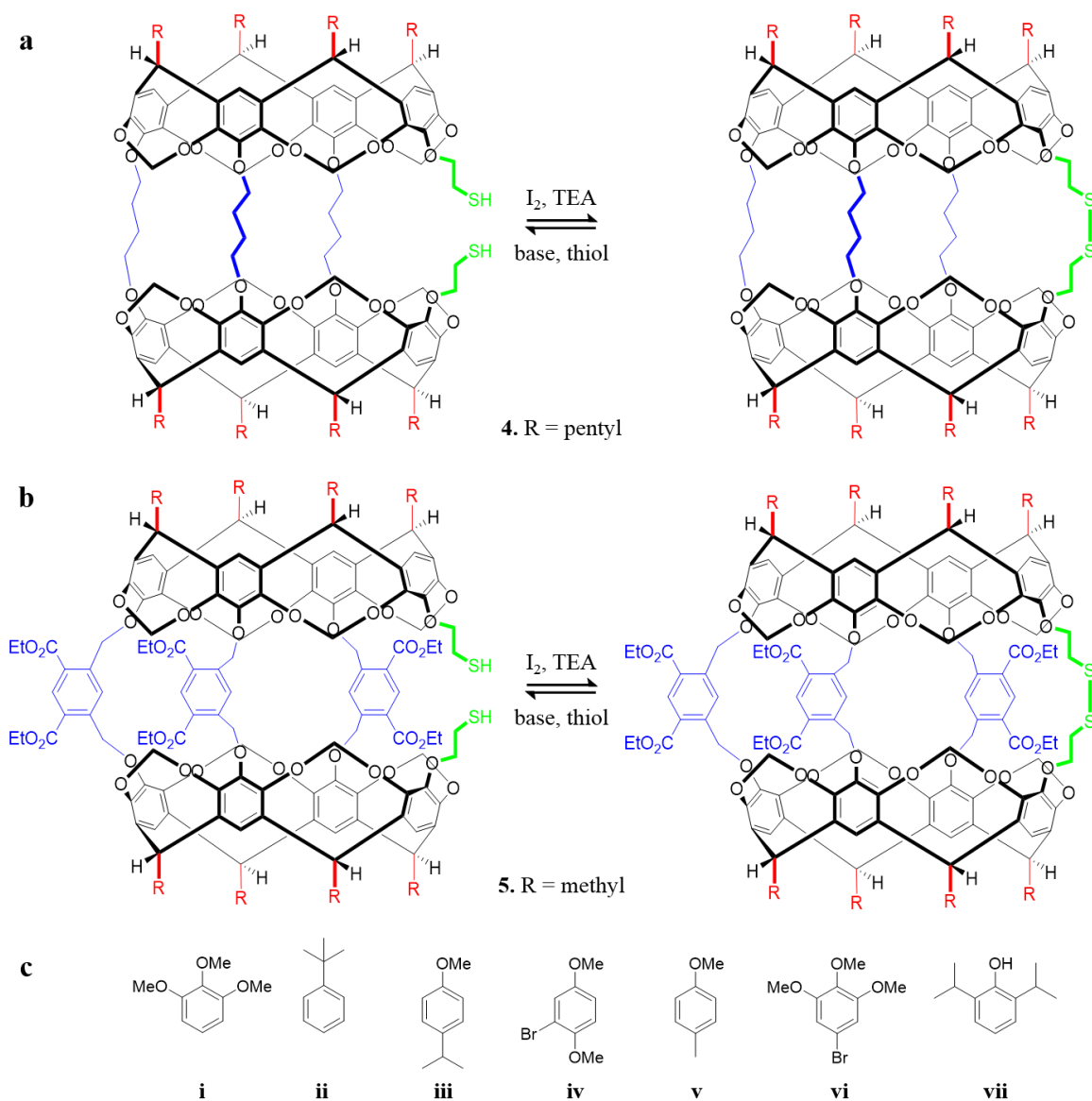


Figure 2.1 a) Redox reaction-gated hemicarcerand **4**.^[1] b) Water-soluble redox reaction-gated hemicarcerand **5** (the “feet” are colored in red, and the polar bridges are colored in blue). c) Guest molecules studied computationally.

The binding properties of the designed water-soluble hemicarcerand **5** with small organic molecules (shown in Figure 2.1c) were studied with molecular mechanics calculations with the OPLS force field and GB/SA solvation model for water in Macromodel.^[3] Conformation

searches were performed on isolated host **5** and the complexes between **5** and guest molecules to locate the global minimum conformation. For simple organic molecules, direct optimization proved to be satisfactory. Binding energy is defined as the energy difference between complex and the isolated host and guest. Both open and closed forms of host **5** were studied.

The optimized structures of the open and closed forms of host **5** are shown in Figure 2.2 (hydrogens are omitted for simplicity). Solvent molecules, in this case water molecules, can also enter the cavity, competing with the other organic guests. Therefore, a simulation on complexation between water and host **5** was carried out. By increasing the number of water molecules inside the cavity, it was determined that the most stable complex between **5** and water molecules is $5 \cdot 2H_2O$.

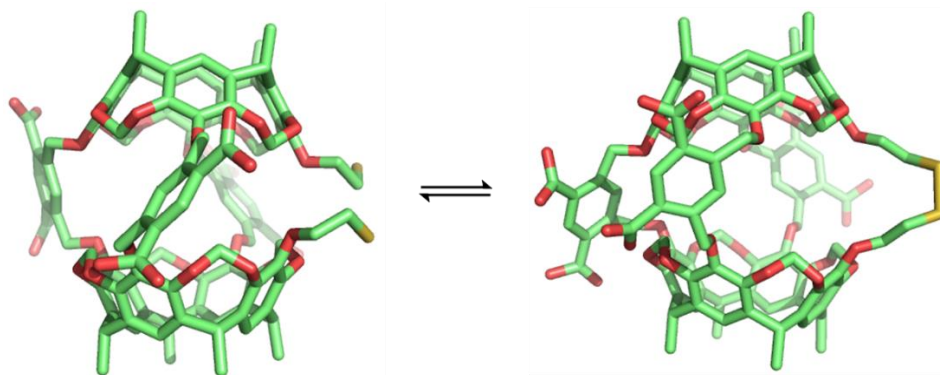


Figure 2.2 Optimized structures of isolated host **5** in water, in both open and closed forms.

The optimized structures of complexes formed between open and closed host **5** and guest molecule **i** are shown in Figure 2.3. In both forms, two methoxy groups on 1,2,3-trimethoxybenzene fit perfectly into the center of the top and bottom cavities without introducing much strain. The dithiol-disulfide interchange induced gate-opening and closing

have little effect on the orientation of the guest in its global minimum conformer. The optimized structures for the remaining complexes are shown in Figure 2.4.

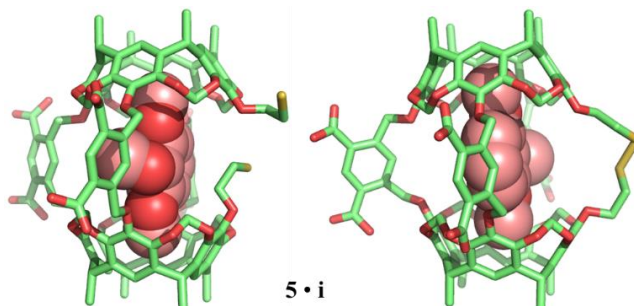


Figure 2.3 Optimized structures of complexes formed between **5** and guests **i** with GB/SA solvation model for water.

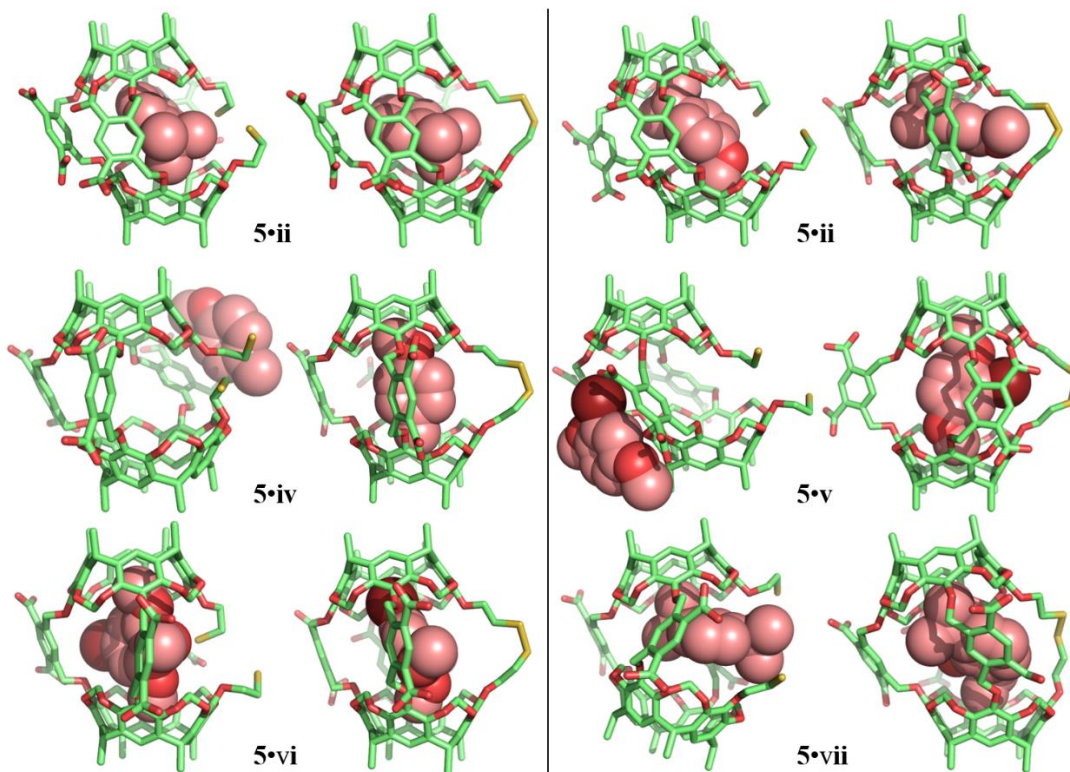


Figure 2.4 Optimized structures of complexes formed between **5** and guests **ii-vii** with GB/SA solvation model for water.

In most cases, the gate-opening and closing involves changes in the host conformation or the orientation of the guest. Guests **iv** and **v** cannot be accommodated by host **5** in its open form; they escape the cavity after optimization (Figure 2.4, middle line). Guest **vii** appears to be too large for **5** in both open and closed forms; the host has to twist to hold the guest molecule inside its cavity. The calculated binding energies ($E_{binding}$) for all complexes shown in Figure 2.3 and Figure 2.4 are shown in Table 2.1.

Table 2.1 Computed binding energies in GB/SA water for complexes between **5** and guests **i-vii**, in kcal/mol.

	i	ii	iii	iv	v	vi	vii
5 (open)	-23	-24	-13			-25	-17
5 (closed)	-29	-27	-20	-30	-19	-30	-26

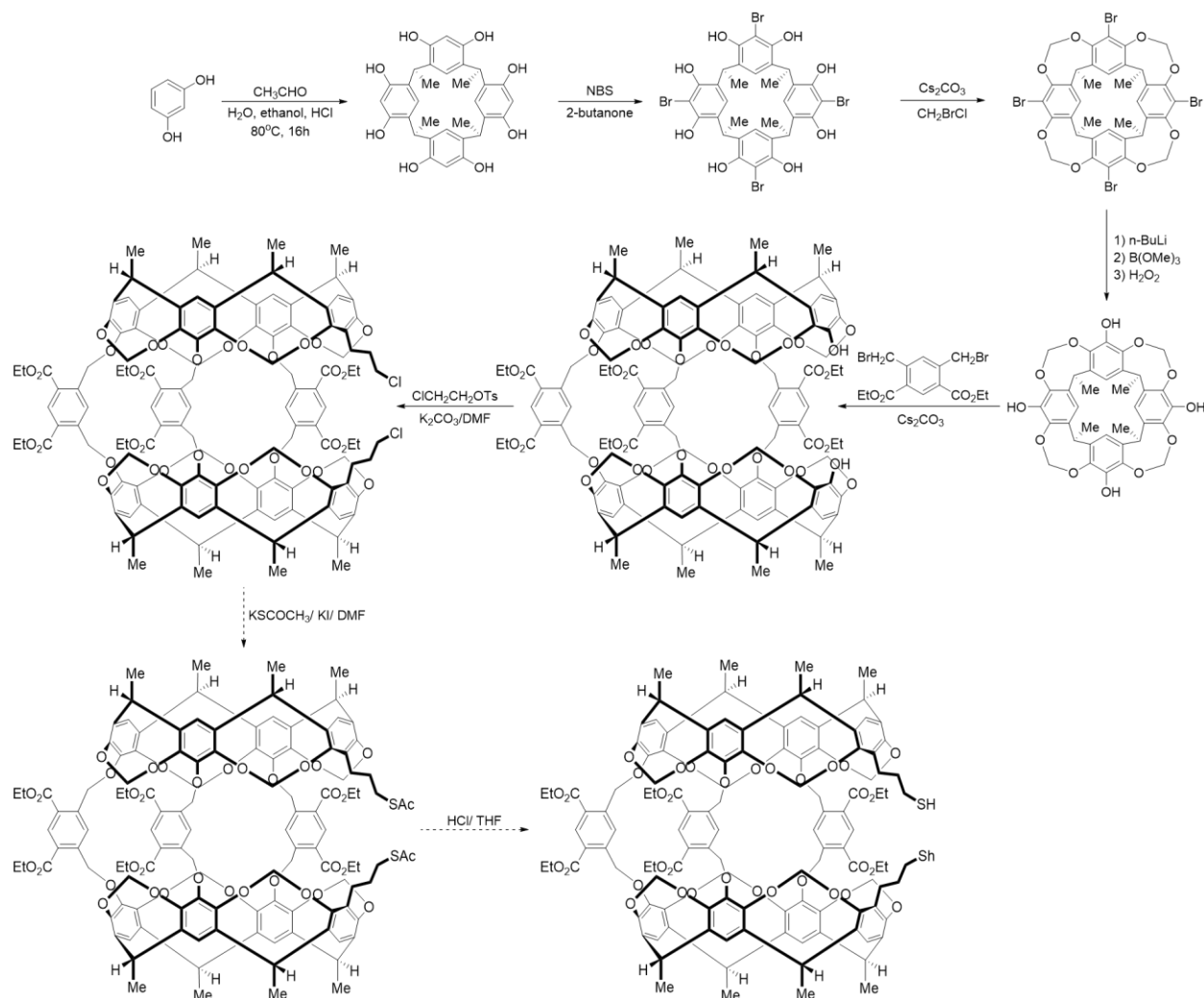
A more negative binding energy indicates a more stable complex formed between **5** and the particular guest. In general, the closed form of **5** binds more strongly with these guests than the open form, with $\Delta E_{binding}$ ranging from 3 to 9 kcal/mol. It is postulated that the lowering in binding energy is responsible for the encapsulation of guests in the closed form of **5** and the release of guests in its open form. This is related to the gating in many enzymes, where gate closure has been postulated to increase the surface area of the binding site and increase enzymes substrate complex stabilities.

2.3 Attempted Synthesis of Gated Hemicarcerand **5**

The synthesis pathway for gated hemicarcerand **5** is presented in Scheme 2.1. The general procedures for preparing cavitands were reported by Cram and coworkers in 1988,

starting with the reaction between resorcinol and acetaldehyde.^[4] The key step in the synthesis of hemicarcerand **5** is the connection of two cavitands by a diester. The yield of this particular step is extremely low, around 5%.

Scheme 2.1 Synthesis of water soluble gated hemicarcerand **5**.



Although I tried to enhance the yield by adding template molecules such as pyrazine and 1,4-dioxane, which have been reported to have a remarkable effect on carceplex formation by Sherman and coworkers,^[5] the formation of the tri-bridged product remained challenging. Another problem is that the solubilities of these molecules in organic solvents are not good. To

get enough starting material for the next three steps, I would have to run this reaction over and over, at least 40 times, assuming each run give 5% yield. This highly demanding project was abandoned until a better synthetic design emerges.

2.4 References

[1] Helgeson, R. C.; Hayden, A. E.; Houk, K. N. Controlled gating of a hemicarcerand by disulfide-dithiol interchange. *J. Org. Chem.* **2010**, *75*, 570-575.

[2] (a) Siemann, D. W.; Beyers, K. L. *In vivo* therapeutic potential of combination thiol depletion and alkylating chemotherapy. *Br. J. Cancer.* **1993**, *68*, 1071-1079. (b) Wong, D. Y.; Hsiao, Y.; Poon, C.; Kwan, P.; Chao, S.; Chou, S.; Yang, C. Glutathione concentration in oral-cancer tissues. *Cancer. Lett.* **1994**, *81*, 111-116. (c) Schnelldorfer, T.; Gansauge, S.; Gansauge, F.; Schlosser, S.; Beger, H. G.; Nussler, A. K. Glutathione depletion causes cell growth inhibition and enhanced apoptosis in pancreatic cancer cells. *Cancer*, **2000**, *89*, 1440-1447.

[3] Macromodel, version 9.1, Schrödinger, LLC, New York, NY, 2006.

[4] Cram, D. J.; Karbach, S.; Kim, H.-E.; Knobler, C. B.; Maverick, E. F.; Ericson, J. L.; Helgeson, R. C. Host-guest complexation. 46. Cavitands as open molecular vessels from solvates. *J. Am. Chem. Soc.* **1988**, *110*, 2229-2237.

[5] Chapman, R. G.; Chopra, N.; Cochien, E. D.; Sherman, J. C. Carceplex formation: scope of a remarkably efficient encapsulation reaction. *J. Am. Chem. Soc.* **1994**, *116*, 369-370.

CHAPTER 3: PHOTOCHEMICALLY-GATED HEMICARCARERANDS

3.1 Photochemically Gated Hemicarcerands

Carceplexes that can be converted to hemicarceplexes by UV radiation were reported by Deshayes and coworkers. One is shown in Figure 3.1.^[1] This host has one bridge with a nitrobenzyl ether group. Upon irradiation at 330 nm, intramolecular hydrogen transfer to the nitro and irreversible CO bond cleavage take place. This opens the gate and allows escape of the trapped guests, either dimethyl acetamide (DMA) or N-methyl-2-pyrrolidinone (NMP).

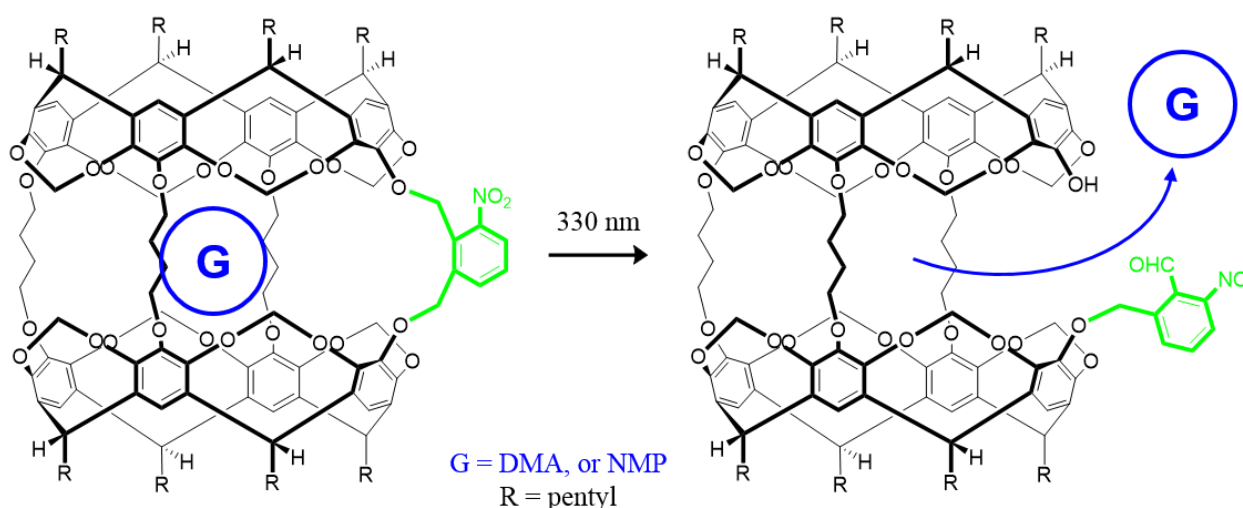


Figure 3.1 Photo-induced release of a guest molecule G from a photoactive hemicarcerand.

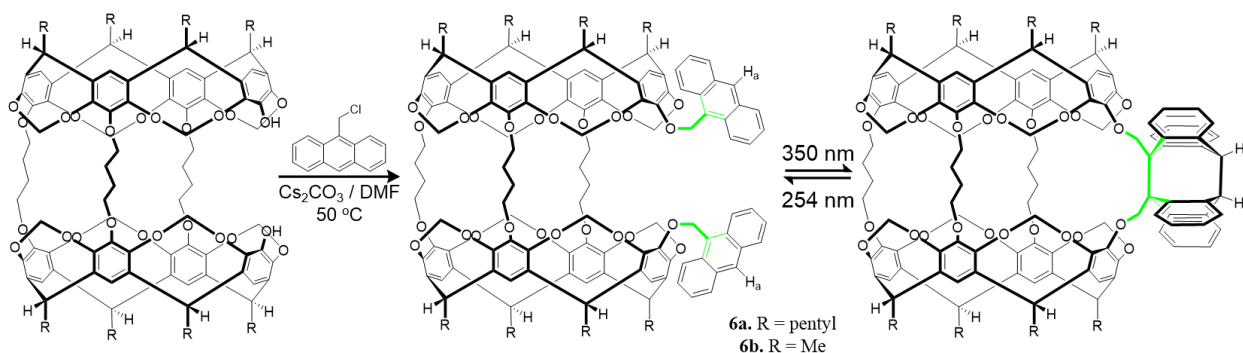
While this demonstrates the photochemical gate-opening that converts a carceplex into a hemicarceplex, we undertook the synthesis and study of a reversibly gated hemicarcerand. We designed a photoswitchable gated hemicarcerand **6a** (Figure 3.2) based on the reversible dimerization of anthracene upon irradiation.^[2] The dimerization of anthracene is known to occur

upon irradiation at relative long wavelength, while the retro-cycloaddition occurs at the shorter wavelength of 254 nm.^[3] I carried out the computational studies of these new hemicarceplexes and the gating phenomenon, while Hao Wang in our group performed the synthesis, aided by Roger Helgeson.

The synthesis of **6a** was achieved by treating the diol with 9-chloromethylantracene in DMF using cesium carbonate as the base (Scheme 3.1). Dimerization of anthracene occurs upon irradiation at 350 nm, resulting in the gate closing. Irradiation at 254 nm causes the gate to open and regenerates the bis-anthracene. The reversibility of gate-opening and closing processes of the hemicarcerand **6a** were confirmed by ¹H NMR and ¹³C NMR spectra, as well as fluorescence spectroscopy. During one cycle of alternate irradiation at 350 nm and 254 nm, the emission band of anthracene decreases in intensity and then recovers to 99% of the original level. Good reversibility was observed from successive photochemical cycles.

Scheme 3.1 Synthesis of hemicarcerands **6a** and its the reversible gate-closing and gate-opening.

The photochemical gates are colored in green.



A complexation study of hemicarcerand **6a** with 1,4-(MeO)₂C₆H₄ was monitored with ¹H NMR spectroscopy. An excess of 1,4-(MeO)₂C₆H₄ was added to a Ph₂O solution of **6a** (open

form). An upfield shift of the methyl protons on 1,4-(MeO)₂C₆H₄ was observed on the ¹H NMR spectrum of the mixture, indicating the formation of complex. When the mixture was irradiated at 350 nm for 1h, the upfield shift of methyl protons was maintained, and the disappearance of the anthracene peaks (H_a) showed that a carceplex was formed involving the gate-closed form of **6a** and the guest. The carceplex was stable indefinitely at ambient temperature without detectable release of the guest. Upon irradiation at 254 nm, a downfield shift of the methyl protons was observed along with the appearance of the anthracene resonances, which indicates the opening of the gate and release of the guest.

3.2 Computational Exploration

I studied computationally the structures of the open and closed host as well as the binding properties between the host and candidate guest molecules. The binding properties of the photochemically gated hemicarcerand **6b** with small organic molecules (shown in Figure 3.2) were studied with molecular mechanics calculations with the OPLS force field and GB/SA solvation model for chloroform. Guests **vii**, and **xii** are small drugs, metronidazole, and propofol, respectively.

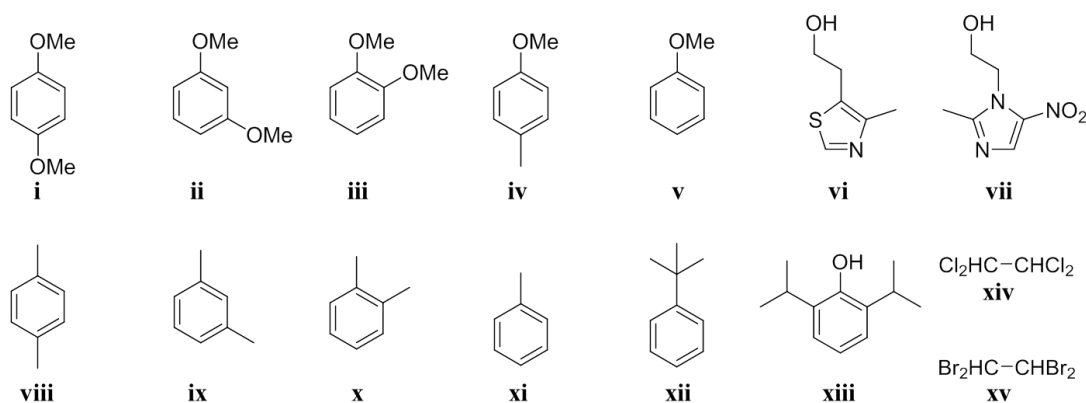


Figure 3.2 Organic molecules **i-xv** tested in complexation study.

Conformation searches were performed on isolated host **6b** and the complexes between **6b** and guest molecules to locate the global minimum conformation. For simple organic molecules, direct optimization proved to be satisfactory. Binding energy is defined as the energy difference between complex and the isolated host and guest. Both open and closed forms of host **6b** were studied.

Calculations on the isolated host showed that the two anthracene moieties in an open-state are parallel to each other, separated by a proper distance so that they are able dimerize without introducing much strain to close the gate, as shown in Figure 3.3a. The participation of solvent in complexation was also taken into consideration. By increasing the number of chloroform molecules inside the cavity, it was determined that the most stable complex between **6b** and chloroform molecules is $5 \cdot \text{CHCl}_3$, as shown in Figure 3.3b.

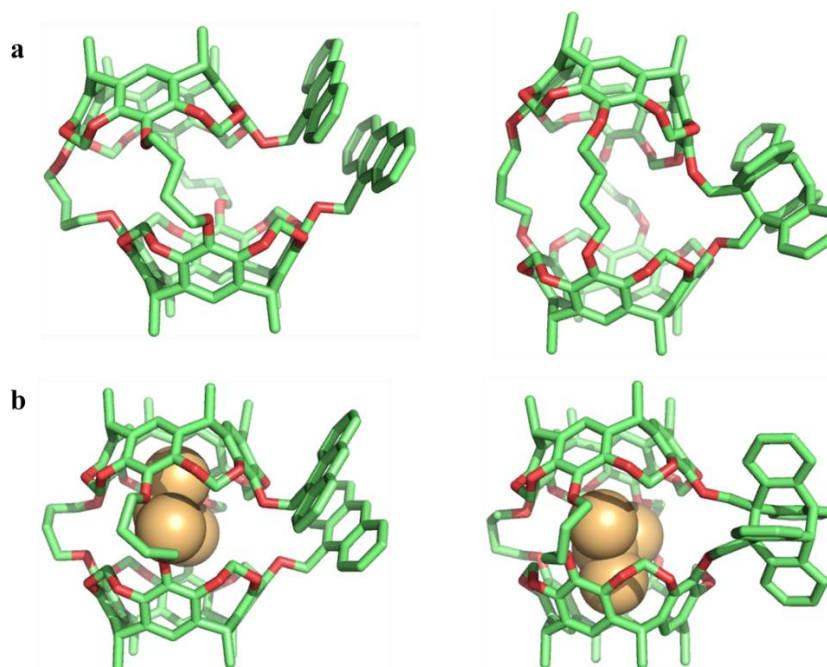


Figure 3.3 Optimized structures of isolated host and complexes between host and chloroform solvent.

Several small organic molecules were studied with molecular mechanics calculations to predict whether a stable complex could be formed with the designed hemicarcerand. Figure 3.4 shows the optimized complexes formed between *para*-dimethoxybenzene and host **6b** in both open and closed states. In both cases, the methoxy groups sit perfectly in the cavities with no obvious strain, indicating that *para*-dimethoxybenzene can form stable complexes with host **6**. This was confirmed by experimental data. The optimized structures for the remaining complexes are shown in Figure 3.5.

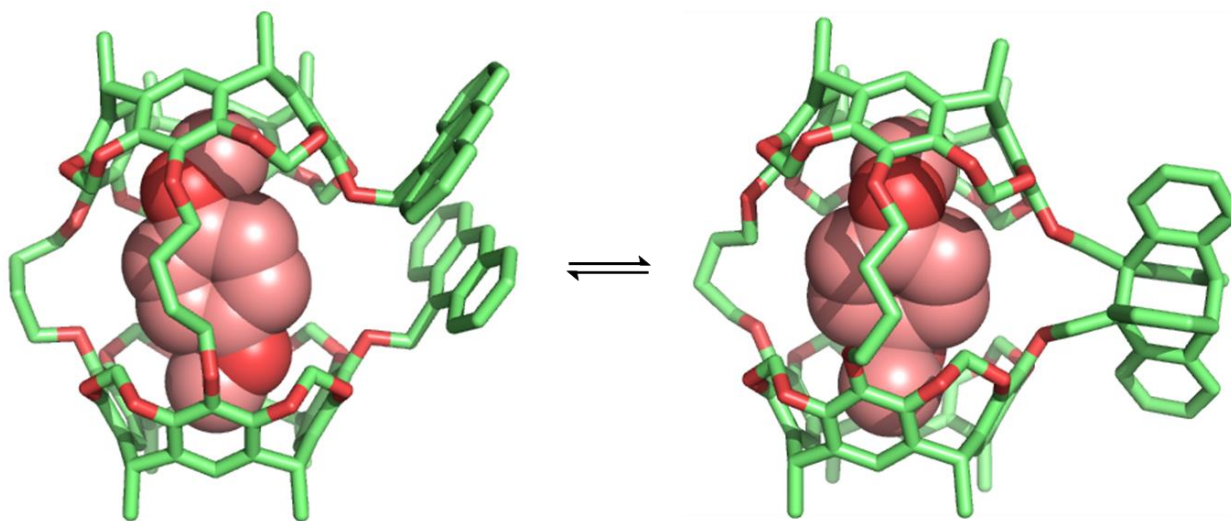


Figure 3.4 Computed structures of complexes formed between *para*-dimethoxybenzene **i** and **6b**

The complexes formed between **6b** with an open gate and guests **ii-xv** maintain the corresponding guests inside the cavity. However, the formation of some of these complexes requires significant twist of the host molecule, such as in **6b•iii**, **6b•vi**, **6b•vii**, **6b•ix**, **6b•xii**, and **6b•xiii** (Figure 3.5). In these six complexes, the gate closing resulting from the dimerization of anthracene shrinks the size of the cavity and causes the guests to exit. No complexes were observed between **6b** with a closed gate and guests **iii**, **vi**, **vii**, **ix**, **xii**, and **xiii**.

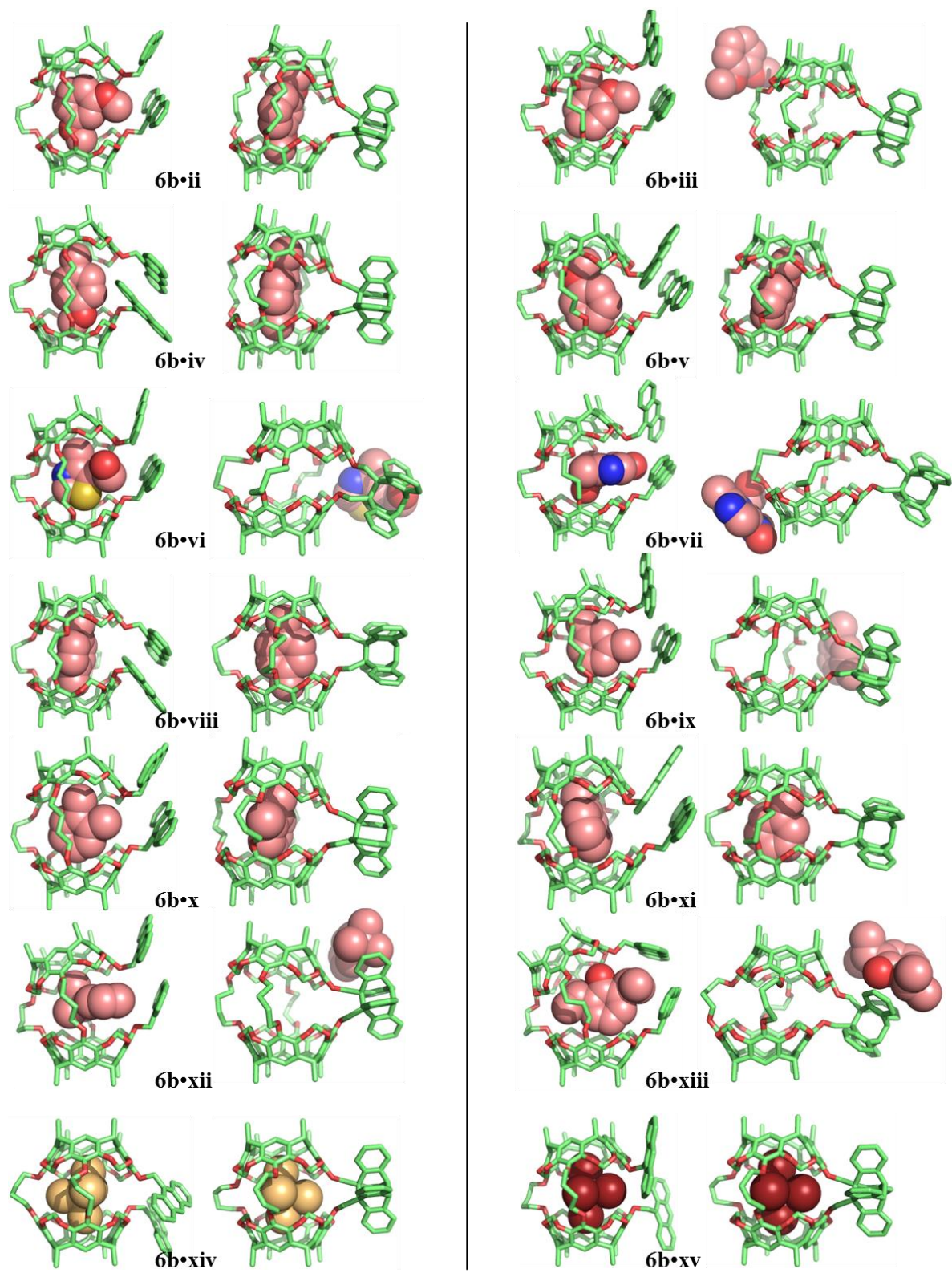


Figure 3.5 Optimized structures of complexes formed between **6b** and guests **ii-xv**.

The binding energies for all thirty complexes are shown in Table 3.1, where the binding is defined as the energy difference between complex **6b**•guest plus chloroform and **6b**•chloroform plus guest ($E_{binding} = E_{host\cdot guest} + E_{solvent} - E_{host\cdot solvent} - E_{guest}$). Most of the guests exhibit positive binding energies with **6b** in its closed form, which suggests complexation between host and solvent molecule is favored over the complexation between host and guest molecule. This prediction was confirmed by the failure to observe complexation of *para*-dimethoxybenzene **i** with **6a** in chloroform. Because of that, bulkier solvent, phenyl ether, was used as solvent for the complexation study, allowing observation of the weakly bound complex of **6a**•**i**.

Table 3.1 Computed binding energies for complexes between **6b** and guests **i**-**xv**, relative to CHCl₃ binding, in kcal/mol.

	6b_open	6b_closed		6b_open	6b_closed
i	0	15	ix	4	
ii	-3	10	x	0	7
iii	-7		xi	-3	7
iv	-2	3	xii	1	
v	-3	3	xiii	26	
vi	-5		xiv	-1	0
vii	-6		xv	-2	0
viii	-6	10			

3.3 References

- [1] Piatnitski, E. L.; Deshayes, K. D. Hemicarceplexes that release guests upon irradiation. *Angew. Chem. Int. Ed.* **1998**, *37*, 970-972.

[2] Wang, H.; Liu, F.; Helgeson, R. C.; Houk, K. N. Reversible photochemically gated transformation of a hemicarcerand to a carcerand. *Angew. Chem. Int. Ed.* **2013**, *52*, 655-659.

[3] (a) Chandross, E. A.; Dempster, C. J. Reversible intramolecular photodimerization of 1,3-bis(.alpha.-naphthyl)propane. *J. Am. Chem. Soc.* **1970**, *92*, 703-704. (b) Bouas-Laurent, H.; Castellan, A.; Desvergne, J.-P. Lapouyade, R. Photodimerization of anthracenes in fluid solution: structural aspects. *Chem. Soc. Rev.* **2000**, *29*, 43-55.

CHAPTER 4: BIOORTHOGONAL CYCLOADDITION

4.1 Introduction to Bioorthogonal Chemistry

The field of bioorthogonal chemistry emerged in the early 2000s, and the term was introduced by Carolyn Bertozzi to describe chemical reactions that occur inside living systems without interfering with natural biochemical processes.^[1] Bioorthogonal reactions have become powerful tools in the study of biomolecules in living system without introducing cellular toxicity. Figure 4.1 shows how bioorthogonal chemistry is used to study cellular processes. The first step involves modification of a cellular substrate with a bioorthogonal functional group, also called a chemical reporter. The modified substrate is then introduced into the cell to determine where the biomolecule is located in the cell. In the second step, a fluorophore probe containing a functional group that can react with the reporter is added to the system to label the biomolecule.

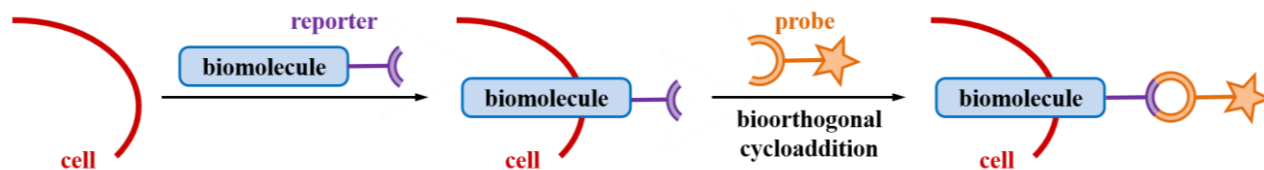


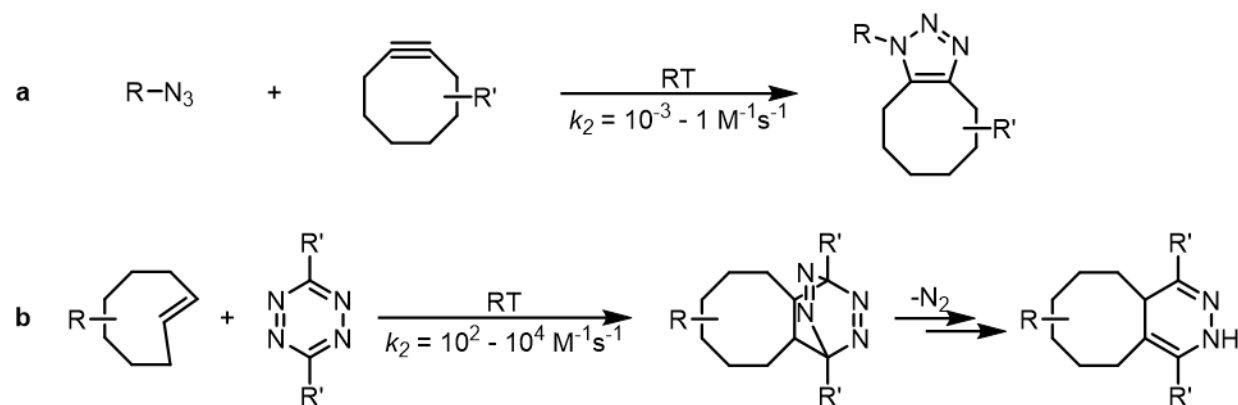
Figure 4.1 Bioorthogonal reactions.

To be considered as bioorthogonal, the functional groups in both reporter and probe should not perturb the chemistry naturally found in the cell. In addition, the cycloaddition between reporter and probe should be fast enough to allow real time labeling in living system. These requirements dictate the guidelines for the development of new reactions.

4.2 Reactivity and Orthogonality

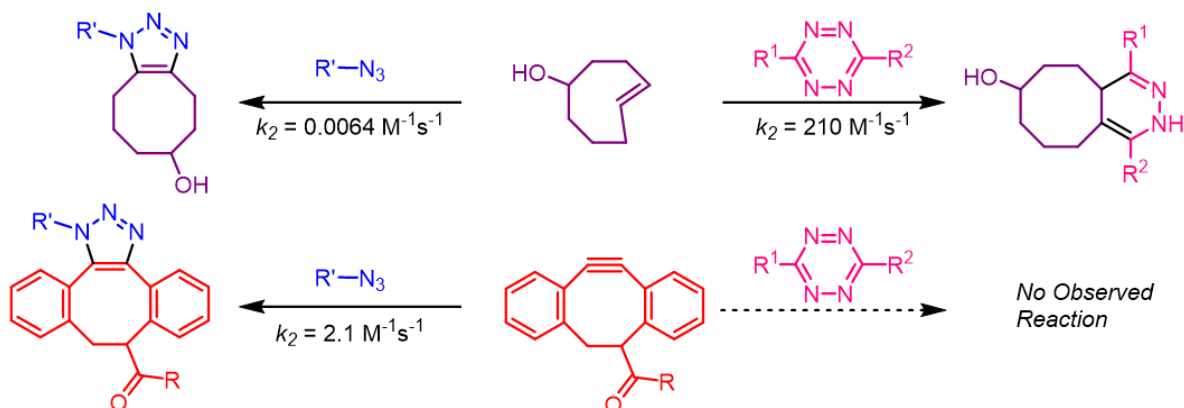
Many effective bioorthogonal reactions have been developed to enrich the toolbox of bioorthogonal chemistry. Among them, azide-cyclooctyne cycloadditions^[2] (Scheme 4.1a) and tetrazine-*trans*-cyclooctene cycloadditions^[3] (Scheme 4.1b) are widely used. Azide cycloadditions were introduced into bioorthogonal chemistry by the Bertozzi group in the early 2000s, and tetrazine cycloadditions emerged later and have received increased attention because of the rapid rates of these reactions.

Scheme 4.1 (a) Azide-cyclooctyne cycloaddition; (b) tetrazine-*trans*-cyclooctene cycloaddition



An interesting phenomenon called mutual orthogonality emerges when one pair of bioorthogonal reagents does not react with a second pair of bioorthogonal reagents. Recently, Hilderbrand and coworkers demonstrated that *trans*-cyclooctene derivatives prefer to react with tetrazines rather than azides (second-order constants measured for the former are four orders of magnitude greater than the latter). On the contrary, dibenzocyclooctyne derivatives only react with azides; while reactions between tetrazines and dibenzocyclooctyne were not observed under physiological conditions.^[4] Such mutual orthogonality is summarized in Scheme 4.2.

Scheme 4.2 Mutual orthogonality in Bioorthogonal Cycloaddition Reactions



To understand the orthogogeneity presented in Scheme 4.2, we explored the cycloaddition reactions of *trans*-cyclooctene **1** and dibenzocyclooctyne **2** with methyl azide **3** and dimethyltetrazine **4** using DFT calculations with *Gaussian 09*.^[5] Geometry optimizations of all the minima and transition states were carried out at the M06-2X level of theory with the 6-311+G(d,p) basis set,^[6] which has been found to give relatively accurate energetics for cycloadditions.^[7] The vibrational frequencies were computed at the same level to verify that optimized structures are energy minima or transition states and to evaluate zero-point vibrational energies (ZPVE) and thermal corrections at 298 K. A quasiharmonic correction was applied during the entropy calculation by setting all positive frequencies that are less than 100 cm^{-1} to 100 cm^{-1} .^[8] Solvation energies were evaluated by a self-consistent reaction field (SCRF) using the CPCM model,^[9] where UFF radii were used.

The optimized transition structures of these reactions are shown in Figure 4.2, with the forming bond distances shown in Å. The computed activation free energies in the gas phase (G_{gas}) and in water (G_{water}) and rate constants (k_2 , based on G_{water} at 298 K) are shown under each

structure, in black, blue, and red. Our results are in good agreement with the experimentally measured rate constants shown in Scheme 4.2. Rate constants are derived from Eyring equation:

$$k_{rel} = \frac{k_B T}{h} e^{\frac{G_{water} - 3.3}{RT}}$$

A constant (3.3 kcal/mol) is subtracted from the computed activation free energy in water (G_{water}) because of systematic overestimation of activation energy. This specific number is used here because it gives relatively accurate rate constants in other bioorthogonal reactions that we have studied.^[10]

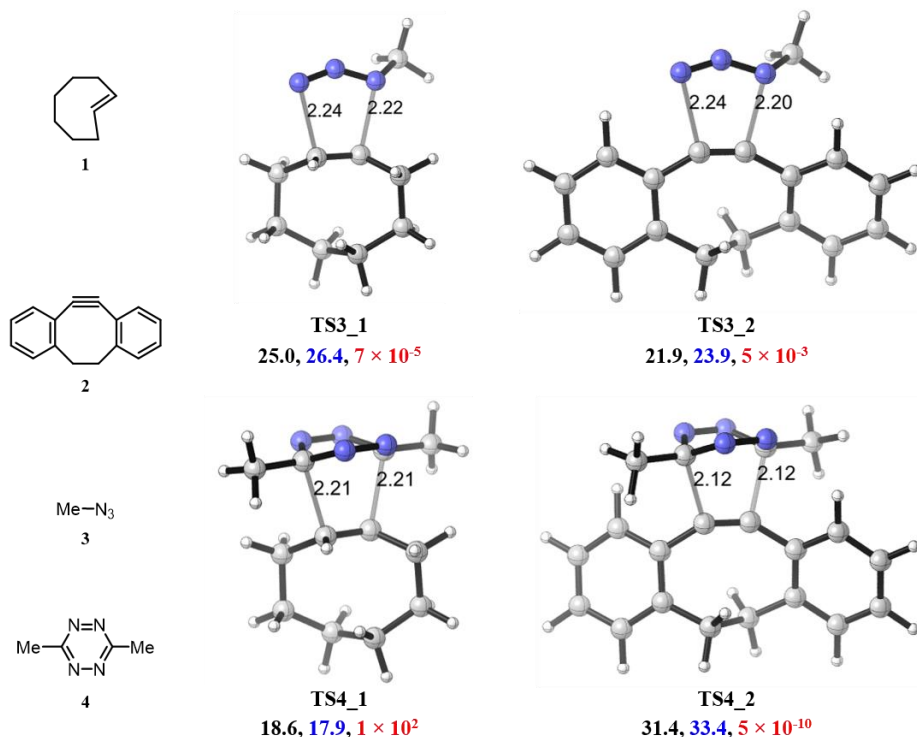


Figure 4.2 M06-2X/6-311+G(d,p)-optimized transition structures for cycloadditions with methyl azide and dimethyltetrazine. The computed activation free energies in the gas phase (G_{gas} , in kcal/mol) and in water (G_{water} , in kcal/mol) and relative rate constants (k_{rel} , in $M^{-1}s^{-1}$) are shown under each structure, in black, blue, and red.

The distortion/interaction analysis, a model developed by our group to analyze the origins of reactivities, especially in cycloaddition reactions,^[11] was applied to these reactions to determine the key factors that contribute to reactivity and orthogonality. The distortion/interaction model is illustrated in Figure 4.3 on the left, with the Diels-Alder reaction between butadiene and ethylene as an example. The solid black curve in Figure 4.3 represents the potential energy along the reaction coordinate for the corresponding reaction. The transition structure is separated into two fragments (distorted butadiene and distorted ethylene), followed by single-point energy calculations on each fragment. The energy difference between the distorted structures and optimized ground-state structures is the distortion energy. The distortion energy of diene ($\Delta E_{dist_4e}^\ddagger$) and dienophile ($\Delta E_{dist_2e}^\ddagger$) can be determined separately. The difference between activation energy (ΔE_{act}^\ddagger) and total distortion energy ($\Delta E_{dist}^\ddagger = \Delta E_{dist_4e}^\ddagger + \Delta E_{dist_2e}^\ddagger$) is the interaction energy (ΔE_{int}^\ddagger).

The relationship between activation, distortion, and interaction energies is shown on the right of Figure 4.3. The lengths of green arrow and blue arrow represent the distortion energy of dienophile ($\Delta E_{dist_2e}^\ddagger$) and distortion energy of diene ($\Delta E_{dist_4e}^\ddagger$), respectively. The total length of green and blue arrows equals the total distortion energy (ΔE_{dist}^\ddagger). The red arrow pointing down starting from the value of total distortion energy represents the interaction energy (ΔE_{int}^\ddagger), which is usually a negative number. The activation energy (ΔE_{act}^\ddagger), represented by a black arrow, is the sum of distortion and interaction energies. The distortion/interaction analyses for cycloaddition reactions of *trans*-cyclooctene **1** and dibenzocyclooctyne **2** with methyl azide **3** and dimethyltetrazine **4** are shown in Figure 4.4.

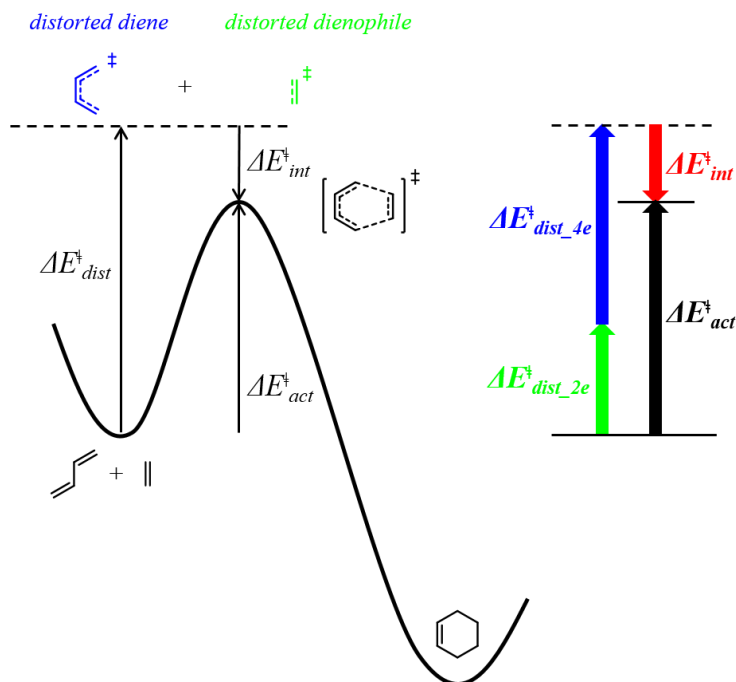


Figure 4.3. Distortion/interaction model.

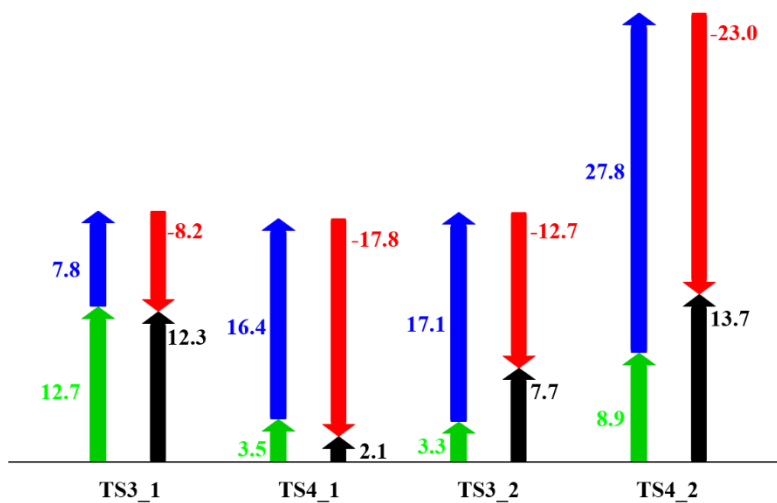


Figure 4.4. Graph of distortion, interaction, and activation energies for reactions of *trans*-cyclooctene **1** and dibenzocyclooctyne **2** with methyl azide **3** and dimethyltetrazine **4** (green: distortion energy of dienophile, blue: distortion energy of diene, red: interaction energy, black: activation energy, in kcal/mol).

With respect to a certain dienophile or dipolarophile, dimethyltetrazine has stronger interaction energies than methyl azide: the differences are about 10 kcal/mol. This large difference in the interaction energies results from the different electronic properties of tetrazines and azides. Frontier Molecular Orbital analysis indicated that the preferred orbital interaction is between the HOMO of *trans*-cyclooctene or dibenzocyclooctyne and the LUMO of methyl azide or a relevant π^* orbital of dimethyltetrazine (Figure 4.5).

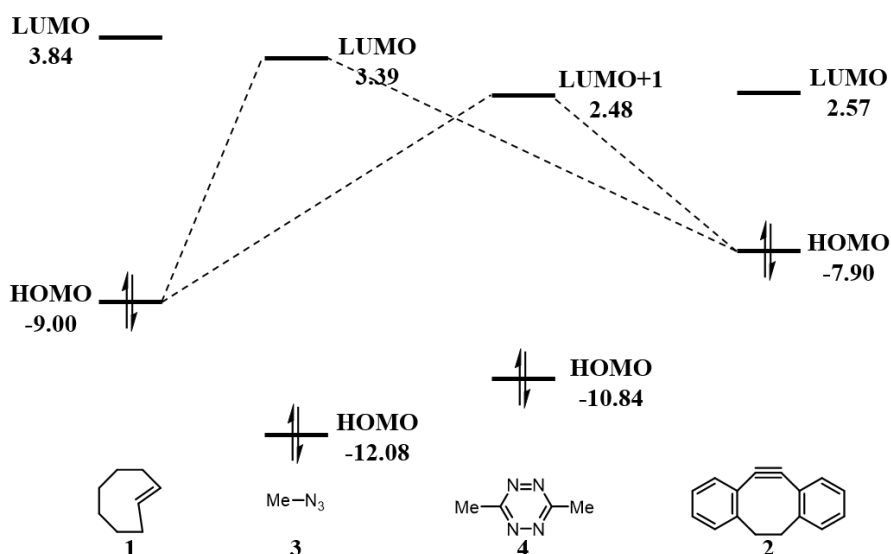


Figure 4.5 FMO diagram for the cycloadditions of *trans*-cyclooctene and dibenzocyclooctyne with methyl azide and dimethyltetrazine. HF//M06-2X/6-311+G(d,p)-computed orbital energies are shown in eV.

Note from the diagram that azide is a much weaker electron acceptor compared with tetrazine, because of its higher LUMO energy. The smaller orbital energy gap between tetrazine LUMO+1 and *trans*-cyclooctyne or dibenzocyclooctyne HOMO is responsible for its stronger interactions presented in Figure 4.4. The distortion energies in cycloadditions of *trans*-cyclooctene with methyl azide and dimethyltetrazine are very close (20.5 and 19.9 kcal/mol,

respectively). Therefore, tetrazines are more reactive than azides in the cycloaddition reactions with *trans*-cyclooctenes, due to greater intrinsic electrophilicities of tetrazines.

However, in the cycloadditions of dibenzocyclooctyne, the advantage of tetrazine over azide in the interaction energy (-23.0 versus -12.7 kcal/mol) is overcome by the extremely high distortion energy (36.7 versus 20.4 kcal/mol), resulting in a higher activation energy (13.7 versus 7.7 kcal/mol). The high distortion energy in the reactions between dibenzocyclooctyne and dimethyltetrazine is due to the steric effect that is illustrated in Figure 4.6 with space-filling models. The steric repulsion between the methyl hydrogen atoms of tetrazine and the *ortho* hydrogen atoms of the aromatic rings of dibenzocyclooctyne forces the tetrazine to tilt away from the orientation that allows perfect orbital overlap between diene and dienophile. The tetrazine has to distort more to compensate for the poor orbital overlap, leading to a high distortion energy.

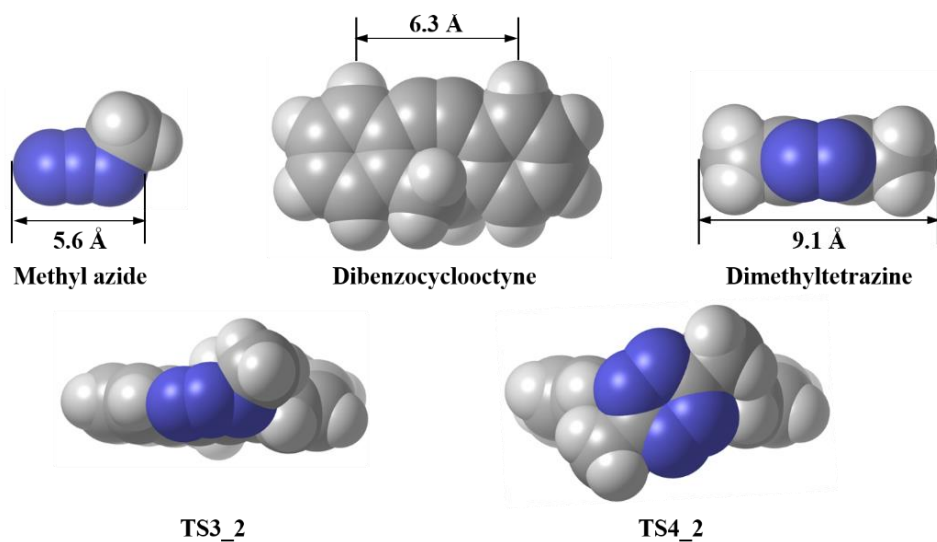


Figure 4.6 Space-filling models of, methyl azide, dibenzocyclooctyne, dimethyltetrazine, and transition states **TS3_2** and **TS4_2** (distances in Å).

4.3 Developing New Bioorthogonal Reagents

Mutual orthogonal reaction pairs are useful in labeling multiple biomolecules in living systems (Figure 4.7). Reporters **a** and **b** are introduced into the cell to label different biomolecules, for example two different sugars; subsequently, probes **c** and **d** are added in succession. Probe **c** selectively reacts with reporter **a**; while probe **d** only reacts with reporter **b** (alternatively, probe **d** can be less selective between reporters **a** and **b** – since **a** has been consumed by probe **c**, **d** can only react with **b**). Therefore, biomolecules **1** and **2** can be simultaneously labeled and studied.

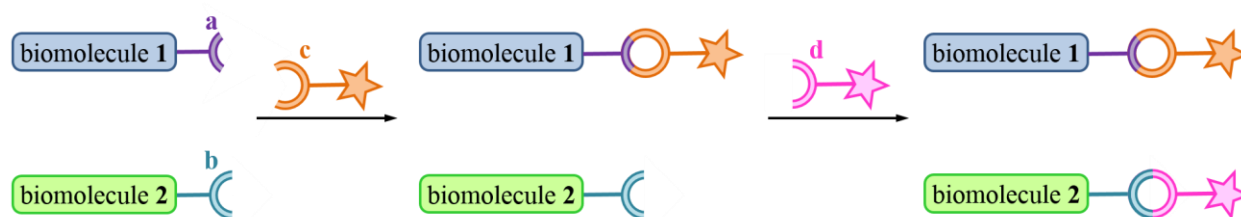


Figure 4.7 Schematic of mutual orthogonality to label two different biomolecules.

Although cycloaddition reactions, especially the 1,3-dipolar (3+2) cycloaddition and the Diels-Alder (4+2) cycloaddition, are widely utilized in various chemical transformations, only a small subcategory of cycloadditions is suitable for modification of biomolecules that typically proceed in water and at ambient temperature. For known bioorthogonal reagents, stabilities in water and the tolerance of biological functionality have been demonstrated by experiments in the literature.^[12] The key to the discovery of new reactions and orthogonality of reaction pairs is to obtain the information about the cycloaddition reactivity and selectivity. We applied the same computational approach to understand the orthogonality and to design new orthogonal reaction pairs.

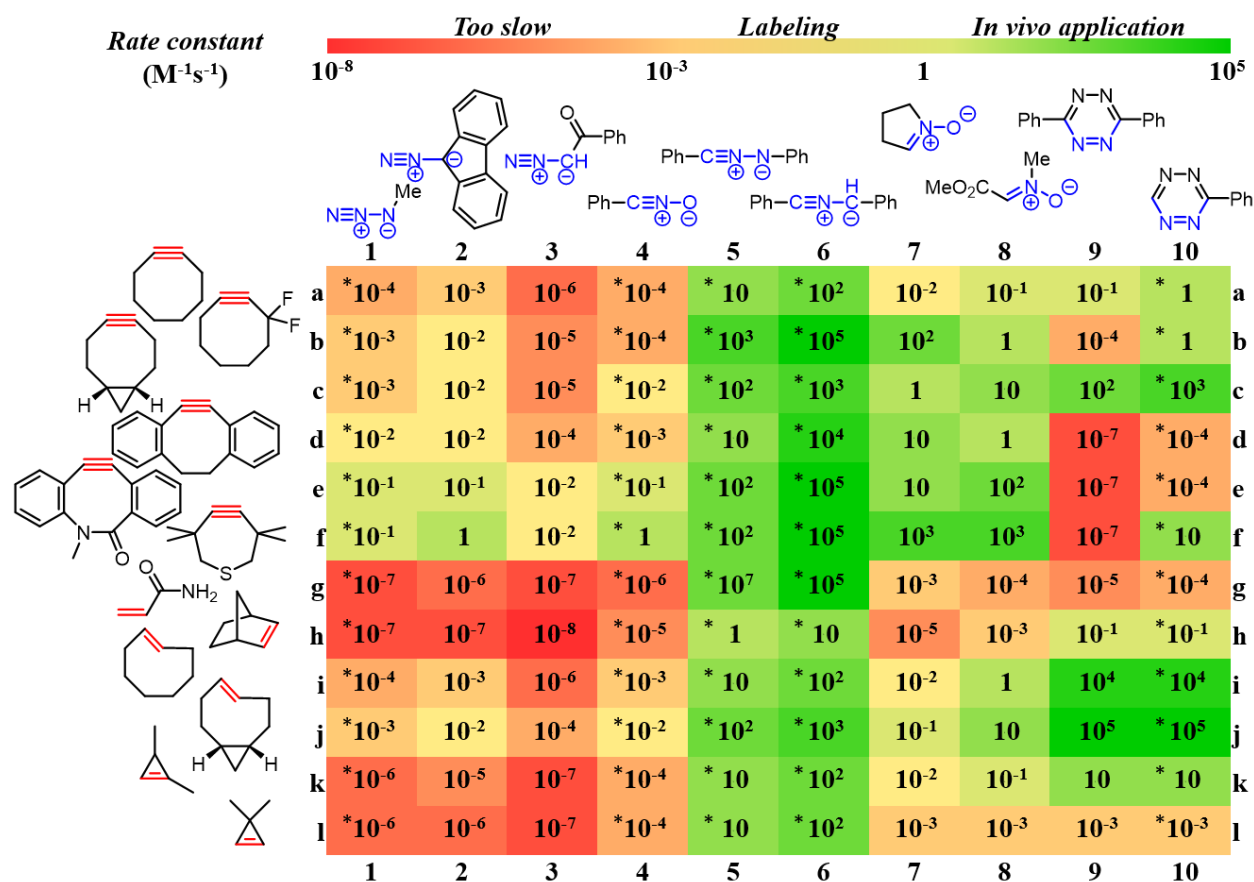


Figure 4.8 Color-coded matrix of rate constants (in $M^{-1} s^{-1}$) for 120 cycloadditions in water to predict reactivity and orthogonality. The activation free energies that were used to predict these rates were computed at the CPCM(water)-M06-2X/6-311+G(d,p)//M06-2X/6-31G(d) level. Calculations done by other group members are marked with *. The meaning of the color code is given at the top.

As shown in Figure 4.8, twenty two bioorthogonal cycloaddition reagents were chosen from the literature and divided into 4π components (1,3-dipoles and dienes) and 2π components (alkenes and alkynes). All these components form a 10×12 matrix of possible bioorthogonal cycloadditions. The rate constants (k_{compt} , based on G_{water} at 298 K) calculated for each reaction are shown in the matrix in Figure 4.8, in $M^{-1} s^{-1}$. To make it easier to follow, the matrix is color-

coded to show the reactivity of each reaction directly. Red shades mean that the corresponding cycloaddition is very slow at room temperature, while yellow indicates that the reactions may be employed as bioorthogonal cycloadditions with moderate rate constants, primarily for labeling and static imaging applications. Green stands for extremely fast cycloadditions, that can be used *in vivo* to track biological processes even at low concentrations of reactants.

Among these 120 cycloadditions, about 30 reactions have been investigated experimentally. It is found that the observed rate constants for these reaction are within one order of magnitude with those calculated from our activation free energies. For instance, Wang's group recently reported that the reaction of cyclooctyne with 3,6-diphenyltetrazine has a rate constant of $0.070 \pm 0.007 \text{ M}^{-1}\text{s}^{-1}$,^[30] which is quantitatively comparable to the predicted one of $0.1 \text{ M}^{-1}\text{s}^{-1}$. The widely investigated azide cycloadditions with cyclooctyne, dibenzocyclooctyne, and 3,3,6,6-tetramethylthiacyclo-4-heptyne exhibit cycloaddition rates with azides at increasing rates along this series: experimental rate constants are 1.2×10^{-3} , 0.12, and $4.0 \text{ M}^{-1}\text{s}^{-1}$, respectively. Calculations predict 10^{-4} , 10^{-2} , $10^{-1} \text{ M}^{-1}\text{s}^{-1}$; all are just one order of magnitude lower than experiments.

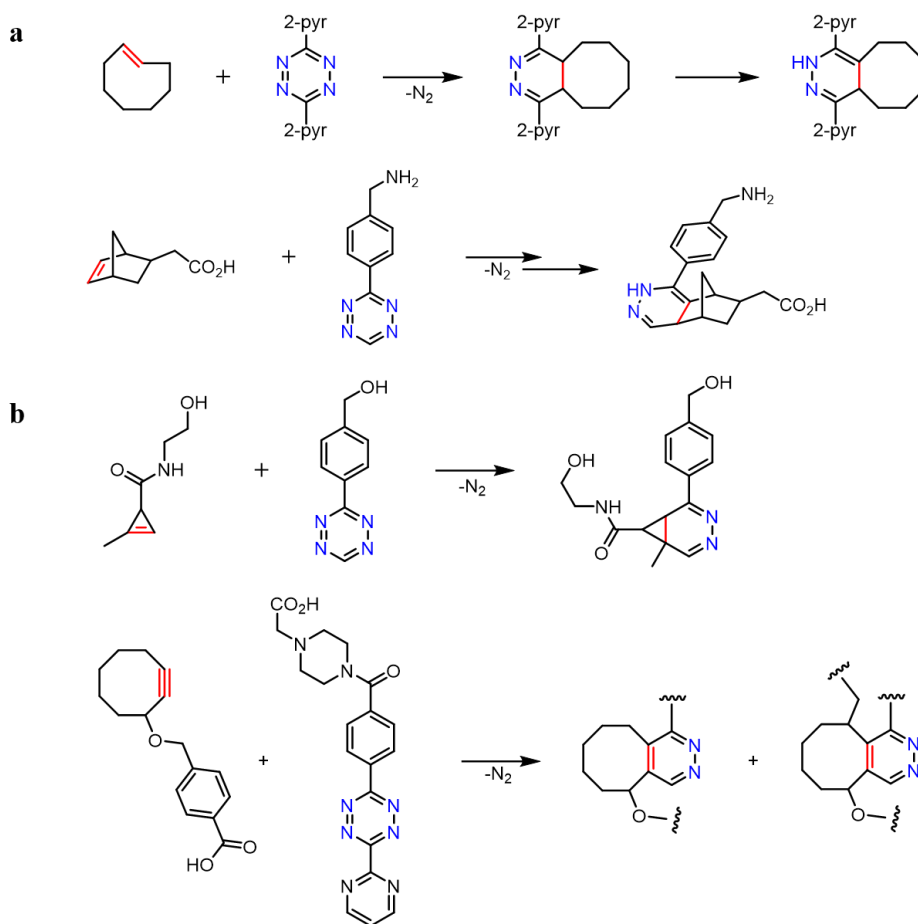
In addition to unveiling additional useful bioorthogonal cycloadditions between two known reagents, this matrix also provides a guide for the discovery of new orthogonal cycloaddition pairs. For azide cycloadditions, the reactivity of 3,3,6,6-tetramethylthiacycloheptyne is much higher than that of 1,3-dimethylcyclopropene, while in the 3,6-disubstituted tetrazine cycloadditions, these reactivity patterns are reversed. Therefore, these two bioorthogonal reaction pairs are mutually orthogonal. There are also several new orthogonal pairs involving nitrile oxides, nitrones, and monosubstituted tetrazines. This provides more

opportunities for designing sequential or simultaneous cycloadditions to monitor multiple biomolecules in biological environments.

4.4 Tetrazines in Bioorthogonal Cycloaddition

Among the reported bioorthogonal cycloaddition reagents, tetrazines have received increased attention since Fox and Hilderbrand reported the use of tetrazine-based cycloadditions in live cell imaging in 2008.^[3] In these pioneering studies, Fox and Hilderbrand reported that strained alkenes such as *trans*-cyclooctene and norbornene undergo rapid reactions as dienophiles in Diels-Alder cycloaddition reactions with tetrazines (Scheme 4.3a).

Scheme 4.3 Cycloadditions of tetrazines with strained alkenes



Later, cyclopropenes^[13] and cyclooctynes^[14] were explored as dienophiles with tetrazines (Scheme 4.3b), adding an extra dimension to strain-promoted, or as we have identified, distortion-promoted,^[15] cycloadditions in bioorthogonal chemistry. The following chapters (Chapter 5-7) explore the Diels-Alder reactivities of tetrazines in detail.

4.5 References

[1] (a) Prescher, J. A.; Dube, D. H.; Bertozzi, C. R. Chemical remodelling of cell surfaces in living animals. *Nature* **2004**, *430*, 873–877. (b) Prescher, J. A.; Bertozzi, C. R. Chemistry in living systems. *Nature Chem. Biol.* **2005**, *1*, 13-21. (c) Sletten, E. M.; Bertozzi, C. R. Bioorthogonal chemistry: fishing for selectivity in a sea of functionality. *Angew. Chem. Int. Ed.* **2009**, *48*, 6974–6998. (d) Bertozzi, C. R. A decade of bioorthogonal chemistry. *Acc. Chem. Res.* **2011**, *44*, 651-653.

[2] (a) Agard, N. J.; Prescher, J. A.; Bertozzi, C. R. A strain-promoted [3+2] azide-alkyne cycloaddition for covalent modification of biomolecules in living systems. *J. Am. Chem. Soc.* **2004**, *126*, 15046-15047. (b) Baskin, J. M.; Prescher, J. A.; Laughlin, S. T.; Agard, N. J.; Chang, P. V.; Miller, I. A.; Lo, A.; Codelli, J. A.; Bertozzi, C. R. Copper-free click chemistry for dynamic *in vivo* imaging. *Proc. Natl. Acad. Sci. USA* **2007**, *104*, 16793-16797.

[3] (a) Blackman, M. L.; Royzen, M.; Fox, J. M. Tetrazine ligation: fast bioconjugation based on inverse-electron-demand Diels-Alder reactivity. *J. Am. Chem. Soc.* **2008**, *130*, 13518-13519. (b) Devaraj, N. K.; Weissleder, R.; Hilderbrand, S. A. Tetrazine-based cycloadditions: application to pretargeted live cell imaging. *Bioconjugate Chem.* **2008**, *19*, 2297-2299.

- [4] Karver, M. R.; Weissleder, R.; Hilderbrand, S. A. Bioorthogonal reaction pairs enable simultaneous, selective, multi-target imaging. *Angew. Chem. Int. Ed.* **2012**, *51*, 920-922.
- [5] Frisch, M. J.; et al. *Gaussian 09*, revision C.01; Gaussian, Inc.: Wallingford, CT, 2010.
- [6] (a) Zhao, Y.; Truhlar, D. G. The M06 suite of density functionals for main group thermochemistry, thermochemical kinetics, noncovalent interactions, excited states, and transition elements: two new functionals and systematic testing of four M06-class functionals and 12 other functionals. *Theor. Chem. Acc.* **2008**, *120*, 215-241. (b) Zhao, Y.; Truhlar, D. G. Density functionals with broad applicability in chemistry. *Acc. Chem. Res.* **2008**, *41*, 157-167.
- [7] (a) Paton, R. S.; Mackey, J. L.; Kim, W. H.; Lee, J. H.; Danishefsky, S. J.; Houk, K. N. Origins of stereoselectivity in the *trans* Diels–Alder paradigm. *J. Am. Chem. Soc.* **2010**, *132*, 9335-9340. (b) Lan, Y.; Zou, L.; Cao, Y.; Houk, K. N. Computational methods to calculate accurate activation and reaction energies of 1,3-dipolar cycloadditions of 24 1,3-dipoles. *J. Phys. Chem. A* **2011**, *115*, 13906-13920.
- [8] (a) Zhao, Y.; Truhlar, D. G. Computational characterization and modeling of buckyball tweezers: density functional study of concave–convex $\pi \cdots \pi$ interactions. *Phys. Chem. Chem. Phys.* **2008**, *10*, 2813-2818. (b) Ribeiro, R. F.; Marenich, A. V.; Cramer, C. J.; Truhlar, D. G. Use of solution-phase vibrational frequencies in continuum models for the free energy of solvation. *J. Phys. Chem. B* **2011**, *115*, 14556-14562.
- [9] (a) Barone, V.; Cossi, M. Quantum calculation of molecular energies and energy gradients in solution by a conductor solvent model. *J. Phys. Chem. A* **1998**, *102*, 1995-2001. (b) Cossi, M.;

Rega, N.; Scalmani, G.; Barone, V. Energies, structures, and electronic properties of molecules in solution with the C-PCM solvation model. *J. Comput. Chem.* **2003**, *24*, 669-681.

[10] We used experimentally measured rate constants to calibrate our calculations. Experimental data are obtained from reference [3] and the following: (a) Baskin, J. M.; Prescher, J. A.; Laughlin, S. T.; Agard, N. J.; Chang, P. V. Miller, I. A.; Lo, A.; Codelli, J. A.; Bertozzi, C. R. Copper-free click chemistry for dynamic in vivo imaging. *Proc. Natl. Acad. Sci. U.S.A.* **2007**, *104*, 16793-16797. (b) Codelli, J. A.; Baskin, J. M.; Agard, N. J.; Bertozzi, C. R. Second-generation difluorinated cyclooctynes for copper-free click chemistry. *J. Am. Chem. Soc.* **2008**, *130*, 11486-11493. (c) Jewett, J. C.; Sletten, E. M.; Bertozzi, C. R. Cu-free click chemistry with readily synthesized biarylazacyclooctynones. *J. Am. Chem. Soc.* **2010**, *132*, 3688-3690. (d) Dommerholt, J.; Schmidt, S.; Temming, R.; Hendriks, L. J. A.; Rutjes, F. P. J. T.; van Hest, J. C. M.; Leferber, D. J.; Friedl, P.; van Delft, F. L. Readily accessible bicyclononynes for bioorthogonal labeling and three-dimensional imaging of living cells. *Angew. Chem. Int. Ed.* **2010**, *49*, 9422-9425. We are preparing a manuscript on this work, where the calibration with experimental data will be discussed in detail.

[11] (a) Nagase, S.; Morokuma, K. An ab initio molecular orbital study of organic reaction. The energy, charge, and spin decomposition analyses at the transition state along the reaction pathway. *J. Am. Chem. Soc.* **1978**, *100*, 1666-1672. (b) Strozier, R. W.; Caramella, P.; Houk, K. N. Influence of molecular distortion upon reactivity and stereochemistry in nucleophilic addition to acetylenes. *J. Am. Chem. Soc.* **1979**, *101*, 1340-1343. (c) Diefenbach, A.; Bickelhaupt, F. M. Activation of H-H, C-H, C-C, and C-Cl bonds by Pd(0). Insight from the activation strain model. *J. Phys. Chem.* **2004**, *108*, 8460-8466. (d) Ess, D. H.; Houk, K. N. Distortion/interaction energy

control of 1,3-dipolar cycloaddition reactivity. *J. Am. Chem. Soc.* **2007**, *129*, 10646-10647. (e) Ess, D. H.; Houk, K. N. Theory of 1,3-dipolar cycloadditions: distortion/interaction and frontier molecular orbital models. *J. Am. Chem. Soc.* **2008**, *130*, 10187-10198.

[12] (a) Lang, K.; Chin, J. W. Bioorthogonal reactions for labeling proteins. *ACS Chem. Biol.* **2014**, *9*, 16-20. (b) Patterson, D. M.; Nazarova, L. A.; Prescher, J. A. Finding the right (bioorthogonal) chemistry. *ACS Chem. Biol.* **2014**, *9*, 592-605.

[13] (a) Patterson, D. M.; Nazarova, L. A.; Xie, B.; Kamber, D. N.; Prescher, J. A. Functionalized cyclopropenes as bioorthogonal chemical reporters. *J. Am. Chem. Soc.* **2012**, *134*, 18638-18643. (b) Yang, J.; Seckute, J.; Cole, C. M.; Devaraj, N. K. Live-cell imaging of cyclopropene tags with fluorogenic tetrazine cycloadditions. *Angew. Chem. Int. Ed.* **2012**, *51*, 7476-7479.

[14] Thomas, J. D.; Cui, H.; North, P. J.; Hofer, T.; Rader, C.; Burke, T. R. Jr. Application of strain-promoted azide-alkyne cycloaddition and tetrazine ligation to targeted Fc-drug conjugates. *Bioconjugate Chem.* **2012**, *23*, 2007-2013.

[15] Liu, F.; Paton, R. S.; Kim, S.; Liang, Y.; Houk, K. N. Diels-Alder reactivities of strained and unstrained cycloalkenes with normal and inverse-electron-demand dienes: activation barriers and distortion/interaction analysis. *J. Am. Chem. Soc.* **2013**, *135*, 15642-15649.

CHAPTER 5: DIELS-ALDER REACTIVITIES OF TETRAZINES

5.1 Introduction to Tetrazine Diels-Alder Reactions

Introduction

Diels-Alder reactions of tetrazines have received increased attention in bioorthogonal chemistry since Fox and Hilderbrand reported the use of tetrazine-based cycloadditions in live cell imaging in 2008.^[1,2] In these pioneering studies, strained alkenes such as *trans*-cyclooctene and norbornene were found to undergo rapid reactions as dienophiles in Diels-Alder cycloaddition reactions with tetrazines. Later, cyclopropenes^[3,4], cyclobutene derivative,^[5] and cyclooctynes^[6] were explored as dienophiles with tetrazines, adding an extra dimension to strain-promoted, or as we have identified, distortion-promoted,^[7] cycloadditions in bioorthogonal chemistry. Figure 5.1 shows the general approach used in living cell labeling. Firstly, a reporter, the strained alkene or alkyne that binds specifically to the target biomolecule, is introduced into the system. A fluorophore-tetrazine probe is then added to the biological medium, and the fast cycloaddition between reporter and probe produces a labeled biomolecule whose location can be determined by imaging of the live cell.

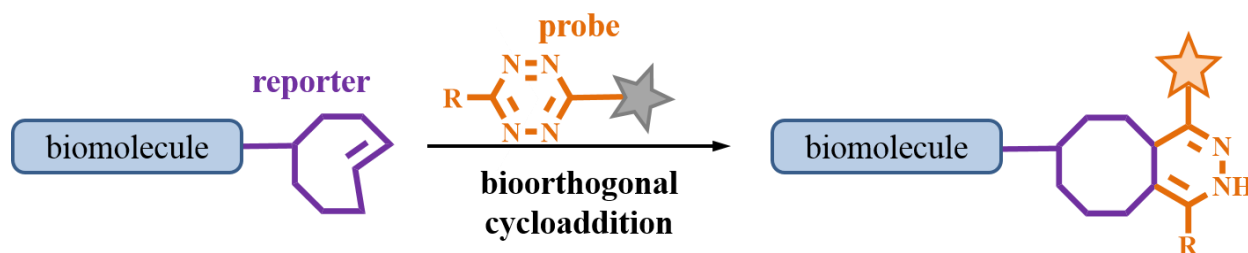
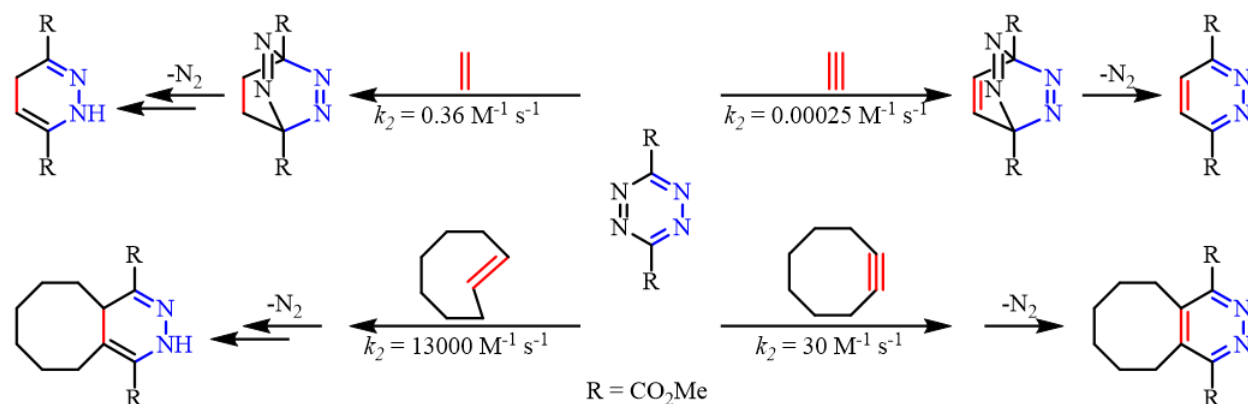


Figure 5.1 Bioorthogonal cycloaddition.

Tetrazine cycloadditions are not limited to bioorthogonal chemistry. These cycloaddition reactions have also been used in syntheses of natural products,^[8] modification of metal-organic frameworks,^[9] and functionalization of carbon nanotubes.^[10] In fact, the Diels-Alder reactions of tetrazines are venerable processes that have been studied in detail by Sauer's group and others over the last four decades.^[11,12] Sauer reported kinetic measurements of cycloaddition reactions of tetrazines with a series of dienophiles. Along with a more comprehensive exploration of substituents, his studies identified significant differences in rate constants between strained and unstrained alkenes and alkynes.^[11c]

Scheme 5.1 Rate constants of Diels-Alder cycloadditions of tetrazines with strained and unstrained alkenes and alkynes.^[11c]



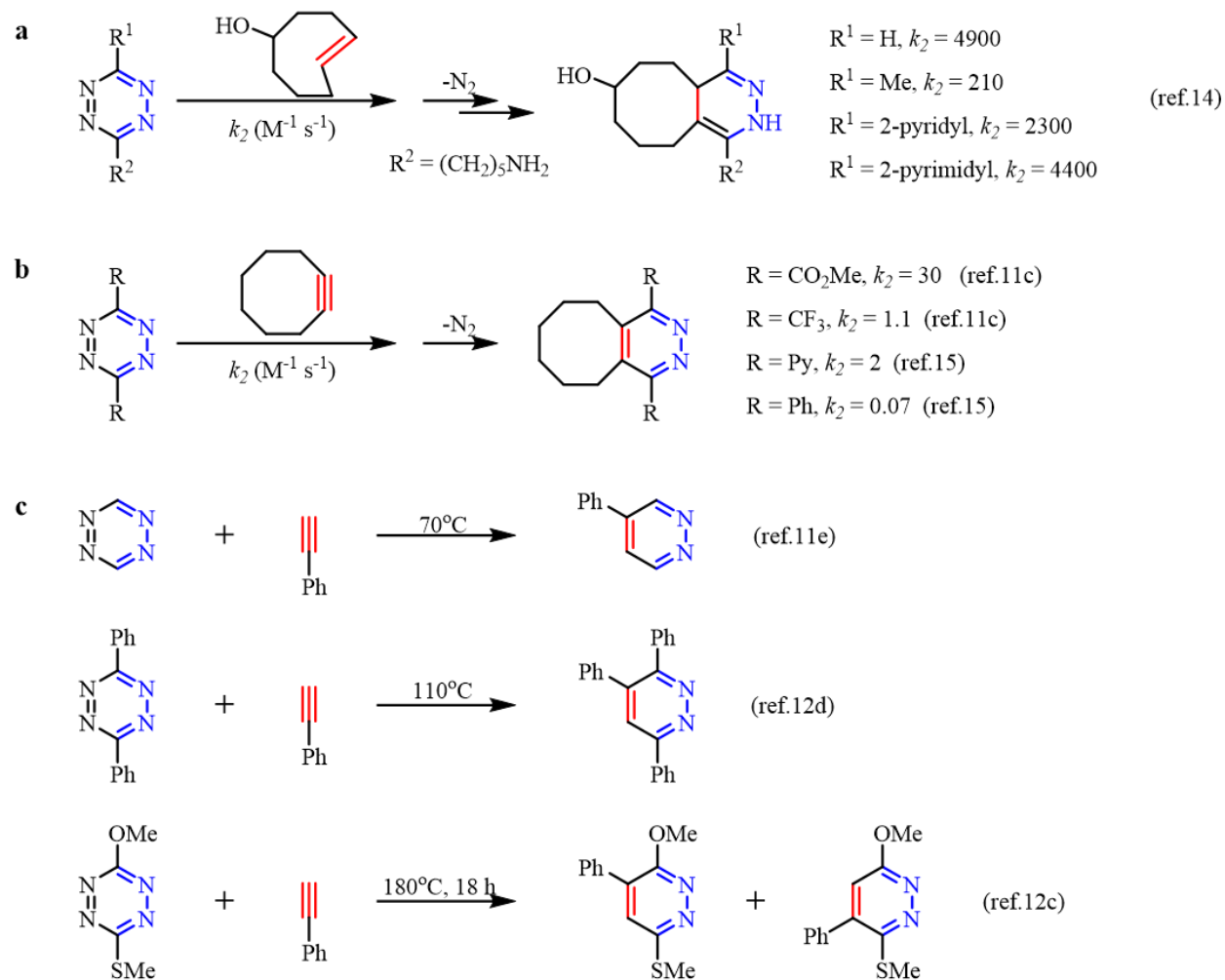
Scheme 5.1 shows the second order rate constants measured experimentally by Sauer et al. for the cycloaddition reactions between dimethyl 1,2,4,5-tetrazine-3,6-dicarboxylate and acetylene, ethylene, cyclooctyne, and *trans*-cyclooctene.^[11c] The rate constants measured with strained dienophiles (cyclooctyne and *trans*-cyclooctene) are about five orders of magnitude greater than the rate constants of unstrained dienophiles (acetylene and ethylene). In addition, the

reactions of alkenes with tetrazine are about 1000 times faster than alkynes. The origin of such striking differences has not been explored previously but are explored here.

The strained dienophiles obviously react faster than unstrained ones, but we have shown previously that this is related to distortion energy differences, not strain release differences.^[7] In the examples in Scheme 1, the reactivity difference between *trans*-cyclooctene and cyclooctyne is not explained by strain release. Conversion of cyclooctyne to *cis*-cyclooctene is 7 kcal/mol more exothermic than conversion of *trans*-cyclooctene to cyclooctane,^[13] yet *trans*-cyclooctene is 10³ more reactive than cyclooctyne. We have undertaken a theoretical investigation of the Diels-Alder reactivities of strained and unstrained alkenes and alkynes and report here the origins of these reactivity differences, as well as those controlled by tetrazine substituents.

There have been many experimental studies of substituent effects of tetrazine cycloadditions. Hilderbrand reported reaction rates for a series of 1,2,4,5-tetrazines in cycloaddition reactions with *trans*-cyclooctenol for bioorthogonal conjugation.^[14] Their study showed that methyl-substituted tetrazines are much less reactive than pyridyl- or pyrimidyl-substituted tetrazines (Scheme 5.2a). The studies of reactions of substituted tetrazines with cyclooctyne showed that trifluoromethyl tetrazine is more reactive than phenyl or pyridyl tetrazines (Scheme 5.2b).^[11c,15] Tetrazines substituted with electron-donor groups are the least reactive species in the tetrazine family. Scheme 5.2c shows a comparison between the parent tetrazine, 3,6-diphenyltetrazine, and 3-methoxy-6-(methylthio)-1,2,4,5-tetrazine. Tetrazine itself reacts with phenylacetylene at 70°C,^[11e] the reaction of diphenyltetrazine and requires higher temperature of 110°C,^[12d] while the reaction between 3-methoxy-6-(methylthio)-1,2,4,5-tetrazine and phenylacetylene occurs only at 180°C.^[12c]

Scheme 5.2 Diels-Alder reactions of substituted tetrazines.



It is well known that tetrazines undergoes inverse-electron-demand Diels-Alder reactions with alkenes or alkynes. Figure 5.2 shows the π orbitals of acetylene (left), the parent tetrazine (middle), and ethylene (right). Because tetrazine is an electron-deficient diene with low-lying vacant orbitals, the interaction between the LUMO+1 (the π^* orbital involved in the Diels-Alder reaction) of tetrazine and HOMO of acetylene or ethylene is a key factor that influences the interaction energy in the Diels-Alder reaction. The LUMO+1 energy of tetrazine is further lowered by an electron-withdrawing substituent, resulting in a decrease in HOMO-LUMO+1 gap,

and an increase in reactivity. On the contrary, electron-donating groups raise LUMO+1 and reduce the reactivity of tetrazine in Diels-Alder reactions.

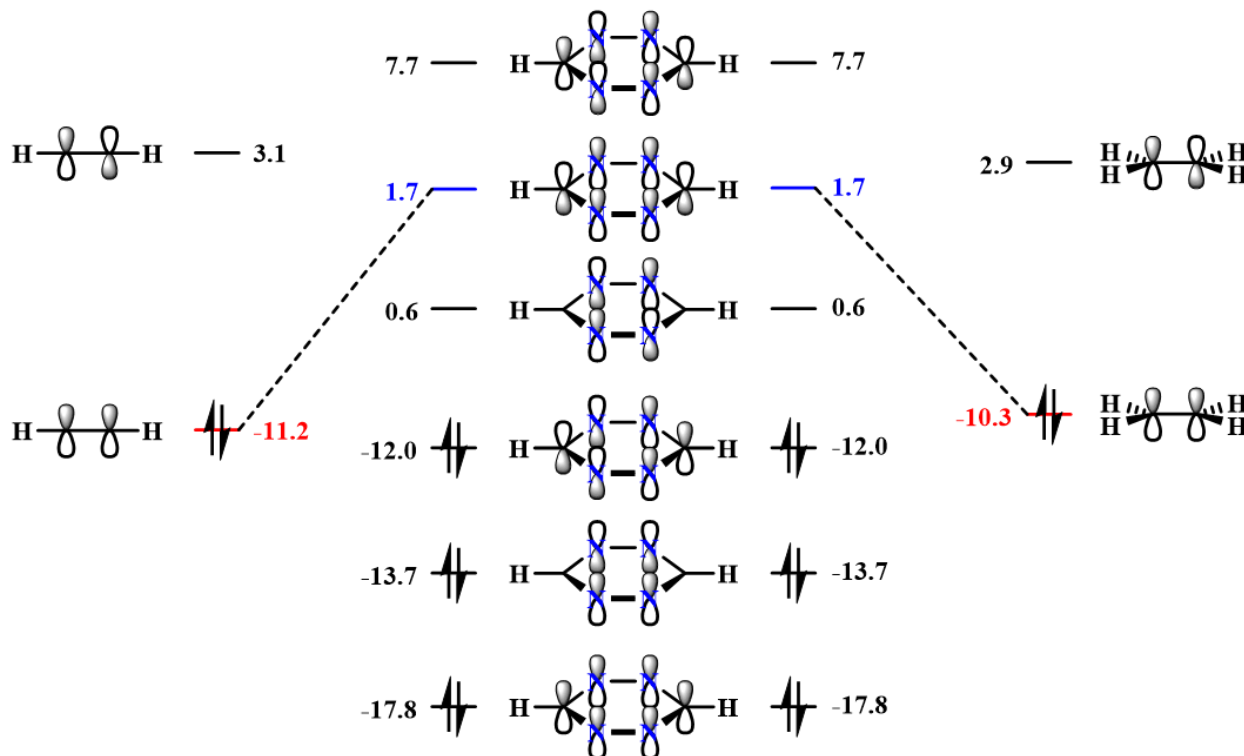


Figure 5.2 The π orbitals of acetylene, parent tetrazine, and ethylene. The HOMO-LUMO+1 interactions between tetrazine and acetylene or ethylene are indicated by dashed lines.

This is shown graphically in Figure 5.3. LUMO+1 orbital energies were calculated with HF/6-311+G(d,p) for a series of substituted tetrazines. The LUMO+1 orbital shapes and energies are shown in Figure 5.3. The lowering of LUMO+1 results in greater reactivity, although diphenyltetrazine is 30 times less reactive than dipyridyltetrazine, in spite of the same energy of LUMO+1 orbitals of the two.

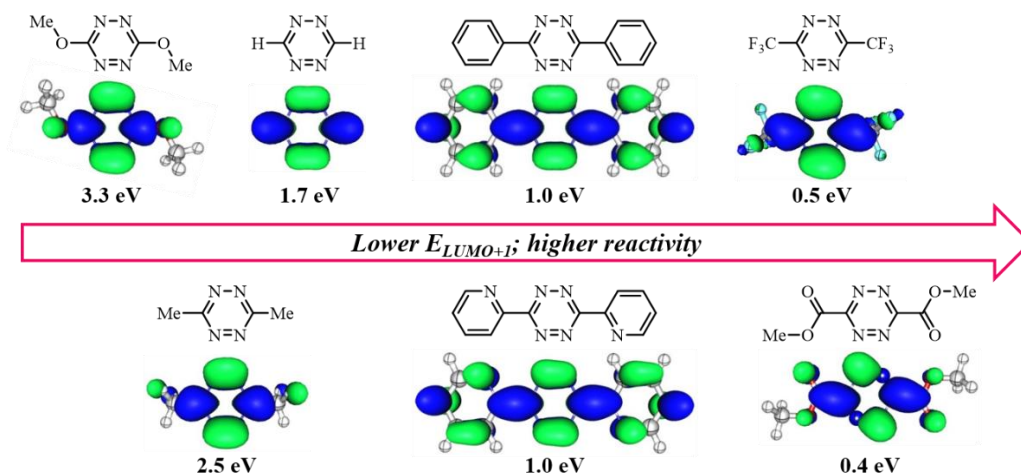


Figure 5.3 Low-lying vacant orbitals involved in the Diels-Alder reactions of tetrazine **1-7**. Energies of these orbitals in eV evaluated by RHF are shown below the orbitals.

In order to better understand these data, we have undertaken a comprehensive investigation of the substituent and strain effects on the rates of the Diels-Alder reactions of tetrazines with a variety of alkenes and alkynes using density functional theory. We provide a detailed analysis of the factors controlling reactivity of the molecules in Figure 5.4. We studied the reactions of electron-donor-substituted tetrazines, **1-2**, conjugating-group-substituted tetrazines, **3** and **5**, the parent tetrazine, **4**, and electron-acceptor-substituted tetrazines **5-7**. The dienophiles studied were strained and unstrained alkenes and alkynes, including 2-butyne **8**, *trans*-2-butene **9**, cyclooctyne **10**, and *trans*-cyclooctene **11**. Computational results are compared to experimental data when available.

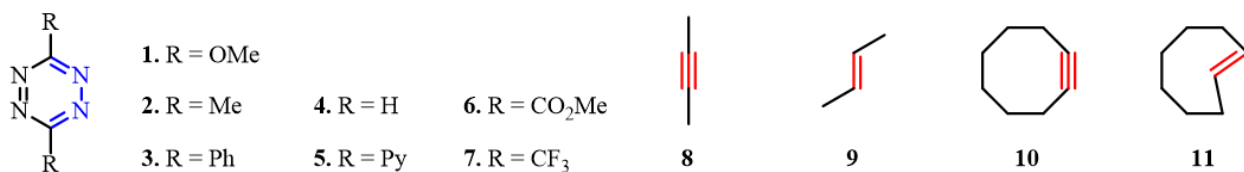


Figure 5.4 Tetrazines and dienophiles investigated in this report.

5.2 Computational Methods

All density functional theory (DFT) calculations were performed with Gaussian 09.^[16] Geometry optimization of all the minima and transition states was carried out at the M06-2X level of theory with the 6-31G(d) basis set,^[17] which has been found to give relatively accurate energetics for cycloadditions.^[18] We also tested the energetics of reactions with a larger basis set, 6-311+G(d,p). There was a systematic increase in activation energy by 0.5-1.0 kcal/mol. Because of the considerably greater cost of these calculations, and the lack of significant change in results, we have used the smaller basis set for the data reported here for the 28 reactions.

The vibrational frequencies were computed to verify that optimized structures are energy minima or transition states and to evaluate zero-point vibrational energies (ZPVE) and thermal corrections at 298 K. A quasiharmonic correction was applied during the entropy calculation by setting all positive frequencies that are less than 100 cm^{-1} to 100 cm^{-1} .^[19] The frontier molecular orbitals (FMOs) and their energies were computed at the HF/6-311+G(d,p) level using the M06-2X/6-31G(d) geometries. For the Diels-Alder reactions of cyclooctyne, solvent effects in 1,4-dioxane were computed at the M06-2X/6-311+G(d,p) level using the gas-phase optimized structures. Solvation energies were evaluated by a self-consistent reaction field (SCRF) using the CPCM model, where UFF radii were used. Distortion and interaction energies, as well as IRCs were carried out at the M06-2X/6-31G(d) level. The scan of distortion angles of tetrazines **1-7** and dienophiles **8-11** was performed by manually fixing the angles followed by optimization of all other parameters with M06-2X/6-31G(d).

5.3 Strain Effects

The transition structures for the Diels-Alder reactions between tetrazine **2** and dienophiles **8-11** are shown in Figure 5.5. The forming bond lengths are shown in Å. The activation enthalpy (ΔH^\ddagger), activation free energy (ΔG^\ddagger), and free energy of reaction (ΔG_{rxn}) for each combination are shown below each structure in kcal/mol in blue, red, and black, respectively.

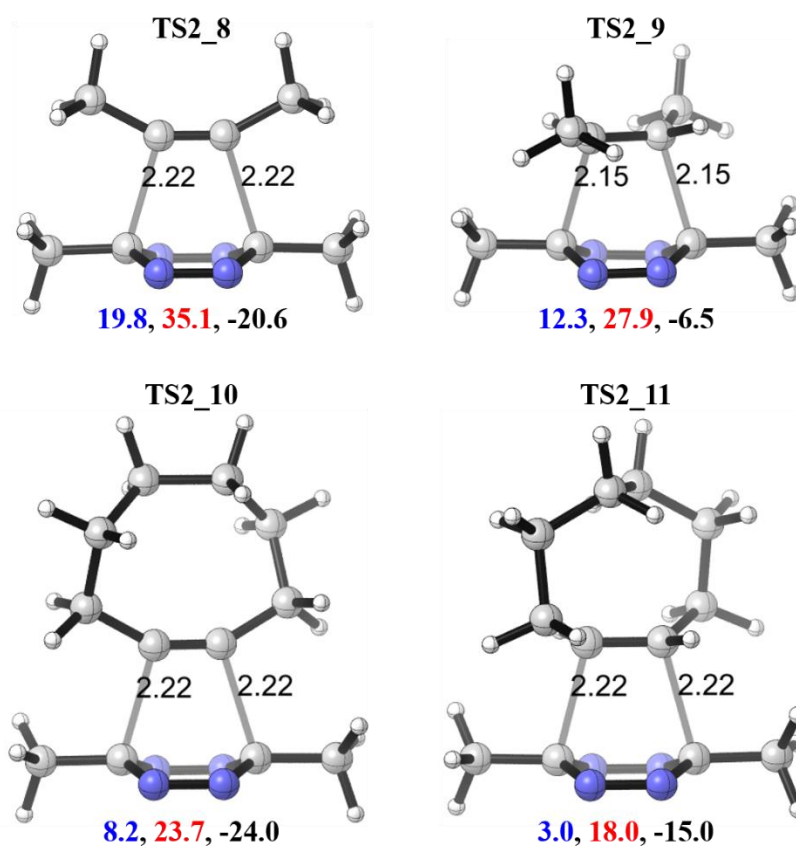


Figure 5.5 M06-2X/6-31G(d)-optimized transition structures for reactions of 3,6-dimethyltetrazine, **2** with 2-butyne, **8**, *trans*-2-butene, **9**, cyclooctyne, **10**, and *trans*-cyclooctene, **11** (forming CC bond distances are labeled on each structure in Å; ΔH^\ddagger , ΔG^\ddagger , ΔG_{rxn} are shown below each structure in kcal/mol in blue, red, and black, respectively.)

The activation free energy for the reaction of 3,6-dimethyltetrazine with *trans*-2-butene **9** is 9.9 kcal/mol higher than that with strained *trans*-cyclooctene **11** (Figure 5.5, **TS2_9** and **TS2_11**), which corresponds to a seven order of magnitude difference in rate constants. This is consistent with the experimental observations in Scheme 5.1. Similarly, the difference in calculated activation free energies for reactions of 3,6-dimethyltetrazine with 2-butyne **8** and strained cyclooctyne **10** is 11.4 kcal/mol (Figure 5.5, **TS2_8** and **TS2_10**), leading to a rate difference of 10^8 . A somewhat smaller difference was found experimentally for the tetrazines shown in Scheme 5.1.

Table 5.1 Activation free energies (ΔG^\ddagger) for Diels-Alder reactions between tetrazines **1-7** and dienophiles **8-11**, in kcal/mol.





	1 (OMe)	2 (Me)	3 (Ph)	4 (H)	5 (Py)	6 (CO₂Me)	7 (CF₃)
8 	32.8	35.1	32.9	29.0	30.3	26.2	25.6
9 	28.6	27.9	26.8	24.0	21.4	18.4	16.0
10 	20.9	23.7	21.5	17.8	18.8	14.0	12.8
11 	18.4	18.0	17.0	13.9	12.1	9.1	7.8

Table 5.1 summarizes the activation free energies of all 28 reactions studied here. The boxes in the table are color coded to show whether the reaction is (green) very rapid at room temperature or below, even for moderately low concentrations. As the colors change to light green, yellow, orange and red, the activation free energies increase, and for red the reactions would require high concentrations and elevated temperatures to be observed at all. The table is arranged in order of increasing reactivity of the tetrazines, as discussed along with Figure 5.3,

from left to right. The dienophiles are also ranked in order of reactivity, increasing from top to bottom.

The range of reactivity is enormous, with activation free energies ranging from 8-35 kcal/mol, corresponding to a 10^{16} range in rate constants at room temperature! Our results and the experiments in Scheme 5.1 showed that alkenes, both unstrained and strained, are better dienophiles than alkyne counterparts in Diels-Alder reactions with tetrazine **2**; the differences in activation free energies are large, 4-10 kcal/mol for *trans*-2-butene/2-butyne and 2-6 kcal/mol for *trans*-cyclooctene/cyclooctyne (Table 5.1). There is also a trend toward higher selectivity with the more reactive tetrazines to the right of Table 5.1. This is unexpected from our previous studies on cycloadditions of twenty-four 1,3-dipoles with ethylene or acetylene, since very similar reactivities of ethylene and acetylene were predicted for the 1,3-dipolar cycloaddition reactions.^[18a,20]

To understand why alkenes are more reactive than alkynes in Diels-Alder reactions with tetrazines, and why strained dienophiles are more reactive than unstrained species, distortion/interaction analyses were performed on all transition states. The distortion/interaction model is illustrated in Figure 5.6 on the left, with the Diels-Alder reaction between parent tetrazine and ethylene as an example. The solid black curve in Figure 5.6 represents the potential energy along the reaction coordinate for the corresponding reaction. The transition structure is separated into two fragments (distorted tetrazine and distorted ethylene), followed by single-point energy calculations on each fragment. The energy difference between the distorted structures and optimized ground-state structures are the distortion energies of diene ($\Delta E_{dist_4e}^\ddagger$) and dienophile ($\Delta E_{dist_2e}^\ddagger$), respectively. The difference between the activation energy (ΔE_{act}^\ddagger) and

the total distortion energy ($\Delta E^{\ddagger}_{dist} = \Delta E^{\ddagger}_{dist_{4e}} + \Delta E^{\ddagger}_{dist_{2e}}$) is the interaction energy ($\Delta E^{\ddagger}_{int}$). The relationships between activation, distortion, and interaction energies are shown on the right of Figure 5.6.

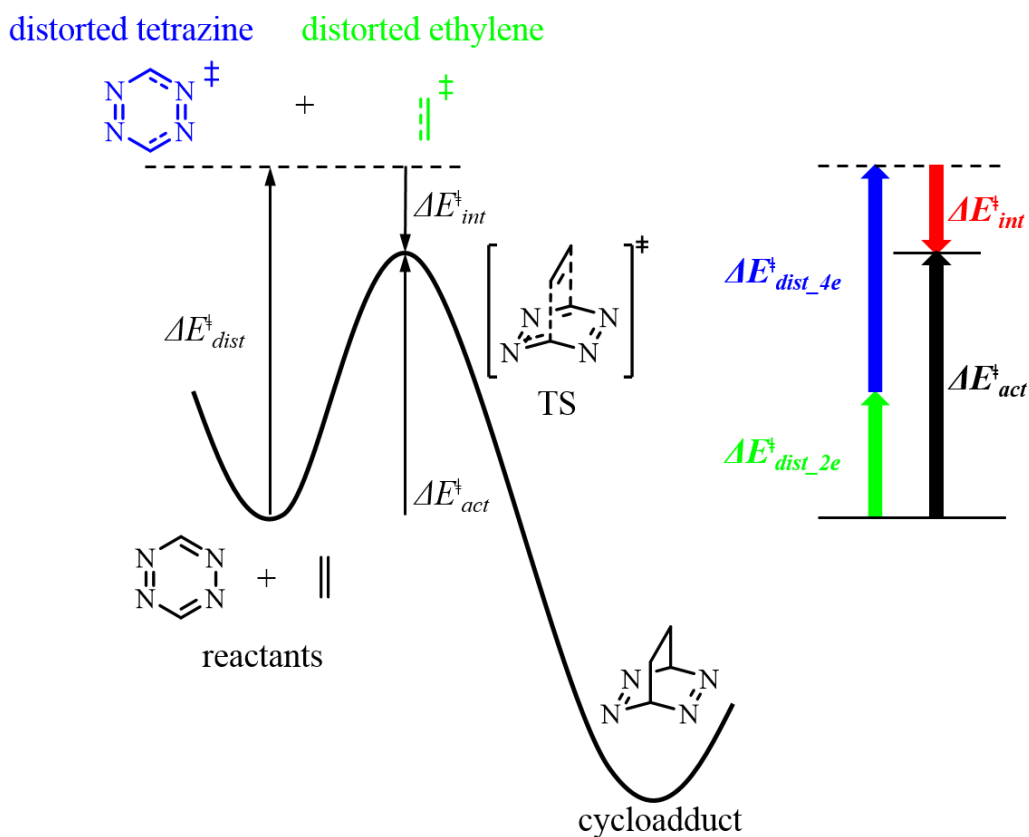


Figure 5.6 Distortion/interaction model.

The activation energies, distortion energies, and interaction energies for each transition structure involving dienophiles **8** and **9** are graphically displayed for each tetrazine (represented by the substituent groups) in Figure 5.7.

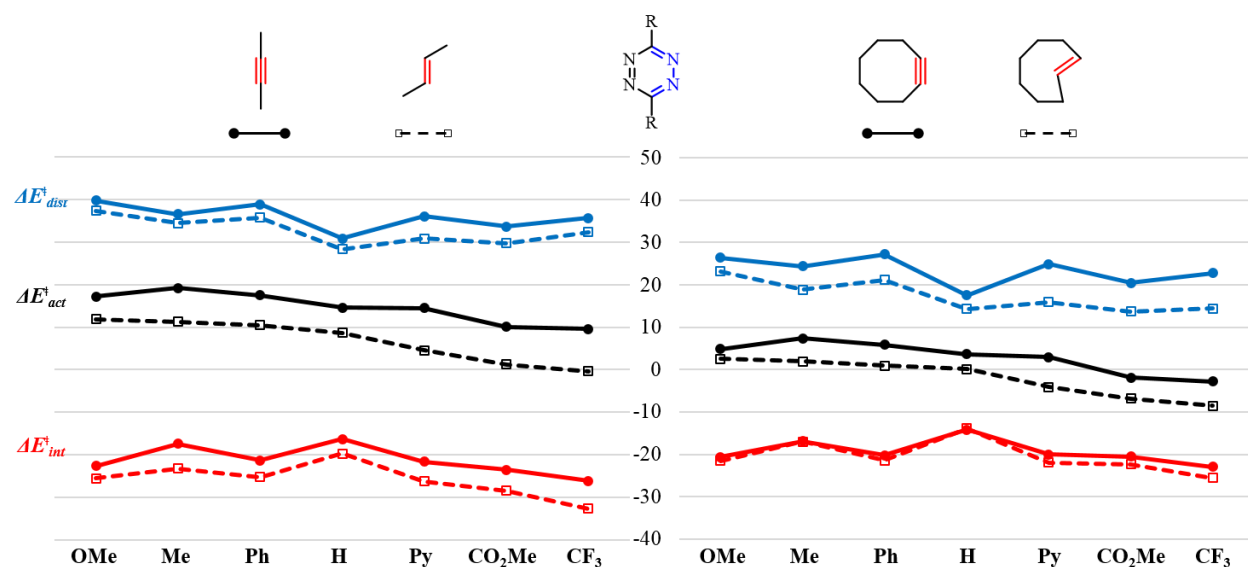


Figure 5.7 Plot of ΔE_{act}^\ddagger (black), ΔE_{dist}^\ddagger (blue), and ΔE_{int}^\ddagger (red) for tetrazines **1-7**, in Diels-Alder reactions with (left) *trans*-2-butene (dashed lines) and 2-butyne (solid lines) and (right) *trans*-cyclooctene (dashed lines) and cyclooctyne (solid lines).

Activation energies, total distortion energies, and interaction energies are shown in black, blue, and red, respectively. Empty squares connected with dashed lines represent the Diels-Alder reactions with *trans*-2-butene **9**; while the solid circles connected with solid lines are for reactions with 2-butyne **8**. The graph shows that the difference in reactivities between alkene and alkyne comes from differences in both distortion and interaction energies. The difference in interaction energies is expected based on FMO theory. Since the alkene has a higher HOMO energy than alkyne (Figure 5.2), the HOMO-LUMO gap between tetrazine and alkene is smaller, resulting in stronger interaction energy. The trend toward larger differences in interaction energies with more electron-deficient tetrazines is also consistent with greater selectivity with the more electrophilic tetrazines. The overall trend, where the interaction energies along the series peak at H, and decrease with donors and acceptors, can be attributed to the increase in

alkene/alkyne HOMO-tetrazine LUMO+1 interaction from left to right, and the shifts from late TS on the left to early TS on the right, which causes a general decrease in interaction energies.

The difference in distortion energies for alkene and alkyne reactions was, however, unexpected. To investigate this phenomenon, we performed constrained optimizations on *trans*-2-butene and 2-butyne, bending substituents (methyl groups or hydrogen atoms) out of planarity or linearity. This is the most significant distortion occurring in the Diels-Alder transition states involving alkenes or alkynes. For *trans*-2-butene, the distortion angle φ , the dihedral angle between the bent bond and the original plane of the carbon skeleton of *trans*-2-butene, as illustrated in Figure 5.8, is gradually changed from 180° (as in ground-state structures) to 160°, in intervals of 2.5°. In the case of 2-butyne, the distortion angle θ , the angle between the bent bond and the triple bond, as illustrated in Figure 5.8, is gradually changed from 180° (as in ground-state structures) to 140°, in intervals of 5°. The energy difference between optimized structure with fixed distortion angle and the ground-state structure is defined as distortion energy of angle ($\Delta E^{\ddagger}_{dist(\varphi)}$ or $\Delta E^{\ddagger}_{dist(\theta)}$). Figure 5.8 shows the plot of these energies versus distortion angles φ and θ . Distortion angles φ and θ range from 167° to 155° and 155° to 151° in transition structures, respectively, as highlighted in orange boxes in Figure 5.8.

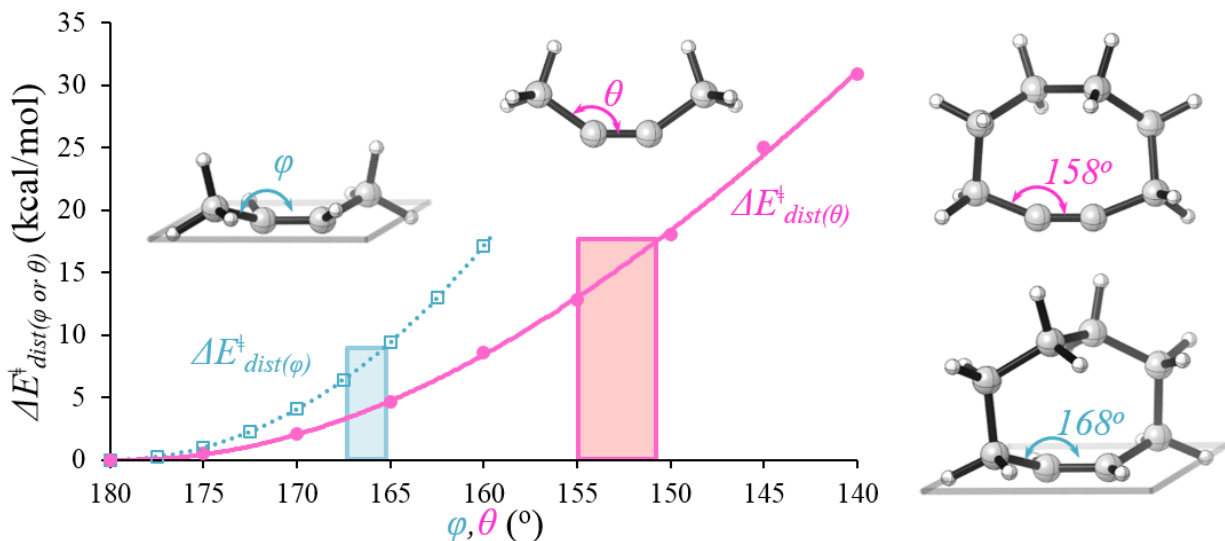


Figure 5.8 Left: plot of distortion energy of angle ($\Delta E^{\ddagger}_{dist(\varphi)}$ or $\Delta E^{\ddagger}_{dist(\theta)}$) versus distortion angle (φ or θ) for *trans*-2-butene (blue) and 2-butyne (pink). The blue and purple boxes show the range of the angle in the transition states for reactions of *trans*-2-butene and 2-butyne, respectively. Right: geometries of ground-state *trans*-cyclooctene and cyclooctyne.

Bending of 2-butyne in this way is easier than bending of *trans*-2-butene, which is in agreement with our previous study of nucleophilic additions of LiH and MeLi to ethylene and acetylene.^[21] However, in Diels-Alder reactions with tetrazines, 2-butyne is bent more than *trans*-2-butene in the transition states, resulting in a higher net distortion energy.

A distortion/interaction analysis was also carried out on reactions of strained dienophiles with tetrazines to understand more quantitatively their extreme reactivities. The energy components for each transition structure of reactions involving dienophiles **10** and **11** are graphically displayed for each tetrazine in Figure 5.7 on the right. In comparison with the plot on the left, it shows that the significant drop in distortion energies involving strained dienophiles

contributes to the decrease in activation energies. A detailed analysis of the distortions and interactions for the dimethyltetrazine reaction is given in Figure 5.9.

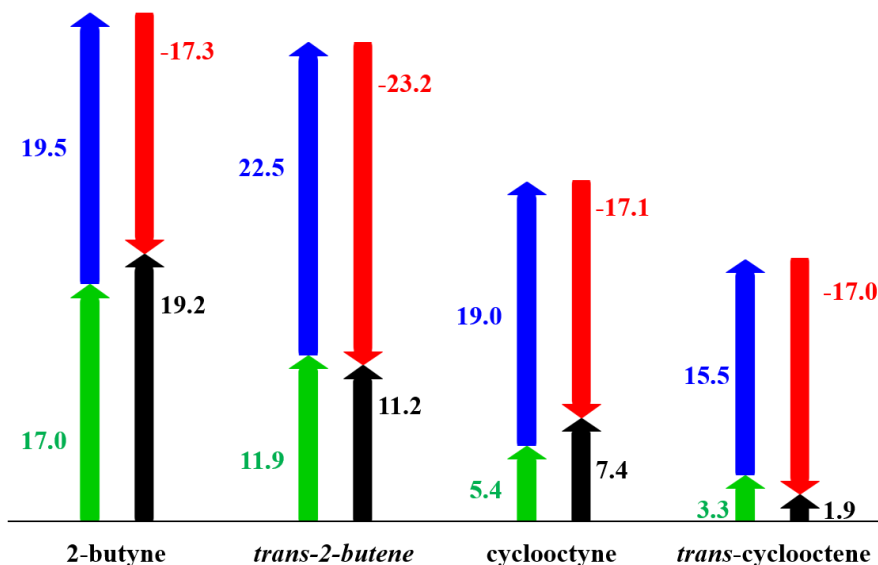


Figure 5.9 Graph of distortion, interaction, and activation energies for transition states of reactions of tetrazines **2** and dienophiles **8-11** (green: distortion energy of dienophile, blue: distortion energy of diene, red: interaction energy, black: activation energy, in kcal/mol).

Comparing the activation energies for 2-butyne and the distorted cyclooctyne, the 12 kcal/mol reduction in the activation barrier is caused by a 12 kcal/mol reduction in distortion energy, primarily due to the pre-distortion of the cyclooctyne.^[22] The same trend is observed upon comparison of *trans*-2-butene and *trans*-cyclooctene. Although the interaction energy is more negative for *trans*-2-butene, due to a somewhat late TS (Figure 5.5), the extremely small distortion energy for *trans*-cyclooctene lowers down the activation energy. The decrease in activation barrier is a result from the decrease in distortion energy. The distortion angles (φ and θ) in ground-state structures of *trans*-cyclooctene and cyclooctyne are 168° and 158°, respectively,

as shown in Figure 5.8 on the right. These values are fairly close to the angles observed in transition structures, where φ ranges from 166° to 163° ; and θ ranges from 154° to 149° . Based on this analysis, we conclude that *trans*-cyclooctene and cyclooctyne are predistorted toward Diels-Alder transition structures and require smaller distortion energies compared to unstrained dienophiles, leading to lower activation barriers.

5.4 Substituent Effects

The transition structures for the Diels-Alder reactions between tetrazines **1-7** and dienophile **9** are shown in Figure 5.10 with the forming bonding distances marked in Å. The activation enthalpy (ΔH^\ddagger), activation free energy (ΔG^\ddagger), and free energy of reaction (ΔG_{rxn}) are shown below each structure in kcal/mol in blue, red, and black, respectively. Dimethoxytetrazine **1** is the least reactive, in agreement with the experimentally observed low reactivity of 3-methoxy-6-(methylthio)-1,2,4,5-tetrazine shown in Scheme 5.2c. Dimethyltetrazine **2** has a slightly lower barrier than **1**, but still not as reactive as parent tetrazine **3**, as demonstrated in Scheme 5.2a. Diphenyltetrazine **4** and dipyridyltetrazine **5** are less reactive than dimethyl-1,2,4,5-tetrazine-3,6-dicarboxylate **6** and bis(trifluoromethyl)tetrazine **7**, in accord with the reactivity trend presented in Scheme 5.2b. Tetrazines substituted with electron-donating groups (**1** and **2**) have late transition states with short forming bond distances and large activation barriers. On the contrary, tetrazines substituted with electron-withdrawing groups (**5-7**) have early transition states with long forming bond distances and small activation barriers.

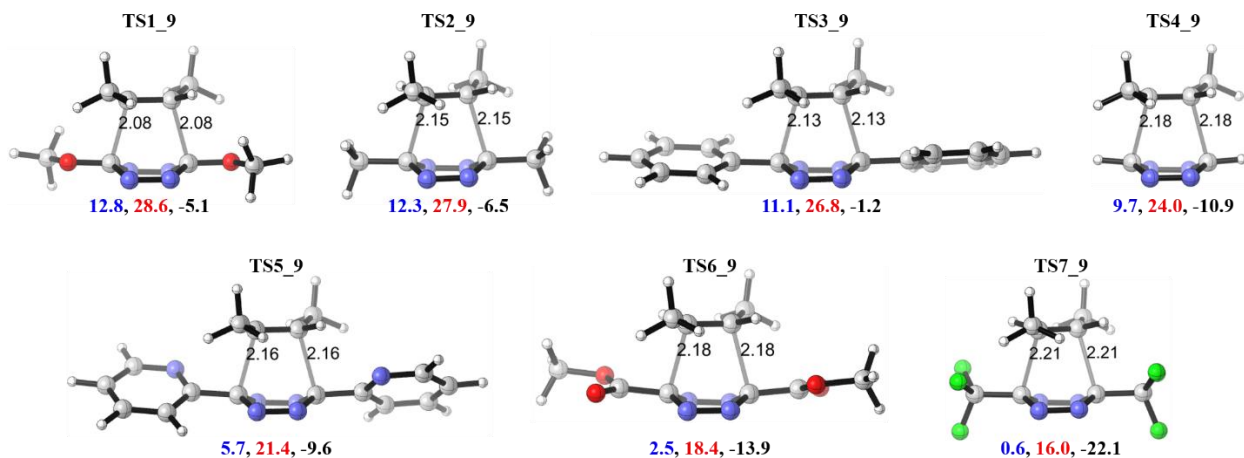


Figure 5.10 M06-2X/6-31G(d)-optimized transition structures for reactions of *trans*-2-butene (forming CC bond distances are labeled on each structure in Å; ΔH^\ddagger , ΔG^\ddagger , ΔG_{rxn} are shown below each structure in kcal/mol in blue, red, and black, respectively).

To understand what controls the reactivity, we did the distortion/interaction analysis on each transition structure, as shown in Figure 5.11. The distortion energy of dienophile (green arrow), distortion energy of diene (blue arrow), interaction energy (red arrow), and activation energy (black arrow) are plotted for each tetrazine involved in the reaction, in kcal/mol. The distortion energy of dienophiles is not sensitive to tetrazine substituents, ranging from 10 to 13 kcal/mol as the substituent varies. Distortion energies of diene for reactions involving donor-substituted tetrazines are higher than for reactions involving acceptor-substituted tetrazines, due to the position of transition states. The tetrazine distortion energies vary from 19 to 25 kcal/mol. The distortion energies are larger for R = donor, where the transition states are relatively late, and become smaller for R = acceptor, where the transition states are relatively early. This difference in distortion energies is not as significant as the difference in interaction energies, which is the major contributor to the variance in activation energies. These vary from -20 to -33 kcal/mol. Tetrazines substituted with electron-withdrawing groups tend to have more negative

interaction energies, leading to low activation energies. This arises in large part due to favorable tetrazine LUMO+1 interaction with alkene HOMO, as discussed earlier.

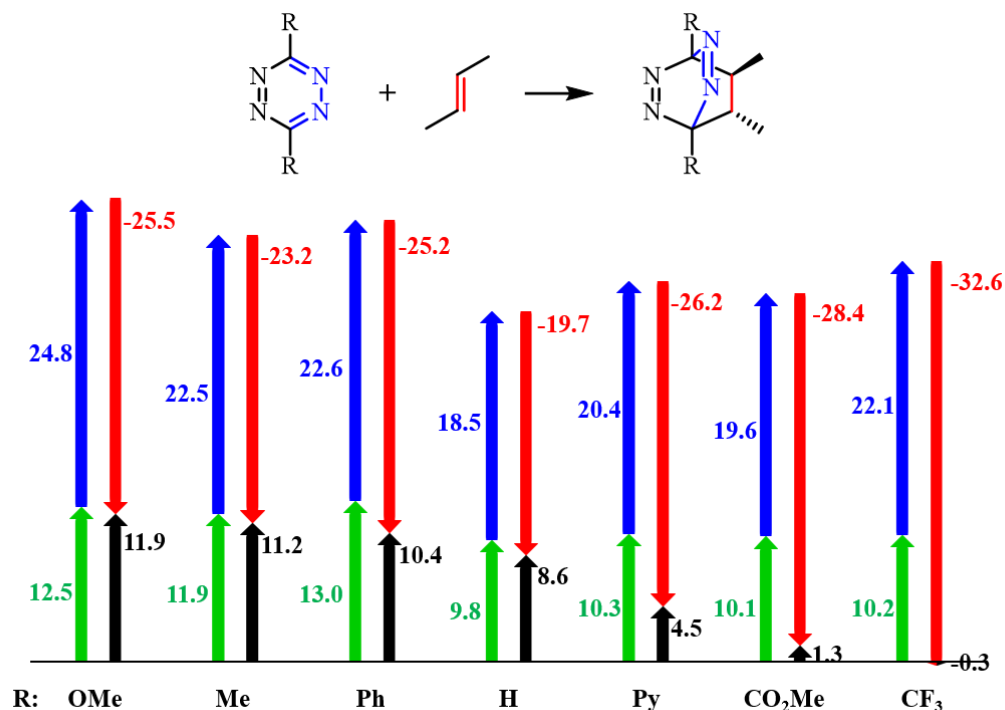


Figure 5.11 Graph of distortion, interaction, and activation energies for transition states of reaction of tetrazines **1-7** and *trans*-2-butene **9** (green: distortion energy of dienophile, blue: distortion energy of diene, red: interaction energy, black: activation energy, in kcal/mol).

In order to provide a more detailed understanding of how the distortion and interaction energies vary as the reaction proceeds, we have examined distortion and interaction energies along the intrinsic reaction coordinate (IRC) for these reactions. The activation energies and energy components are plotted against the forming CC bond distance for points along the IRC in Figure 5.12. This type of analysis has been used extensively by Bickelhaupt and in our earlier work.^[23] Total, distortion, and interaction energies are shown as solid lines, dashed-dotted lines, and dashed lines, respectively. These energy profiles are colored according to the tetrazines

involved in the reactions. The positions of transition states are marked with diamonds in corresponding colors. The energy values at these positions correspond to the activation energy (ΔE_{act}^\ddagger), total distortion energy (ΔE_{dist}^\ddagger), and interaction energy (ΔE_{int}^\ddagger) defined in Figure 5.6. At the transition state, the derivative of the distortion energy is equal and opposite in sign to the derivative of the interaction energy. Clearly, an early transition state, with a relatively long forming CC bond distance, corresponds to a low activation barrier, while a late transition state is accompanied by a high activation barrier.

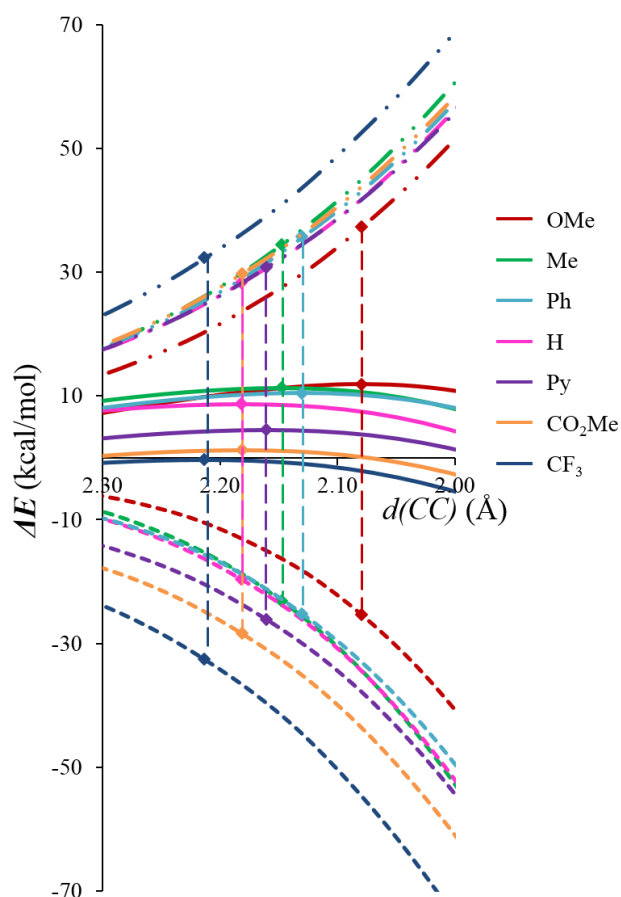


Figure 5.12 Total energy ΔE_{act} (solid), distortion energy ΔE_{dist} (dashed-dotted), and interaction ΔE_{int} (dashed) along the reaction coordinate (forming bond distance in Å) for reactions of tetrazines **1-7** with *trans*-2-butene.

At a certain forming bond distance, reactions involving tetrazines substituted with electron-withdrawing groups have stronger interaction energies than reactions of tetrazines substituted with electron-donating groups (Figure 5.12, dashed lines). These differences in interaction energies can be explained by FMO theory. The variation in LUMO+1 energies of tetrazines **1-7** in Figure 5.3 corresponds approximately with the vertical displacement of the dashed lines in Figure 5.12. Tetrazines substituted with electron-withdrawing groups have lower LUMO+1 energies, leading to smaller HOMO-LUMO gaps and stronger interactions. To our surprise, such correlation between energies and with the electronegativities of the substituents does not hold true for the distortion energies (Figure 5.12, dashed-dotted lines). At a certain forming bond distance, reaction of dimethoxytetrazine **1** has a much smaller distortion energy than reaction of bis-(trifluoromethyl)tetrazine **7**, while the reactions involving tetrazines **2-6** have very close distortion energies. Does that suggest dimethoxytetrazine **1** is easier to be distorted than bis-(trifluoromethyl)tetrazine **7**? To answer this question, we analyzed four critical structures along the IRC for reactions of **1** and **7**, including two transition structures and structures with similar forming bond distances with the transition structure, as shown in Figure 5.13.

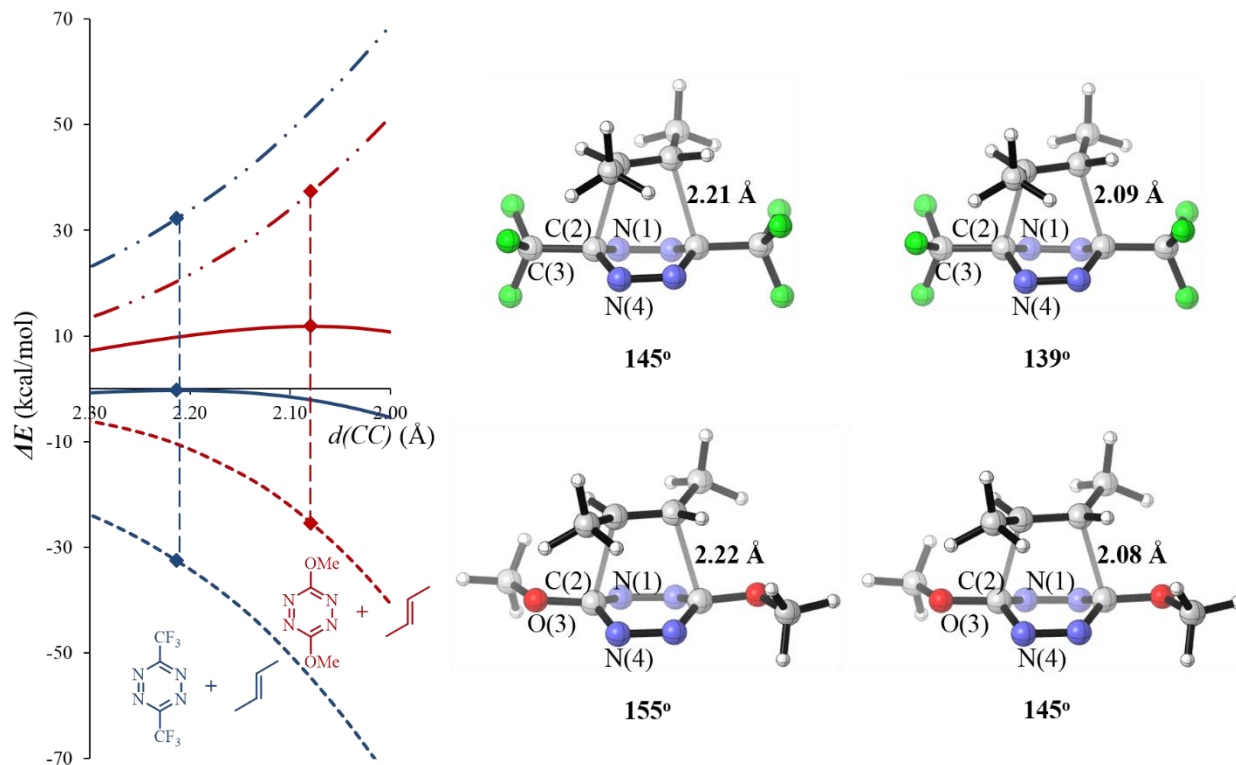


Figure 5.13 Left: Total energy ΔE_{act} (solid), distortion energy ΔE_{dist} (dashed-dotted), and interaction ΔE_{int} (dashed) along the reaction coordinate (forming bond distance in Å) for reactions of tetrazines **1** (R = OMe, red) and **7** (R = CF₃, blue) with *trans*-2-butene. Right: transition structures involving **1** and **7** and corresponding IRC points with similar forming bond distances. The distortion angles N(1)-C(2)-C(3)-C(4) or N(1)-C(2)-C(3)-O(4) are shown below each structure.

At a similar forming bond distance, dihedral N(1)-C(2)-C(3)-O(4) is larger than dihedral N(1)-C(2)-C(3)-C(4) (155° vs. 145° or 145° vs. 139°, shown in Figure 5.13 on the right), indicating that dimethoxytetrazine is less bent out of planarity than bis(trifluoromethyl)tetrazine when separated from *trans*-2-butene at a fixed distance. This explains why the distortion energy curve for reaction involving dimethoxytetrazine is lower than that for bis(trifluoromethyl)-

tetrazine—not because the former is easier to distort but because the former is distorted to a less degree.

To compare the ease of distortion in substituted tetrazines, a scan of the out-of-plane distortion, which is a prominent distortion in the transition state (Figure 5.14), was carried out. For each tetrazine, the out-of-plane dihedral angle ω , which is 0° for planar ground-state structures and 12 - 18° for transition structures, was gradually increased from 2.5° to 20.0° in intervals of 2.5° . The energy difference between optimized structure with fixed dihedral angles and the ground-state structure is defined as distortion energy of angle ($\Delta E_{dist_ \omega}^\ddagger$). Figure 5.14 shows the plot of $\Delta E_{dist_ \omega}^\ddagger$ versus the dihedral angle ω .

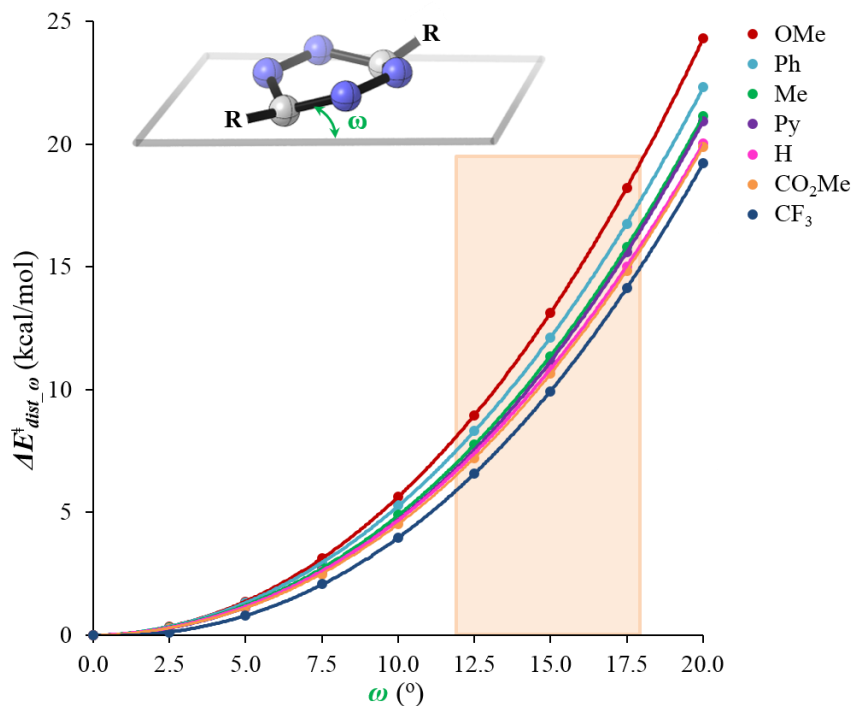


Figure 5.14 Plot of distortion energy of angle ($\Delta E_{dist_ \omega}^\ddagger$) versus distortion angle (ω) for tetrazines **1-7**. The orange box shows the range of the dihedral angle in the transition states for reactions of substituted tetrazines with dienophiles **8-11**.

The distortion energy increases as this dihedral angle increases. At a certain angle within the transition zone (highlighted with an orange box in Figure 5.14 with $\omega = 12-18^\circ$), the distortion energies of tetrazines substituted with electron-withdrawing groups are significantly lower than the distortion energies of tetrazines substituted with electron-donating groups. The acceptor-substituted tetrazines are easier to distort compared than the donor-substituted tetrazines. This trend is consistent with the distortion/interaction analysis in the previous discussion as well as the Diels-Alder reactivities of different tetrazines. This occurs because donor stabilize the tetrazines, while acceptors destabilize them. Tetrazines are electron-deficient and benefit from electron-donation and this interaction is reduced by bending. We calculated the isodesmic reaction energies for the process shown in Figure 5.15. The isodesmic reaction energy, ΔH_{stab} , is very favorable (35 kcal/mol stabilization) for the powerful donor, MeO, and becomes destabilizing up to -13 kcal/mol for CF₃. The distortion energy at various values of ω are plotted versus ΔH_{stab} in Figure 5.15. The ease of distortion in substituted tetrazines is related to the stability of the ground-state structures. Tetrazines substituted by electron-donating groups are more stable and hard to distort, while tetrazines substituted by electron-withdrawing groups are less stable and easy to distort into Diels-Alder transition states.

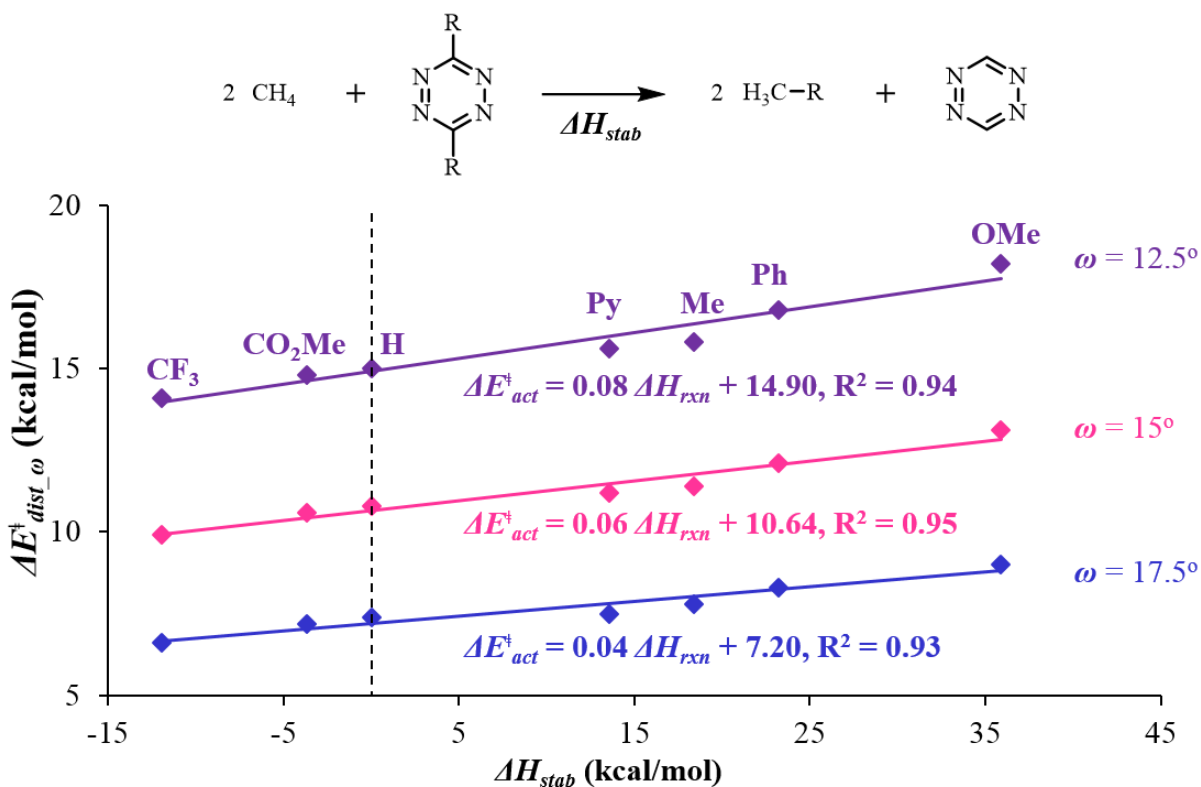


Figure 5.15 Correlation between angular distortion energies at fixed distortion angles ($\omega = 12.5^\circ$, 15.0° , and 17.5°) and the reaction enthalpies of the corresponding isodesmic reactions.

5.5 Correlation between Activation Energies, Distortion Energies, and HOMO-LUMO Gaps

Finally, we summarize the factors that control reactivities of tetrazines. Figure 5.16 shows a plot of activation energies ($\Delta E_{act}^{\ddagger}$) versus total distortion energies ($\Delta E_{dist}^{\ddagger}$) or reaction energies ($\Delta E_{rxn}^{\ddagger}$). The blue and red data points on the plot are for the Diels-Alder reactions of tetrazines **1-7** with alkenes and alkynes, respectively. The solid and empty data points are for reactions involving strained and unstrained dienophiles, respectively. The linear correlations for all data are shown at the bottom right of each plot. The activation energies correlate very roughly with reaction energies as shown in Figure 5.16b. The Diels-Alder reactions of strained

dienophiles (*trans*-cyclooctene and cyclooctyne) are about 10 kcal/mol more exothermic and about 5 kcal/mol more kinetically favored than those of the unstrained dienophiles, *trans*-2-butene and 2-butyne. As noted earlier, alkenes (blue), generally, are more reactive than alkynes (red), and this shows up quite dramatically in Figure 5.16b.

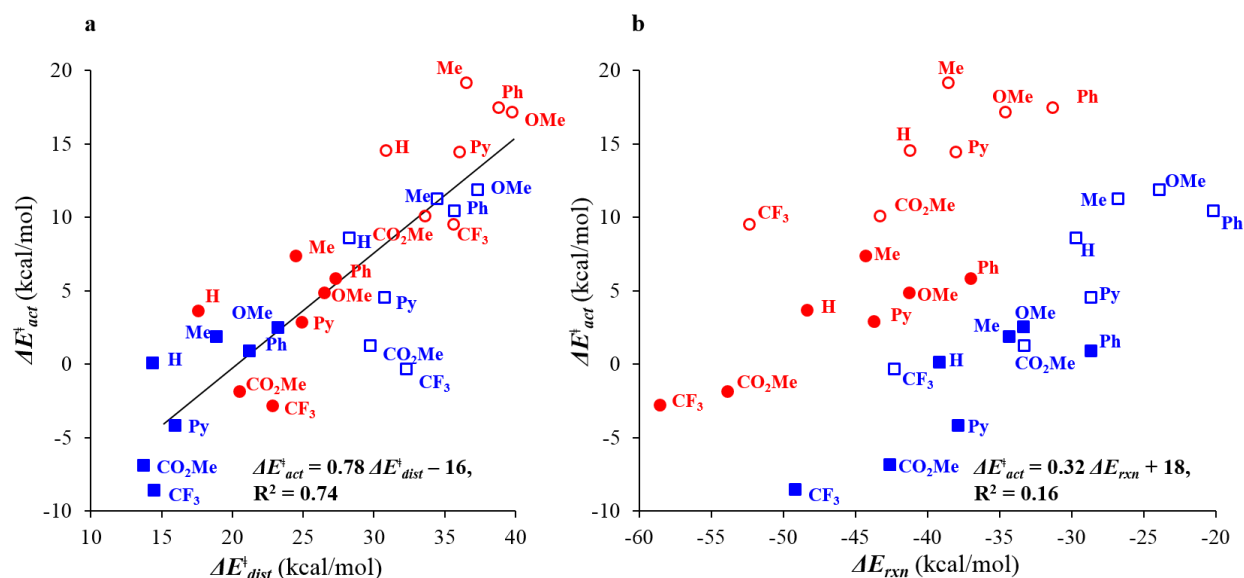


Figure 5.16 Plots of activation energy ($\Delta E_{act}^{\ddagger}$) vs (a) total distortion energy ($\Delta E_{dist}^{\ddagger}$) and (b) reaction energy ($\Delta E_{rxn}^{\ddagger}$). Solid blue squares: *trans*-cyclooctene; empty blue squares: *trans*-2-butene; Solid red circle: cyclooctyne; empty red circle: 2-butyne. The labels shown besides each data point refer to the substituent groups on the tetrazines involved in the corresponding reactions.

The correlation between activation energy and distortion energy is much better, with R^2 equal to 0.74. The activation energies increase as the distortion energies increase. In general, this correlation indicates that the reactivity is distortion-controlled. Deviations from this line result from the fact that interaction energies are not constant. Tetrazines substituted with electron-

donating groups lie at or above the correlation line, and tetrazines substituted with electron-donating groups lie, for the most part, at or below this line, due to their more favorable interaction energies. The interaction energy differences cause deviations from the linear correlation with distortion energies.

Interaction energies arise from a variety of factors, such as charge-transfer, electrostatic, and polarization stabilization, as well as closed-shell (Pauli) repulsion. The differences in interaction energies are largely determined by differences in charge-transfer stabilization due to dienophile HOMO-tetrazine LUMO+1 interactions in the reaction studied here. According to perturbation theory,^[24] the stabilization energy arising from this interaction is proportional to $1/(E_{HOMO} - E_{LUMO+1})$. Based on this, we expect a larger interaction energy for the tetrazines substituted by electron-withdrawing groups. This is only qualitatively the case, as shown by the plot of ΔE_{int}^\ddagger versus $1/(E_{HOMO} - E_{LUMO+1})$ in Figure 5.17. The significant deviations arise from the complication that the interaction energies are altered by the position of the transition states.

For each type of dienophile, a “volcano” correlation is observed. Figure 5.17b shows this for the trans-2-butene, but the same general shape is observed. The largest stabilizing interaction energies are at the lower left of the graph, and poorer acceptors give less stabilization as the HOMO-(LUMO+1) gap increases. The methyl and methoxy compounds have higher LUMO+1 energies, and larger HOMO-LUMO+1 gaps, but nevertheless more negative interaction energies due to their later transition states. This leads to the deviation of data points for R = OMe and R = Me from the linear correlations.

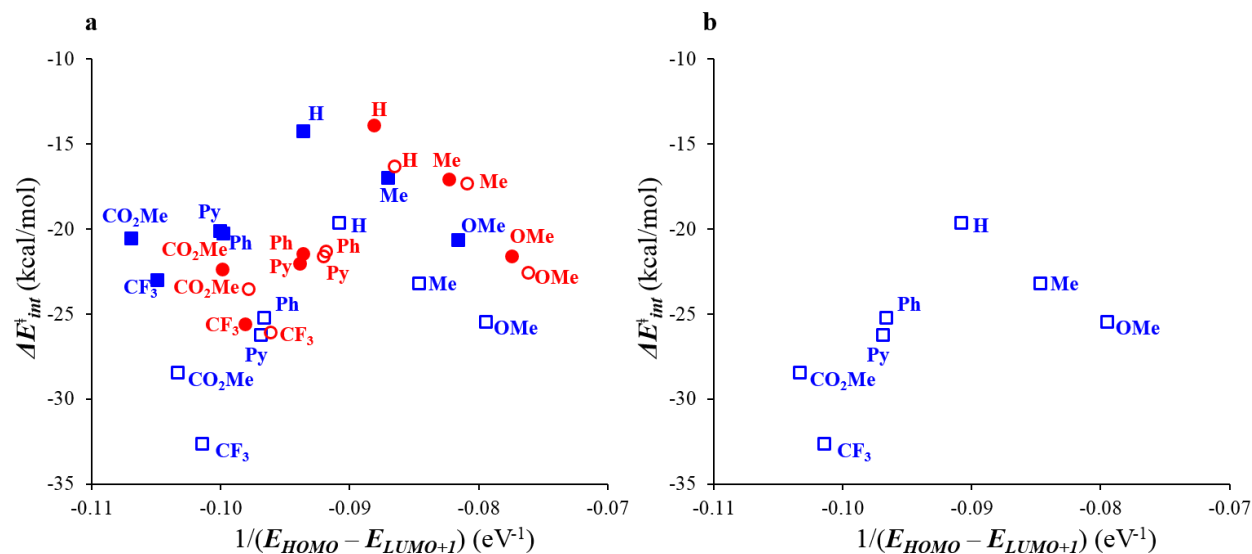


Figure 5.17 a) Plots of interaction energy ($\Delta E_{int}^{\ddagger}$) vs inverse of the FMO energy gap ($1/(E_{HOMO} - E_{LUMO+1})$). Solid blue squares: *trans*-cyclooctene; empty blue squares: *trans*-2-butene; Solid red circle: cyclooctyne; empty red circle: 2-butyne. The labels shown besides each data point refer to the substituent groups on the tetrazines involved in the corresponding reactions. b) Same plot for *trans*-2-butene only.

In addition, the differences in interaction energies between different dienophiles for a given HOMO-LUMO+1 gap is related to the position of transition state, as well. In particular, *trans*-2-butene (Figure 5.17, empty squares) has lower HOMO energy than *trans*-cyclooctene (Figure 5.17, solid squares),^[25] and larger HOMO-LUMO+1 gaps, but more favorable interaction energies due to later transition states.

We have studied dienophile strain and tetrazine substituent effects on rates of Diels-Alder reactions of tetrazines. Electron-withdrawing substituents on tetrazines lower the LUMO+1 energy, which leads to stronger interaction energy in Diels-Alder reactions with dienophiles, and facilitates the crucial out-of-plane distortion that controls distortion energies. Small distortion

energies and high interaction energies explain the high reactivities of tetrazines substituted by electron-withdrawing-groups. Electron-donating substituents affect reactivities in the opposite fashion. We have demonstrated that alkenes are in general more reactive than alkynes in Diels-Alder reactions with tetrazines. Alkenes have relatively higher HOMO energies than alkynes, and therefore stronger interaction energies with electrophilic tetrazines. In addition, the distortion energies required for alkenes to achieve their transition structures are less than alkynes. Strained dienophiles are extremely reactive in Diels-Alder reactions with tetrazine because they are pre-distorted towards the transition structures. Consequently, smaller distortion energies are required to achieve the transition-state geometries.

5.6 References

- [1] Blackman, M. L.; Royzen, M.; Fox, J. M. Tetrazine ligation: fast bioconjugation based on inverse-electron-demand Diels-Alder reactivity. *J. Am. Chem. Soc.* **2008**, *130*, 13518-13519.
- [2] Devaraj, N. K.; Weissleder, R.; Hilderbrand, S. A. Tetrazine-based cycloadditions: application to pretargeted live cell imaging. *Bioconjugate Chem.* **2008**, *19*, 2297-2299.
- [3] Patterson, D. M.; Nazarova, L. A.; Xie, B.; Kamber, D. N.; Prescher, J. A. Functionalized cyclopropenes as bioorthogonal chemical reporters. *J. Am. Chem. Soc.* **2012**, *134*, 18638-18643.
- [4] Yang, J.; Seckute, J.; Cole, C. M.; Devaraj, N. K. Live-cell imaging of cyclopropene tags with fluorogenic tetrazine cycloadditions. *Angew. Chem. Int. Ed.* **2012**, *51*, 7476-7479.
- [5] Pipkorn, R.; Waldeck, W.; Ddinger, B.; Koch, M.; Mueller, G.; Wiessler, M.; Braun, K. Inverse-electron-demand Diels-Alder reaction as a highly efficient chemoselective ligation

procedure: synthesis and function of a BioShuttle for temozolomide transport into prostate cancer cell. *J. Pept. Sci.* **2009**, *15*, 235-241.

[6] Thomas, J. D.; Cui, H.; North, P. J.; Hofer, T.; Rader, C.; Burke, T. R. Jr. Application of strain-promoted azide–alkyne cycloaddition and tetrazine ligation to targeted Fc-drug conjugates. *Bioconjugate Chem.* **2012**, *23*, 2007-2013.

[7] Liu, F.; Paton, R. S.; Kim, S.; Liang, Y.; Houk, K. N. Diels–Alder reactivities of strained and unstrained cycloalkenes with normal and inverse-electron-demand dienes: activation barriers and distortion/interaction analysis. *J. Am. Chem. Soc.* **2013**, *135*, 15642-15649.

[8] (a) Boger, D. L.; Wolkenberg, S. E. Total synthesis of amaryllidaceae alkaloids utilizing sequential intramolecular heterocyclic azadiene Diels–Alder reactions of an unsymmetrical 1,2,4,5-tetrazine. *J. Org. Chem.* **2000**, *65*, 9120-9124. (b) Boger, D. L.; Hong, J. Asymmetric total synthesis of ent(-)-roseophilin: assignment of absolute configuration. *J. Am. Chem. Soc.* **2001**, *123*, 8515-8519. (c) Hamasaki, A.; Zimpleman, J. M.; Hwang, I.; Boger, D. L. Total synthesis of ningalin D. *J. Am. Chem. Soc.* **2005**, *127*, 10767-10770. (d) Oakdale, J. S.; Boger, D. L. Total synthesis of lycogarubin C and lycogalic acid. *Org. Lett.* **2010**, *12*, 1132-1134. (e) Fu, L.; Gribble, G. W. Total synthesis of lycogarubin C utilizing the Kornfeld-Boger ring contraction. *Tetrahedron Lett.* **2010**, *51*, 537-539.

[9] Chen, C.; Allen, C. A.; Cohen, S. M. Tandem postsynthetic modification of metal-organic frameworks using an inverse-electron-demand Diels–Alder reaction. *Inorg. Chem.* **2011**, *50*, 10534-10536.

[10] (a) Hayden, H.; Gun'ko, Y. K.; Perova, T. S. Chemical modification of multi-walled carbon nanotubes using a tetrazine derivative. *Chem. Phys. Lett.* **2007**, *435*, 84-89. (b) Hayden, H.; Gun'ko, Y. K.; Perova, T.; Grudinkin, S.; Moore, A.; Obraztsova, E. D. Investigation of tetrazine functionalized single walled carbon nanotubes. *Plast. Rubber. Compos.* **2009**, *38*, 253-256. (c) Zhu, J.; Hiltz, J.; Lennox, R. B.; Schirmacher, R. Chemical modification of single walled carbon nanotubes with tetrazine-tethered gold nanoparticles *via* a Diels-Alder reaction. *Chem. Commun.* **2013**, *49*, 10275-10277.

[11] (a) Sauer, J.; Mielert, A.; Lang, D.; Peter, D. Eine Studie der Diels-Alder reaktion, III: umsetzungen von 1,2,4,5-tetrazinen mit olefinen. Zur struktur von dihydropyridazinen. *Chem. Ber.* **1965**, *98*, 1435-1445. (b) Sauer, J.; Heinrichs, G. Kinetik und umsetzungen von 1,2,4,5-tetrazinen mit winkelgespannten und elektronenreichen doppelbindunge. *Tetrahedron Lett.* **1966**, *41*, 4979-4984. (c) Thalhammer, F.; Wallfahrer, U.; Sauer, J. Reaktivitat einfacher offenkettiger und cyclischer dienophile bei Diels-Alder-reaktionen mit inversem elektronenbedarf. *Tetrahedron Lett.* **1990**, *31*, 6851-6854. (d) Meier, A.; Sauer, J. Donor-akzeptor substituierte dienophile bei Diels-Alder-reaktionen mit inversem elektronenbedarf. *Tetrahedron Lett.* **1990**, *31*, 6855-6858. (e) Cioslowski, J.; Sauer, J.; Hetzenegger, J.; Karcher, T.; Hierstetter, T. Ab initio quantum-mechanical and experimental mechanistic studies of Diels-Alder reactions between unsubstituted and phenyl-substituted acetylenes and 1,2,4,5-tetrazines. *J. Am. Chem. Soc.* **1993**, *115*, 1353-1359. (f) Sauer, J.; Heldmann, D. K.; Hetzenegger, J.; Krauthan, J.; Sichert, H.; Schuster, J. 1,2,4,5-tetrazine: synthesis and reactivity in [4+2] cycloadditions. *Eur. J. Org. Chem.* **1998**, 2885-2896.

- [12] (a) Boger, D. L.; Panek, J. S. Inverse electron demand Diels-Alder reactions of heterocyclic azadienes: formal total synthesis of streptonigrin *J. Am. Chem. Soc.* **1985**, *107*, 5745-5754. (b) Boger, D. L.; Boyce, C. W.; Labroli, M. A.; Sehon, C. A.; Jin, Q. Total synthesis of ningalin A, lamellarin O, lukianol A, and permethyl storniamide A utilizing heterocyclic azadiene Diels-Alder reactions. *J. Am. Chem. Soc.* **1999**, *121*, 54-62. (c) Sakya, S.; Groskopf, K. K.; Boger, D. L. Preparation and inverse electron demand Diels-Alder reactions of 3-methoxy-6-methylthio-1,2,4,5-tetrazine. *Tetrahedron Lett.* **1997**, *38*, 3805-3808. (d) Carboni, R. A.; Lindsey, R. V. Jr. Reactions of tetrazines with unsaturated compounds. A new synthesis of pyridazine. *J. Am. Chem. Soc.* **1959**, *81*, 4342-4346.
- [13] Bach, R. D. Ring strain energy in the cyclooctyl system. The effect of strain energy on [3+2] cycloaddition reactions with azide. *J. Am. Chem. Soc.* **2009**, *131*, 5233-5243.
- [14] Karver, M. R.; Weissleder, R.; Hilderbrand, S. A. Synthesis and evaluation of a series of 1,2,4,5-tetrazines for bioorthogonal conjugation. *Bioconjugate Chem.* **2011**, *22*, 2263-2270.
- [15] Chen, W.; Wang, D.; Dai, C.; Hamelberg, D.; Wang, B. Clicking 1,2,4,5-tetrazine and cyclooctynes with tunable reaction rates. *Chem. Commun.* **2012**, *48*, 1736-1738.
- [16] Frisch, M. J.; et al. *Gaussian 09*, revision C.01; Gaussian, Inc.: Wallingford, CT, 2010.
- [17] (a) Zhao, Y.; Truhlar, D. G. The M06 suite of density functionals for main group thermochemistry, thermochemical kinetics, noncovalent interactions, excited states, and transition elements: two new functionals and systematic testing of four M06-class functionals and 12 other functionals. *Theor. Chem. Acc.* **2008**, *120*, 215-241. (b) Zhao, Y.; Truhlar, D. G. Density functionals with broad applicability in chemistry. *Acc. Chem. Res.* **2008**, *41*, 157-167. (c)

We also tested the importance of basis set for three typical cases. The barriers increase on the order of 1 kcal/mol in cases ranging from the methyl through CF₃-substituted tetrazines with *trans*-2-butene, presumably due to the reducing of basis set superposition error. Because we find only a small systematic error, we have used only the 6-31G(d) basis set in the calculations reported here.

[18] (a) Lan, Y.; Zou, L.; Cao, Y.; Houk, K. N. Computational methods to calculate accurate activation and reaction energies of 1,3-dipolar cycloadditions of 24 1,3-dipoles. *J. Phys. Chem. A* **2011**, *115*, 13906-13920. (b) Paton, R. S.; Mackey, J. L.; Kim, W. H.; Lee, J. H.; Danishefsky, S. J.; Houk, K. N. Origins of stereoselectivity in the *trans* Diels-Alder paradigm. *J. Am. Chem. Soc.* **2010**, *132*, 9335-9340.

[19] (a) Zhao, Y.; Truhlar, D. G. Computational characterization and modeling of buckyball tweezers: density functional study of concave-convex $\pi \cdots \pi$ interactions. *Phys. Chem. Chem. Phys.* **2008**, *10*, 2813-2818. (b) Ribeiro, R. F.; Marenich, A. V.; Cramer, C. J.; Truhlar, D. G. Use of solution-phase vibrational frequencies in continuum models for the free energy of solvation. *J. Phys. Chem. B* **2011**, *115*, 14556-14562.

[20] (a) Ess, D. H.; Houk, K. N. Distortion/interaction energy control of 1,3-dipolar cycloaddition reactivity. *J. Am. Chem. Soc.* **2007**, *129*, 10646-10647. (b) Ess, D. H.; Houk, K. N. Theory of 1,3-dipolar cycloadditions: distortion/interaction and frontier molecular orbital models. *J. Am. Chem. Soc.* **2008**, *130*, 10187-10198.

[21] (a) Strozier, R. W.; Caramella, P.; Houk, K. N. Influence of molecular distortion upon reactivity and stereochemistry in nucleophilic addition to acetylenes. *J. Am. Chem. Soc.* **1979**, *101*, 1340-1343. (b) Houk, K. N.; Rondan, N. G.; Schleyer, P. v. R.; Kaufmann, E.; Clark, T.

Transition structures for additions of lithium hydride and methyllithium to ethylene and acetylene. *J. Am. Chem. Soc.* **1985**, *107*, 2821-2823.

[22] Liang, Y.; Mackey, J. L.; Lopez, S. A.; Liu, F.; Houk, K. N. Control and design of mutual orthogonality in bioorthogonal cycloadditions. *J. Am. Chem. Soc.* **2012**, *134*, 17904-17907.

[23] (a) de Jong, G. T.; Bickelhaupt, F. M. Transition-state energy and position along the reaction coordinate in an extended activation strain model. *ChemPhysChem* **2007**, *8*, 1170-1181.

(b) Fernandez, I.; Bickelhaupt, F. M. Alder-ene reaction: aromaticity and activation-strain analysis. *J. Comput. Chem.* **2012**, *33*, 509-516. (c) Hayden, A. E.; Houk, K. N. Transition state distortion energies correlate with activation energies of 1,4-dihydrogenations and Diels-Alder cycloadditions of aromatic molecules. *J. Am. Chem. Soc.* **2009**, *131*, 4084-4089.

[24] Houk, K. N. Frontier molecular orbital theory of cycloaddition reactions. *Acc. Chem. Res.* **1975**, *8*, 361-369.

[25] HOMO energies of trans-2-butene and trans-cyclooctene are calculated to be -9.3 and -9.0 eV, respectively, with HF/6-311+G(d,p)/M06-2X/6-31G(d).

CHAPTER 6: DIELS-ALDER REACTIVITIES OF CYCLOALKENES

6.1 Introduction to Cycloalkene Diels-Alder Reactions

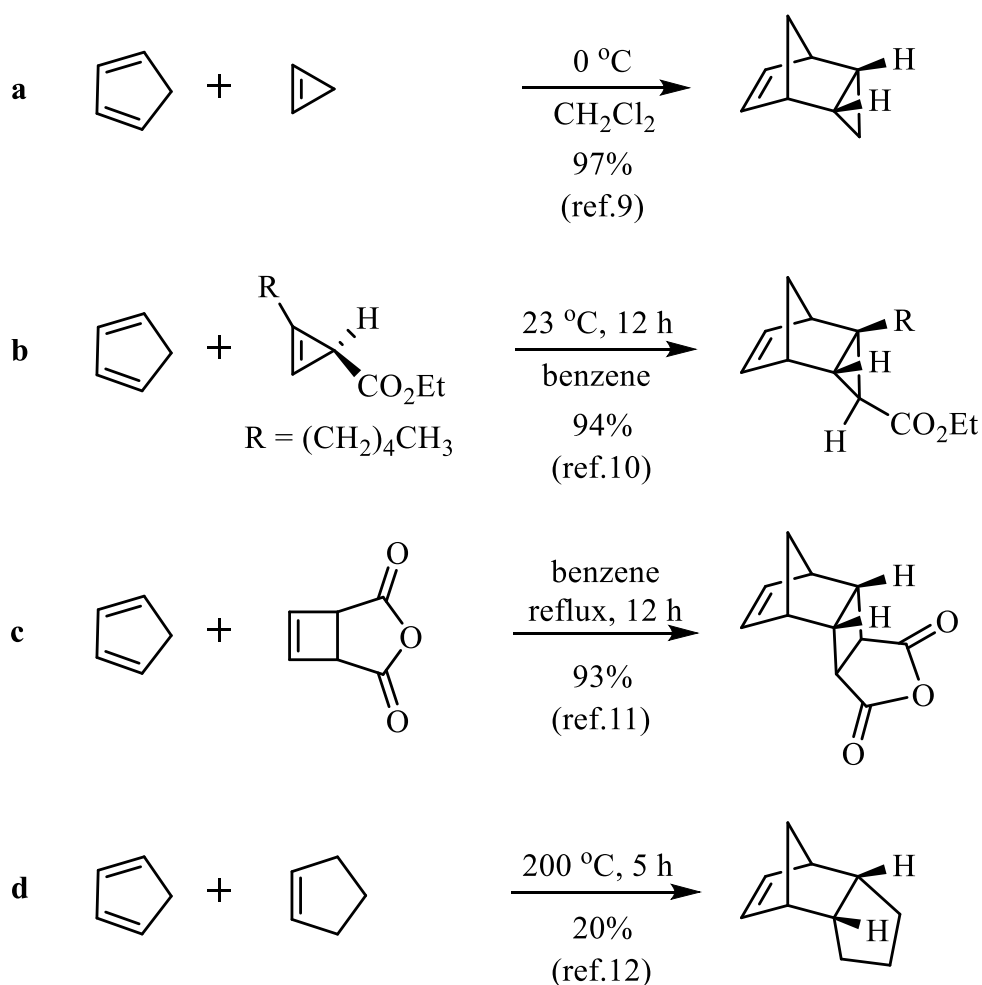
The high reactivity of cyclobutenone in the Diels-Alder reaction with cyclopentadiene was recently reported by Danishefsky and was analyzed by our group using the distortion/interaction model^[1] (or activation strain model^[2]). The reactivities of strained cycloalkenones were found to be a result of distortion-acceleration. The distortion energies — the energies to distort the reactants into the transition-state geometries — correlated well with the activation energies.^[3] By contrast, a poor correlation was observed between the activation energies and the reaction energies.

These trends in reactivity extend to cycloalkenes. Cyclopropenes are highly reactive dienophiles in Diels-Alder reactions even at low temperature,^[4] and have been applied in total synthesis^[5] and bioorthogonal labeling.^[6-8] Cyclobutenes and cyclopentenenes are less reactive than cyclopropenes in Diels-Alder cycloadditions. The differences in the reactivities of cycloalkenes are apparent when one compares the cycloaddition reactions of cyclopropenes, cyclobutenes, and cyclopentenenes with the same diene — cyclopentadiene (Scheme 6.1).^[9-12]

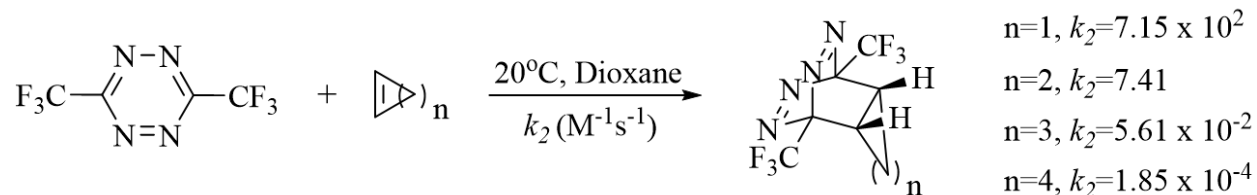
The Diels-Alder reaction of cyclopropene with cyclopentadiene takes place at 0 °C (Scheme 6.1a), and a cyclopropene derivative reacts with cyclopentadiene at room temperature (Scheme 6.1b). Both reactions give excellent yields of adducts. The cycloaddition of a cyclobutene derivative with cyclopentadiene requires higher temperature of 80 °C, but still gives a good yield (Scheme 6.1c). The reaction of cyclopentene with cyclopentadiene requires heating

to temperature as high as 200 °C and gives a low yield (Scheme 6.1d). The Diels-Alder reactivities of cycloalkenes with cyclopentadiene increase from cyclopentene to cyclopropene. Similar trends of reactivity were found in the inverse-electron-demand Diels-Alder reactions of a 1,2,4,5-tetrazine with cycloalkenes, reported by Sauer *et al.* (Scheme 6.2).^[13] The cycloaddition of cyclopropene and tetrazine is extremely fast, and an increase in the size of cycloalkenes by one roughly corresponds to a 100-fold decrease in the rate constant k_2 .

Scheme 6.1 Reactions of Cyclopentadiene with Cycloalkenes in Diels-Alder Reactions.



Scheme 6.2 Reactivities of Cycloalkenes in Diels-Alder Reactions with 3,6-Bis(trifluoromethyl)tetrazine.



The high reactivity of three and four membered cycloalkenes has been attributed to strain-release, which is a thermodynamic factor, especially in ring-opening reactions.^[14] However, the Diels-Alder reactions of cycloalkenes are different from ring-opening reactions in the sense that ring-strains are not fully released. If ring-strain accounts for the reactivity of cycloalkenes in Diels-Alder reactions, the difference between strain energy of cycloalkenes (reactants) and the strain energy of the corresponding cycloalkanes that represents the strain energy of the cycloadduct should correlate with the rate constants shown in Scheme 6.2. Table 6.1 shows the strain energies (*SE*) of cycloalkenes and cycloalkanes obtained from the heat of combustion^[15] and the strain energy differences (ΔSE).

Table 6.1 Strain Energies (*SE*, in kcal/mol) of cycloalkenes and cycloalkanes.

	<i>SE</i> (kcal/mol)		<i>SE</i> (kcal/mol)	ΔSE (kcal/mol)
Cyclopropene	55.2	Cyclopropane	27.5	27.7
Cyclobutene	28.4	Cyclobutane	26.5	1.9
Cyclopentene	4.1	Cyclopentane	6.2	-2.1
Cyclohexene	-0.3	Cyclohexane	0	-0.3

If strain-release were controlling reactivities, the orderly decrease in rate constants (k_2) from cyclopropene to cyclohexene should correspond to an orderly decrease in strain energy differences (ΔSE). However, the ΔSE values shown in Table 6.1 are erratic and really significant only for cyclopropene reactions. The Diels-Alder reactions of cyclopentene with 3,6-bis(trifluoromethyl)tetrazine is about 300 times faster than cyclohexene (Scheme 6.2), but strain energy changes would predict the opposite! Strain-release only influences the reactivity of cyclopropene and is not a general descriptor of reactivity. As we show later, cyclopropene is extraordinary in other ways as well.

Along the same line, the relationship between the heats of reaction and the activation enthalpies suggested by Brønsted, Marcus and Bell-Evans-Polanyi were tested in previous studies of cycloaddition reactions. In general, these quantities correlate much less well with the activation barriers than distortion energies for cycloaddition reactions.^[1,16-17]

Here we apply the distortion/interaction model to study the reactivities of cyclic alkenes including cyclopropene **5**, cyclobutene **6**, cyclopentene **7**, and cyclohexene **8**, and acyclic alkene (*cis*-2-butene **9**) towards a series of dienes. Cyclopentadiene **1** and the electron-deficient 1,3-bis(trifluoromethyl)tetrazine **4** were selected in the study so that the computational results could be compared to experimental data. To investigate the electronic effect of dienes, the electron-rich 1,3-dimethoxybutadiene **2**, which is a simplified model for Danishefsky's diene **2'**,^[18] and the less electron-deficient 3,6-dimethyltetrazine **3**, were also included in the study (Figure 6.1).

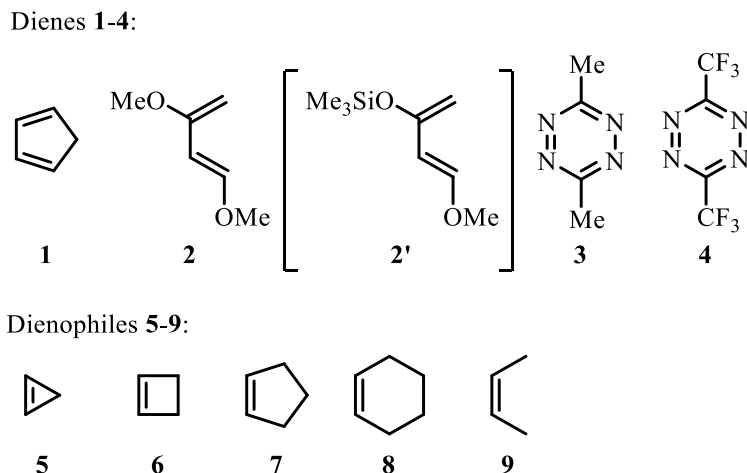


Figure 6.1 Dienes and dienophiles investigated.

6.2 Computational Methods

All density functional theory (DFT) calculations were performed with Gaussian 09.^[19] Geometry optimization of all the minima and transition states involved was carried out at the M06-2X level of theory with the 6-31G(d) basis set,^[20-21] which has been found to give relatively accurate energetics for cycloadditions.^[22-23] The vibrational frequencies were computed at the same level to check whether each optimized structure is an energy minimum or a transition state and to evaluate its zero-point vibrational energy (ZPVE) and thermal corrections at 298 K. A quasiharmonic correction was applied during the entropy calculation by setting all positive frequencies that are less than 100 cm^{-1} to 100 cm^{-1} .^[24-25] The frontier molecular orbitals (FMOs) and their energies were computed at the HF/6-311+G(d,p) level using the M06-2X/6-31G(d) geometries. Fragment distortion and interaction energies were computed at the M06-2X/6-31G(d) level. For the Diels-Alder reactions of 3,6-bis(trifluoromethyl)tetrazine, solvent effects in 1,4-dioxane were computed at the M06-2X/6-311+G(d,p) level using the gas-phase optimized structures. Solvation energies were evaluated by a self-consistent reaction field (SCRF) using the

CPCM model,^[26-27] where UFF radii were used. The scan of out-of-plane distortion dihedral angles of dienophiles **5-9** was performed by manually fixing the dihedral angles followed by an optimization at the M06-2X/6-31G(d) level. The formal atomic-hybridization states were obtained by a natural bond orbital (NBO)^[28] analysis at the M06-2X/6-31G(d) level.

6.3 Comparison of Reactivities

The *endo* transition-state structures calculated at the M06-2X/6-31G(d) level for the Diels-Alder reactions between dienes **1** and dienophiles **5-9** are shown in Figure 6.2, top row. The *exo*-transition state structures are provided in Figure 6.3. The *endo* transition states are favored over the *exo* transition states by 1.8 to 4.3 kcal/mol in terms of free energy. The preference for *endo* transition states of cyclopentadienes arise from favorable CH--- π interactions in the *endo* structures^[29] and unfavorable steric repulsion between methylene hydrogens on cyclopentadiene and alkenes in the *exo* structures. The activation enthalpy (ΔH^\ddagger), activation free energy (ΔG^\ddagger), and free energy of reaction (ΔG_{rxn}) are shown below each structure in kcal/mol in blue, red, and black, respectively. The activation enthalpies and free energies of the Diels-Alder reactions of cycloalkenes with cyclopentadiene increase from cyclopropene to cyclohexene, in agreement with the reported decrease in reactivities (Scheme 6.1). Cyclopropene readily undergoes Diels-Alder cycloaddition with cyclopentadiene at room temperature or below, which corresponds to a free energy barrier of about 20 kcal/mol. The reaction between cyclobutene derivative and cyclopentadiene must be performed in refluxing benzene (80 °C), in accord with the calculated higher barrier of 27.8 kcal/mol. The reaction of cyclopentene with cyclopentadiene requires even higher temperature of 200 °C, and accordingly the calculated barrier is larger, at 30.4 kcal/mol.

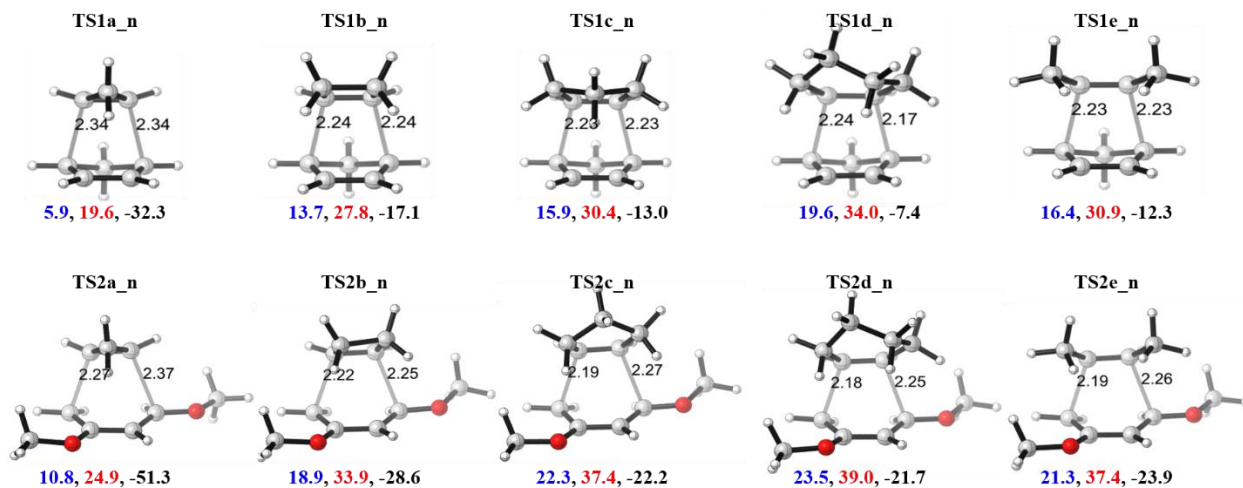


Figure 6.2 M06-2X/6-31G(d)-optimized *endo* transition structures for reactions of cyclopentadiene and 1,3-dimethoxybutadiene (forming CC bonds are labeled in Å; ΔH^\ddagger , ΔG^\ddagger , and ΔG_{rxn} are shown below the structures in blue, red, and black, respectively, in kcal/mol).

Cyclohexene is calculated to be less reactive still than cyclopentene with a higher barrier (34.0 kcal/mol) and the reactivity of acyclic *cis*-2-butene falls in between cyclopentene and cyclohexene. The computed free energies of reaction increase from cyclopropene to cyclohexene, in accordance with the increase in activation energies.

The lengths of forming bonds are marked on transition-state structures in Å in Figure 6.2. Cyclohexene has an asynchronous transition state in which the forming bond distances differ by 0.07 Å resulting from the unsymmetrical structure of cyclohexene (Figure 6.2, **TS1d_n**). The other four dienophiles undergo synchronous cycloadditions with identical forming bond distances. Cyclopropene has an extremely early transition state (Figure 6.2, **TS1a_n**), consistent with the anomalously high exergonicity of this reaction ($\Delta G_{rxn} = -32.3$ kcal/mol) whereas the other ΔG_{rxn} values range from -7.4 to -17.1 kcal/mol. This change in transition state position is in accordance with the Hammond's postulate. The forming bond distances are 0.1 Å larger than that

observed in the transition state of cyclobutene with cyclopentadiene (Figure 6.2, **TS1b_n**). The transition state of cyclopentene and *cis*-2-butene fall between cyclobutene and cyclohexene. The trend of early to late transition state as measured by forming bond distance is: cyclopropene \gg cyclobutene $>$ cyclopentene \approx *cis*-2-butene $>$ cyclohexene, but only cyclopropene varies much from the others.

1,3-Dimethoxybutadiene (diene **2**) is a reasonable analog to Danishefsky's diene, and has a similar free energy barrier in the Diels-Alder reaction with cyclobutene, as described in the footnote.^[18] The *endo* transition-state structures of the Diels-Alder reactions of diene **2** with dienophiles **5-9** are shown in Figure 6.2, bottom row (for each transition state, all possible conformations of the methoxy groups have been calculated and the one with the lowest energy is shown here). The Diels-Alder reactions of 1,3-dimethoxybutadiene with alkenes **5-9** have asynchronous transition states compared to reactions of cyclopentadiene (Figure 6.2, **TS2a_n** through **TS2e_n**). C4 has the largest HOMO coefficient and most negative charge; therefore it is the most nucleophilic carbon. In addition C4 is less hindered than C1, so the forming bond on C4 is 0.03-0.10 Å shorter than C1 in transition states. The *exo* transition-state structures are provided in Figure 6.3. The *endo* transition states are favored over the *exo* transition states by 0.4 to 1.7 kcal/mol. The preference for the *endo* transition states is less significant compared to that in the Diels-Alder reactions of cyclopentadiene, because there are less unfavorable steric repulsions in the *exo* transition states involving 1,3-dimethoxybutadiene. Similar trends of activation energies (ΔH^\ddagger and ΔG^\ddagger) and reaction energies (ΔG_{rxn}) are found as in the reactions of dienes **2** and **1** with dienophiles **5-9**. The most significant difference between diene **1** and **2** is in terms of reactivity: 1,3-dimethoxybutadiene has a higher free energy barrier of 5.4-8.6 kcal/mol than cyclopentadiene in the cycloaddition to the same alkene. The electron-rich diene is 10^3 - 10^6 less

reactive than cyclopentadiene, presumably due to the much larger distortion energy of the acyclic diene, as described in detail later. The trend of early/late transition states and reaction barriers with **2** are the same as those observed in the Diels-Alder reactions of alkenes with cyclopentadiene, **1**.

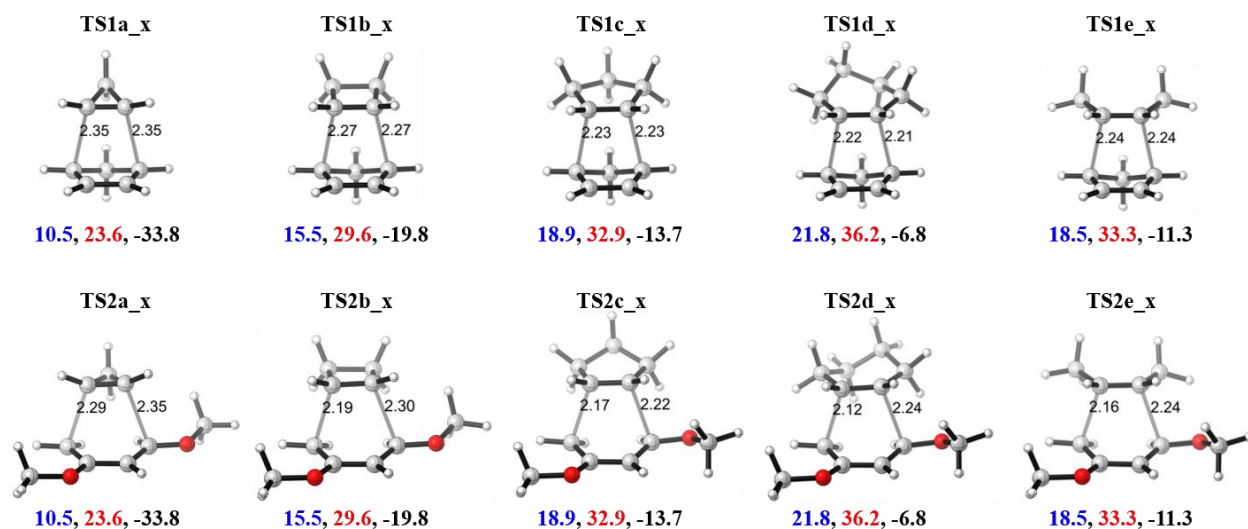


Figure 6.3 M06-2X/6-31G(d)-optimized *exo* transition structures for reactions of cyclopentadiene and 1,3-dimethoxybutadiene (forming CC bonds are labeled in Å; ΔH^\ddagger , ΔG^\ddagger , and ΔG_{rxn} are shown below the structures in blue, red, and black, respectively, in kcal/mol).

To understand this trend of Diels-Alder reactivity, each transition structure was separated into two fragments (the distorted dienophile and diene), followed by single point energy calculations on each fragment. The energy differences between the distorted structures and optimized ground-state structures are the distortion energy of dienophile ($\Delta E^\ddagger_{dist_2e}$) and diene ($\Delta E^\ddagger_{dist_4e}$), respectively. The interaction energy (ΔE^\ddagger_{int}) is the difference between the activation energy (ΔE^\ddagger_{act}) and the total distortion energy ($\Delta E^\ddagger_{dist} = \Delta E^\ddagger_{dist_2e} + \Delta E^\ddagger_{dist_4e}$). The energy

components for each *endo* transition-state structure are plotted in Figure 6.4 (the analysis of the *exo* transition states is shown in Figure 6.5).

Figure 6.4a shows the distortion/interaction analysis of the five Diels-Alder reactions with cyclopentadiene. The lengths of the green arrows represent the distortion energies of dienophiles ($\Delta E_{dist_2e}^\ddagger$), which increase from 6 to 12 kcal/mol as the dienophile changes from cyclopropene to cyclohexene, while *cis*-2-butene falls in between cyclopentene and cyclohexene. The lengths of the blue arrows represent the distortion energies of cyclopentadienes ($\Delta E_{dist_4e}^\ddagger$). There is an increase in $\Delta E_{dist_4e}^\ddagger$ as the dienophile changes from cyclopropene to cyclohexene, consistent with the trend of early/late transition states. The geometry of early transition state is closer to the geometry of ground state, making the distortion energy smaller, and *vice versa*. The total length of blue and green arrows equals the total distortion energy (ΔE_{dist}^\ddagger). The interaction energies (ΔE_{int}^\ddagger) are represented by the red arrows pointing down starting from the values of total distortion energies. The interaction energy remains essentially constant across the series, ranging only from -11.0 to -10.5 kcal/mol. The distortion energies determine reactivities. Similar trends of distortion and activation energy are found in the distortion/interaction analysis of reactions of diene **2** in Figure 6.4b. A significant difference between Figure 6.4b and Figure 6.4a is that 1,3-dimethoxybutadiene exhibits larger $\Delta E_{dist_4e}^\ddagger$ than cyclopentadiene, resulting in larger reaction barriers. Details are discussed later in the paper.

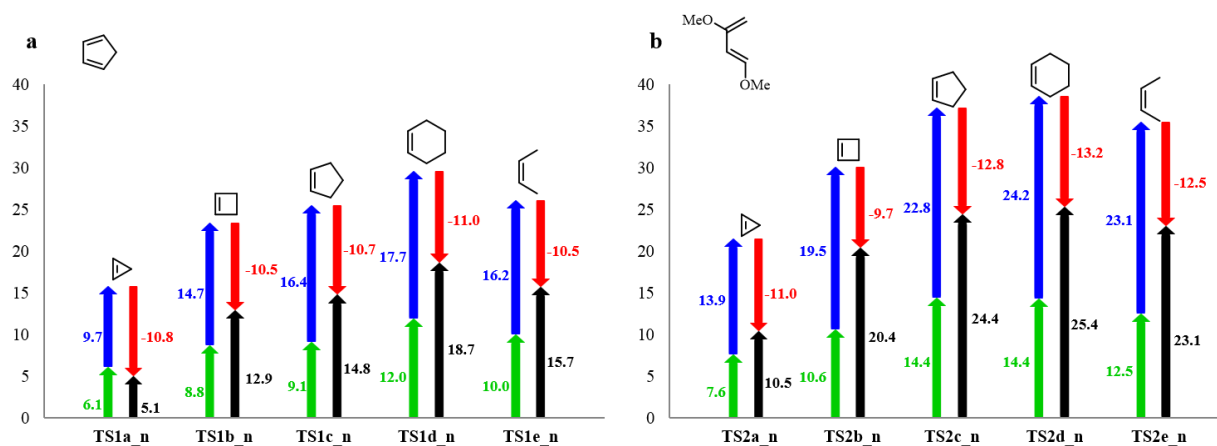


Figure 6.4. Graph of distortion, interaction, and activation energies for *endo* reactions of dienes **1** and **2** with dienophiles **5-9** (green: distortion energy of dienophile, blue: distortion energy of diene, red: interaction energy, black: activation energy, in kcal/mol).

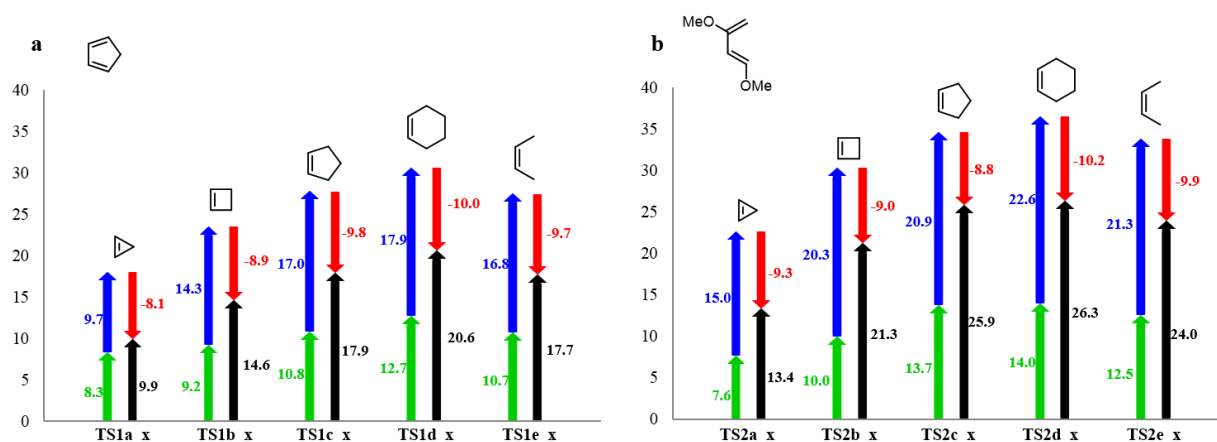


Figure 6.5 Graph of distortion, interaction, and activation energies for *exo* reactions of dienes **1** and **2** with dienophiles **5-9** (green: distortion energy of dienophile, blue: distortion energy of diene, red: interaction energy, black: activation energy, in kcal/mol).

Figure 6.6 shows the relationship between activation energy (ΔE_{act}^\ddagger) and distortion energy ($\Delta E_{dist_{2e}}^\ddagger$ and ΔE_{dist}^\ddagger) and ΔE_{act}^\ddagger with the reaction energy (ΔE_{rxn}). The blue and red dots on the plot are for the Diels-Alder reactions of dienophiles **5-9** with diene **1** and **2**, respectively. For

reactions of a given diene (Figure 6.6, either red or blue plot), both distortion energies and reaction energies correlate well with activation energies, R^2 values range from 0.92 to 1.00. Taking the two sets of reactions together, the correlation between activation energy and reaction energy disappears ($R^2=0.16$). In particular, the Diels-Alder reactions of cyclopentadiene are over 10 kcal/mol less exothermic than 1,3-dimethoxybutadiene due to the less stable tricyclic adducts from the reactions, but the activation barriers are over 5 kcal/mol lower than the corresponding reactions of 1,3-dimethoxybutadiene. The correlation between distortion energy and activation energy is much better, with $R^2=0.94$ and 0.98 (Figure 6.6, black lines).

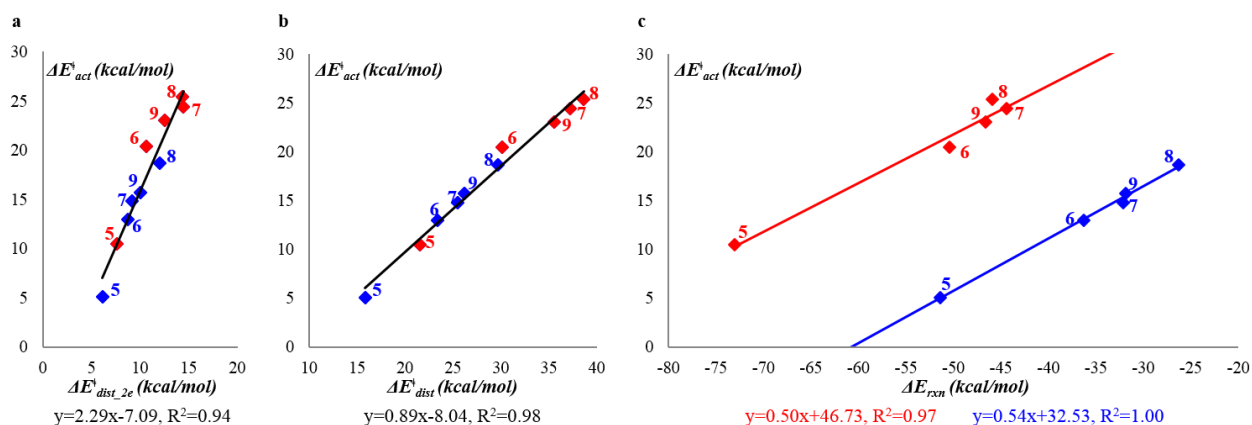


Figure 6.6 Plots of activation energy (ΔE_{act}^\ddagger) versus (a) distortion energy of dienophile ($\Delta E_{dist_2e}^\ddagger$), (b) total distortion energy (ΔE_{dist}^\ddagger), and (c) reaction energy (ΔE_{rxn}). Blue: cyclopentadienes; red: 1,3-dimethoxybutadiene; black: overall correlation of all ten reactions. Linear correlation functions are shown below each plot in corresponding colors. The numbers shown besides each data point refer to the dienophiles involved in the corresponding reactions.

Comparing Figures 6.4a and 6.4b, the average interaction energy (ΔE_{int}^\ddagger) in Figure 6.4b is 1.1 kcal/mol larger than in Figure 6.4a due to the smaller HOMO-LUMO gap involving diene **2** (see later discussion in the paper). However, the acyclic diene **2** exhibits large distortion energies

due to the conformational change from *s-trans* to *s-cis* ($\Delta E = 2.2$ kcal/mol) and the steric repulsion of terminal hydrogen atoms in the transition states. Cyclopentadiene is pre-distorted towards the transition state geometry and requires very little distortion energy, only bending and some bond length changes. The average distortion energy of 1,3-dimethoxybutadiene is 5.8 kcal/mol higher than of cyclopentadiene (Figure 6.4). The extra cost of distortion energies of 1,3-dimethoxybutadiene overtakes its advantage in interaction energies, resulting in a higher activation barrier of about 5 kcal/mol for each reaction compared with cyclopentadiene.

Figure 6.7 shows the transition-state structures calculated at M06-2X/6-31G(d) level for the inverse-electron-demand Diels-Alder reactions between dienes **3-4** and dienophiles **5-9**. The activation enthalpy (ΔH^\ddagger), activation free energy (ΔG^\ddagger), and free energy of reaction (ΔG_{rxn}) are shown below each structure in kcal/mol in blue, red, and black, respectively. The lengths of forming bonds are marked on transition-state structures in Å. The reactions of both tetrazines and cyclopropene have very early transition states. Along the series of dienophiles changing from cyclopropene to cyclohexene, shorter forming bonds are observed. The more electrophilic tetrazine **4** has an earlier transition state than tetrazine **3** for each reaction. Each transition state in the bottom row in Figure 6.7 has longer forming bonds of 0.1 Å and a lower free energy barrier of 10 kcal/mol than the corresponding transition state in the top row.

The activation free energies in the 1,4-dioxane solution ΔG_{sol}^\ddagger for reactions between diene **4** and dienophiles **5-8** have been calculated. The rate constants derived from calculated barriers by transition state theory correlate well with the rate constants measured in experiments (Scheme 6.2), although theory consistently underestimates the barrier by 1-2 kcal/mol. The activation free energies in other solvents, including cyclohexane, dichloromethane, acetonitrile, and water, have

been calculated as well (Table 6.2). The activation free energies in solution are higher than the gas phase results by 2-3 kcal/mol, because solvents stabilize tetrazine significantly.

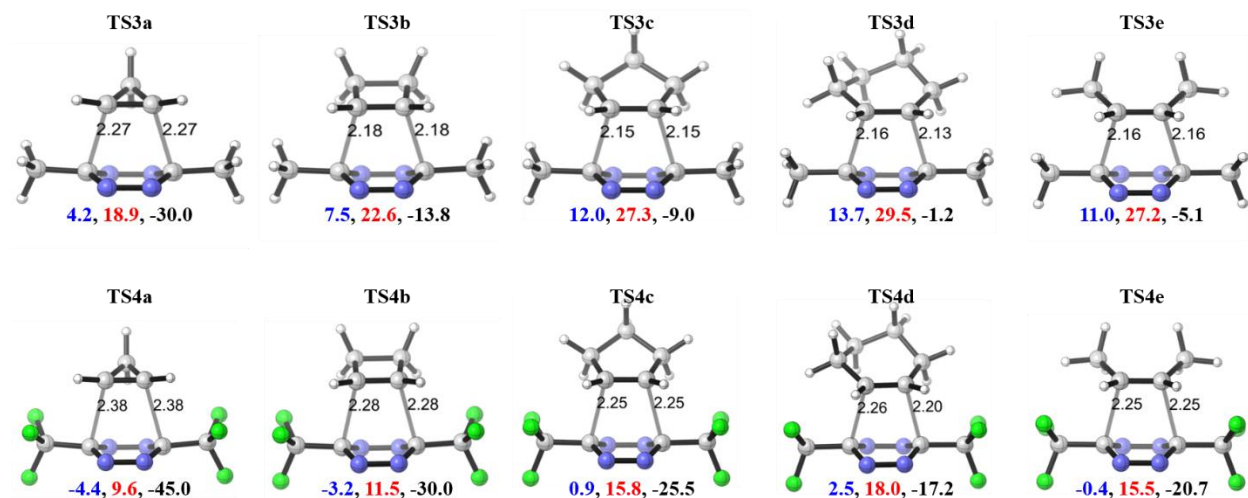


Figure 6.7 M06-2X/6-31G(d)-optimized transition structures for reactions of dienes **3** and **4** (forming CC bonds are labeled in Å; ΔH^\ddagger , ΔG^\ddagger , and ΔG_{rxn} are shown below the structures in blue, red, and black, respectively, in kcal/mol).

Table 6.2 Calculated activation free energies and rate constants in comparison with experimental data.

	ΔG^\ddagger_{cal} (kcal/mol)	ΔG^\ddagger_{exp} (kcal/mol)	k_2_{cal} ($M^{-1}s^{-1}$)	k_2_{exp} ($M^{-1}s^{-1}$)	ΔG^\ddagger_{gas} (kcal/mol)	ΔG^\ddagger_{Cy} (kcal/mol)	$\Delta G^\ddagger_{CH_2Cl_2}$ (kcal/mol)	$\Delta G^\ddagger_{CH_3CN}$ (kcal/mol)	$\Delta G^\ddagger_{H_2O}$ (kcal/mol)
TS4a	12.1	13.6	9.22×10^3	7.15×10^2	9.6	12.0	12.8	12.9	13.0
TS4b	14.1	16.4	3.43×10^2	7.41	11.5	14.0	14.6	14.7	14.7
TS4c	18.4	19.3	2.44×10^{-1}	5.61×10^{-2}	15.8	18.3	18.8	18.9	19.0
TS4d	20.6	22.7	6.66×10^{-3}	1.85×10^{-4}	18.0	20.5	20.9	21.0	21.0

The distortion/interaction analysis for the inverse-electron-demand Diels-Alder reactions is shown in Figure 6.8. Leaving out the reaction between cyclopropene and 3,6-dimethyltetrazine, which has an extremely early transition state, the interaction energies of the other four reactions

fall in the small range of -21.6 to -18.0 kcal/mol. The activation barriers increase along with the distortion energies from cyclobutene to cyclohexene. In other words, the reactivity differences of cycloalkenes in Diels-Alder reactions with 3,6-dimethyltetrazine originate from the distortion energy differences. Figure 6.8b shows the same trend of distortion and interaction energies. The activation barriers are much lower than Figure 6.8a due to stronger interaction energies, which result from smaller HOMO-LUMO gaps that are discussed later in the paper. Both the distortion energy and reaction energy correlate linearly with the activation energy for a single tetrazine (Figure 6.9), R^2 values range from 0.74 to 1.00. The correlation between the distortion energy and the activation energy has a slight advantage over that of the reaction energy. Taking the two sets of reactions together, the correlations between distortion energies and activation energies are abolished due to the huge difference in interaction energies of diene **3** and **4**. The interaction energies of diene **4** are 3.9 to 7.6 kcal/mol stronger (more negative) than diene **3** in reactions with each dienophile, resulting in low-lying data points on the distortion-activation plot.

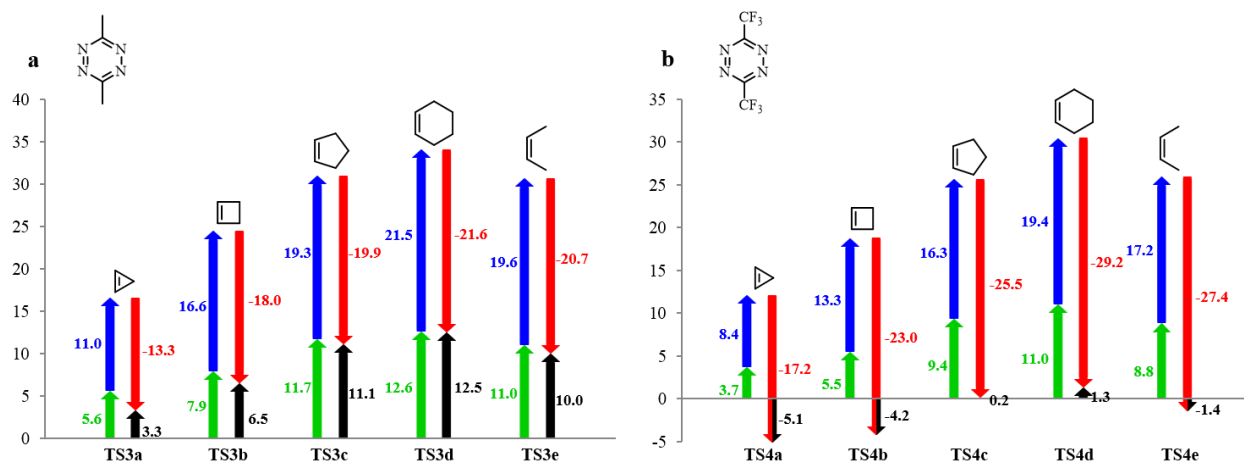


Figure 6.8 Graph of distortion, interaction, and activation energies for reactions of dienes **3** and **4** with dienophiles **5-9** (green: distortion energy of dienophile, blue: distortion energy of diene, red: interaction energy, black: activation energy, in kcal/mol).

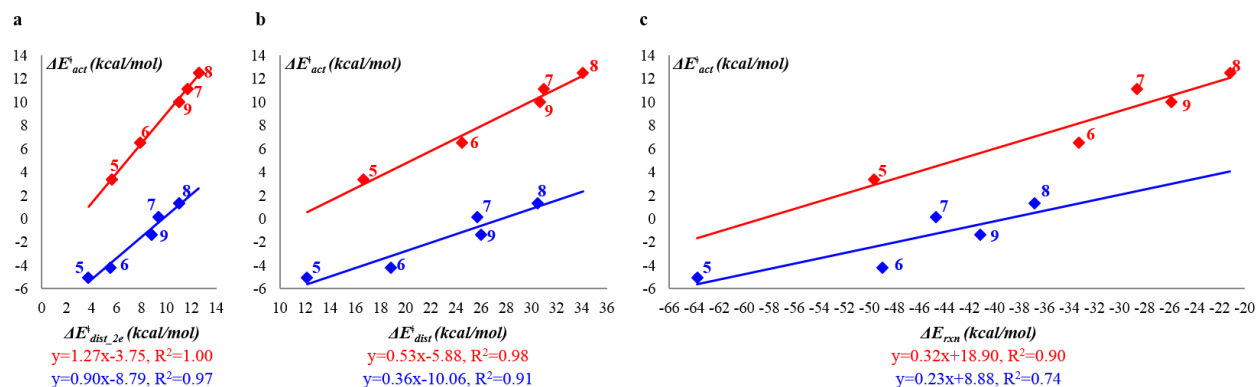


Figure 6.9 Plots of activation energy ($\Delta E_{act}^{\ddagger}$) versus (a) distortion energy of dienophile ($\Delta E_{dist_2e}^{\ddagger}$), (b) total distortion energy ($\Delta E_{dist}^{\ddagger}$), and (c) reaction energy (ΔE_{rxn}). Blue: 3,6-bis(trifluoromethyl)tetrazine; red: 3,6-dimethyltetrazine. Linear correlation functions are shown below each plot in corresponding colors. The numbers shown besides each data point refer to the dienophiles involved in the corresponding reactions.

To better understand the interaction energy differences, the energies of relevant frontier orbitals were calculated at HF/6-311+G(d,p) level based on M06-2X/6-31G(d)-optimized reactants or transition-state geometries, because Kohn-Sham orbitals often provide poor estimates of ionization potentials of simple organic molecules, and the medium size 6-31G(d) basis set often gives inaccurate unoccupied orbital eigenvalues.^[30] As shown in Figure 6.10, the left column of each region shows the HOMOs and LUMOs of ground-state reactants, including the five alkenes and four dienes; the right column of each region shows the HOMOs and LUMOs of corresponding reactants distorted to the transition-state geometries of the reactions of dienes **1-4** and *cis*-2-butene, *i.e.* **TS1e_n**, **TS2e_n**, **TS3e** and **TS4e**.

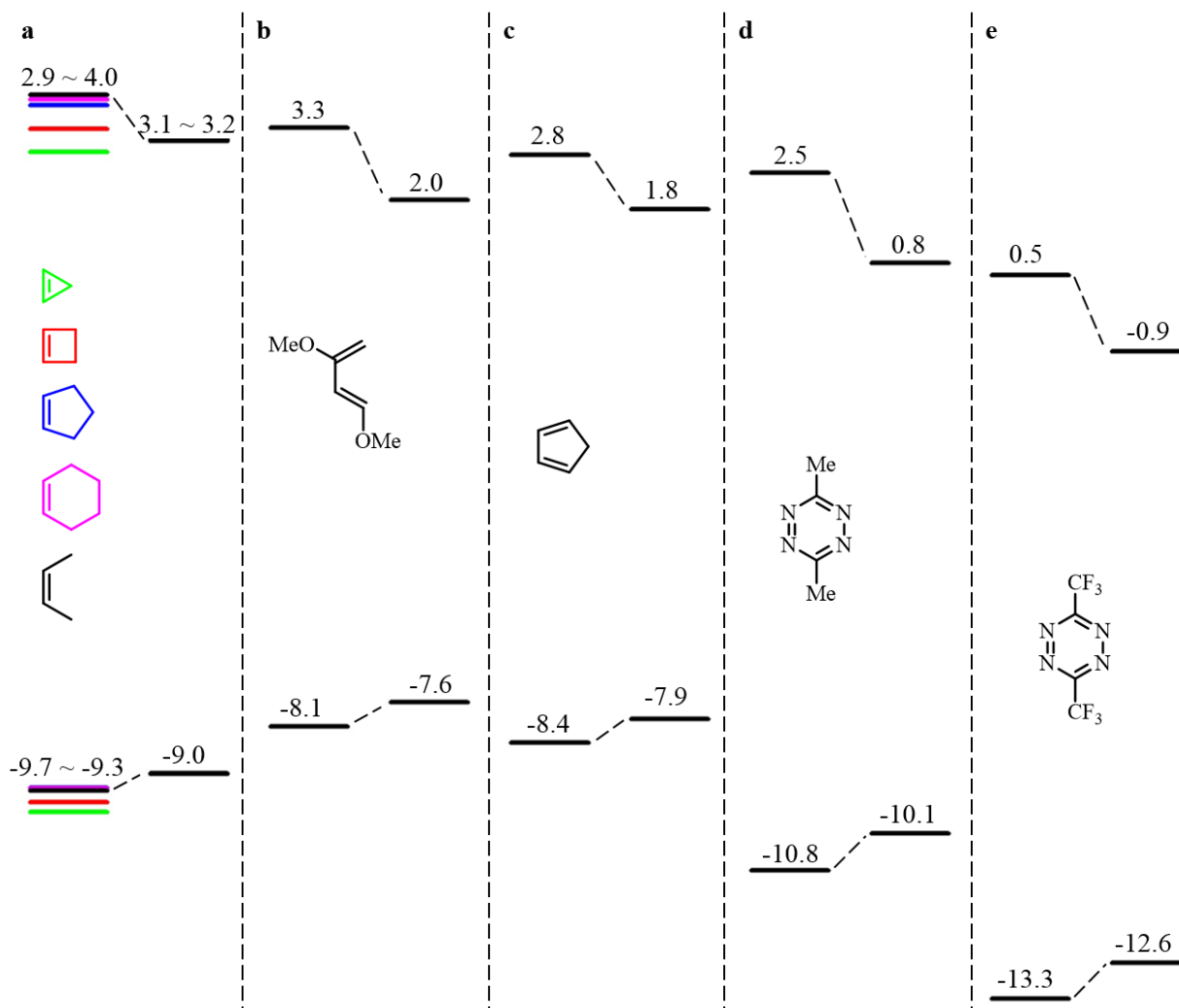


Figure 6.10 FMO energies for (a) alkenes (cyclopropene, cyclobutene, cyclopentene, cyclohexene, and *cis*-2-butene) and (b-e) dienes (1,3-dimethoxybutadiene, cyclopentadienes, 3,6-dimethyltetrazine, and 3,6-bis(trifluoromethyl)tetrazine). HF/6-311+G(d,p)//M06-2X/6-31G(d)-computed orbital energies are shown in eV. The dashed lines indicate the change from ground state reactant (left in each column) to distorted geometry in transition state (right in each column).

Calculations indicate that cycloalkenes have very similar HOMO and LUMO energies with the increase of ring size (Figure 6.10a). The HOMO energies range from -9.7 to -9.3 eV and the LUMO energies range from 2.9 to 4.0 eV. These data are close to experimental values

measured from photoelectron spectroscopy (cyclopropene, -9.86 eV; cyclobutene, -9.59 eV; cyclopentene, -9.18 eV; cyclohexene, -8.94 eV)^[31] and the electron affinities established from electron transmission spectroscopy (cyclopropene, 1.73 eV; cyclobutene, 2.00 eV; cyclopentene, 2.14 eV; cyclohexene, 2.13 eV).^[32] The HOMO and LUMO energies of various dienes decrease from the most electron-rich 1,3-dimethoxybutadiene to the most electron-deficient 3,6-bis(trifluoromethyl)tetrazine (Figure 6.10b-e). In normal Diels-Alder reactions, the HOMO of diene interacts with the LUMO of the dienophile and smaller HOMO-LUMO gap gives better interaction. Since the HOMO of 1,3-dimethoxybutadiene is 0.2 eV higher than cyclopentadiene (Figure 6.11), it is expected that the interaction energies in Diels-Alder reactions of 1,3-dimethoxybutadiene are stronger than cyclopentadiene as discussed in Figure 6.4. In inverse-electron-demand Diels-Alder reactions, which involve the interaction between HOMOs of dienophiles and the LUMOs of dienes, the more electron-deficient 3,6-bis(trifluoromethyl)tetrazine has stronger interaction energies because the interacting unoccupied orbital is 2.0 eV lower than that of 3,6-dimethyltetrazine (Figure 6.11).

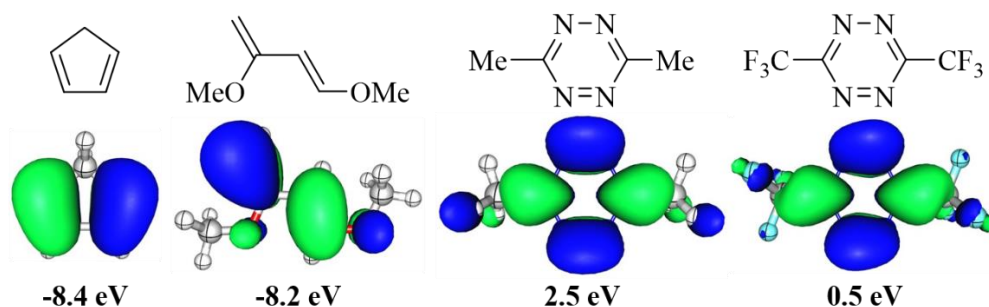


Figure 6.11 Important frontier molecular orbitals involved in the Diels-Alder reactions of dienes **1-4**: the HOMOs of cyclopentadiene and 1,3-dimethoxybutadiene and the low-lying vacant orbitals of 3,6-dimethyltetrazine and 3,6-bis(trifluoromethyl)tetrazine.

As the reactants are distorted into transition-state geometry, a decrease in LUMO energy by about 1 eV and an increase in HOMO energy by about 0.5 eV are observed (right columns of Figure 6.10a-e). The HOMO-LUMO gap shrinks by about 1.5 eV compared to that in ground-state reactants. The distortion of reactants facilitates the interaction between molecular orbitals of interest, namely the π and π^* orbitals.

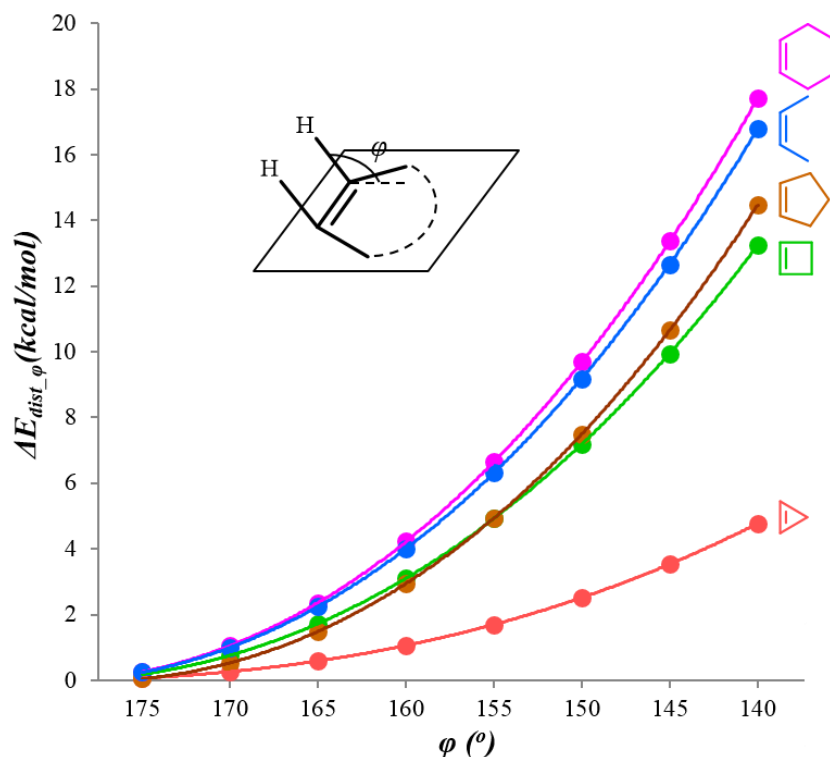


Figure 6.12. Plot of distortion energy (ΔE_{dist_ϕ}) versus out-of-plane distortion angle (ϕ) for dienophiles **5-9**. Red: cyclopropene; green: cyclobutene; brown: cyclopentene; purple: cyclohexene; blue: *cis*-2-butene.

The Diels-Alder relative reactivities of different alkenes originate from the distortion energies. The trends of distortion energies are confirmed by a scan of out-of-plane distortion, which is a prominent distortion in the transition state (Figure 6.12). For each alkene, the out-of-

plane dihedral angles, which are around 180° for ground-state structure and 140°-155° for transition-state structure, were gradually changed from 175° to 140° at intervals of 5°. The energy difference between optimized structure with fixed dihedral angles and the ground-state structure is called distortion energy of the dihedral angle (ΔE_{dist_φ}). Figure 5.10 shows the plot of ΔE_{dist_φ} versus the dihedral angle φ .

For each alkene, the distortion energy increases as the dihedral angle decreases. At a certain dihedral angle within the transition zone ($\varphi = 140^\circ$ - 155°), the distortion energy of cyclopropene is significantly lower than other dienophiles, and as size increase from cyclopropene to cyclohexene, the distortion energy increases. This trend is consistent with the Diels-Alder reactivities of different alkenes discussed in this paper. The increase in distortion energy of dihedral angles indicates an increase of out-of-plane bending force constants from cyclopropene to cyclohexene, which is confirmed by the C-H out-of-plane vibration frequency observed in IR spectra of cycloalkenes (γ -CH out-of-plane bend of cycloalkenes **5-8** are 570 cm⁻¹,^[33] 635 cm⁻¹,^[34] 695 cm⁻¹,^[35] and 718 cm⁻¹,^[36] respectively). This trend in bending force constants is in accord with the change of hybridization states of the olefinic carbons suggested by the natural bond orbital (NBO) analysis. The corresponding hybridization states in cycloalkenes **5-8** (cyclopropene to cyclohexene) are sp^{1.54}, sp^{1.92}, sp^{2.17}, and sp^{2.43}, respectively.

The reactivities of cycloalkenes as dienophiles are controlled by distortion energies. Cyclopropene is more reactive than other alkenes because of the low distortion energy to achieve transition-state geometry. A larger degree of s character of the olefinic carbon results in relatively less sensitivity to out-of-plane bending, leading to a smaller force constant and distortion energy. Distortion energy increases from cyclopropene to cyclohexene, resulting in a

decrease in Diels-Alder reactivities along the series. The reactivities of different dienes are controlled by both distortion energy and interaction energy. Acyclic electron-rich 1,3-dimethoxybutadiene has stronger interaction energies than cyclopentadiene, but the extra distortion energies resulting from the *s-trans* to *s-cis* transformation and steric repulsion between terminal hydrogens of 1,3-dimethoxybutadiene are the dominant factor. Cyclopentadiene is more reactive than 1,3-dimethoxybutadiene, because it is pre-distorted towards transition state geometries and requires less distortion energies. Tetrazines undergo inverse-electron-demand Diels-Alder reactions with alkenes. The more electron-deficient 3,6-bis(trifluoromethyl)tetrazine has stronger interaction energies due to its low-lying π^* orbital. In addition, 3,6-bis(trifluoromethyl)tetrazine has earlier transition states than 3,6-dimethyltetrazine, resulting in smaller distortion energies.

6.4 References

- [1] Paton, R. S.; Kim, S.; Ross, A. G.; Danishefsky, S. J.; Houk, K. N. Experimental Diels-Alder reactivities of cycloalkenones and cyclic dienes explained through transition-state distortion energies. *Angew. Chem., Int. Ed.* **2011**, *50*, 10366-10368.
- [2] van Zeist, W.-J.; Bickelhaupt, F. M. The activation strain model of chemical reactivity. *Org. Biomol. Chem.* **2010**, *8*, 3118-3127.
- [3] (a) Ess, D. H.; Houk, K. N. Distortion/interaction energy control of 1,3-dipolar cycloaddition reactivity. *J. Am. Chem. Soc.* **2007**, *129*, 10646-10647. (b) Ess, D. H.; Houk, K. N. Theory of 1,3-dipolar cycloadditions: distortion/interaction and frontier molecular orbital models. *J. Am. Chem. Soc.* **2008**, *130*, 10187-10198. (c) Fernández, I.; Cossío, F. P.; Bickelhaupt, F. M. Aromaticity and activation strain analysis of [3+2] cycloaddition reactions between group 14

heteroallenes and triple bonds. *J. Org. Chem.* **2011**, *76*, 2310-2314. (d) Lan, Y.; Wheeler, S. E.; Houk, K. N. Extraordinary difference in reactivity of ozone (OOO) and sulfur dioxide (OSO): a theoretical study. *J. Chem. Theory Comput.* **2011**, *7*, 2104-2111. (e) Fernandez, I.; Bickelhaupt, F. M. Alder-ene reaction: aromaticity and activation-strain analysis. *J. Comput. Chem.* **2012**, *33*, 509-516. (f) Gordon, C. G.; Mackey, J. L.; Jewett, J. C.; Sletten, E. M.; Houk, K. N.; Bertozzi, C. R. Reactivity of biarylazacyclooctynones in copper-free click chemistry. *J. Am. Chem. Soc.* **2012**, *134*, 9199-9208. (g) Liang, Y.; Mackey, J. L.; Lopez, S. A.; Liu, F.; Houk, K. N. Control and design of mutual orthogonality in bioorthogonal cycloadditions. *J. Am. Chem. Soc.* **2012**, *134*, 17904-17907. (h) Fernández, I.; Bickelhaupt, F. M.; Cossío, F. P. Type-I dyotropic reactions: understanding trends in barriers. *Chem. Eur. J.* **2012**, *18*, 12395-12403. (i) Lopez, S. A.; Houk, K. N. Alkene distortion energies and torsional effects control reactivities, and stereoselectivities of azide cycloadditions to norbornene and substituted norbornenes. *J. Org. Chem.* **2013**, *78*, 1778-1783. (j) Fernández, I.; Sola, M.; Bickelhaupt, F. M. Why do cycloaddition reactions involving C₆₀ prefer [6,6] over [5,6] bonds? *Chem. Eur. J.* **2013**, *19*, 7416-7422.

[4] (a) Rubin, M.; Rubina, M.; Gevorgyan, V. Recent advances in cyclopropene chemistry. *Synthesis* **2006**, 1221-1245. (b) Zhu, Z.-B.; Wei, Y.; Shi, M. Recent developments of cyclopropene chemistry. *Chem. Soc. Rev.* **2011**, *40*, 5534-5563.

[5] Wilson, M. R.; Taylor, R. E. Strained alkenes in natural product synthesis. *Angew. Chem., Int. Ed.* **2013**, *52*, 4078-4087.

[6] (a) Patterson, D. M.; Nazarova, L. A.; Xie, B.; Kamber, D. N.; Prescher, J. A. Functionalized cyclopropenes as bioorthogonal chemical reporters. *J. Am. Chem. Soc.* **2012**, *134*, 18638-18643. (b) Kamber, D. N.; Nazarova, L. A.; Liang, Y.; Lopez, S. A.; Patterson, D. M.; Shih, H.-W.;

Houk, K. N. Prescher, J. A. Isomeric cyclopropenes exhibit unique bioorthogonal reactivities. *J. Am. Chem. Soc.* **2013**, *135*, 13680-13683.

[7] (a) Yang, J.; Seckute, J.; Cole, C. M.; Devaraj, N. K. Live-cell imaging of cyclopropene tags with fluorogenic tetrazine cycloadditions. *Angew. Chem. Int. Ed.* **2012**, *51*, 7476-7479. (b) Cole, C. M.; Yang, J.; Šečkute, J.; Devaraj, N. K. Fluorescent live-cell imaging of metabolically incorporated unnatural cyclopropene-mannosamine derivatives. *ChemBioChem* **2013**, *14*, 205-208. (c) Šečkute, J.; Yang, J.; Devaraj, N. K. Rapid oligonucleotide-templated fluorogenic tetrazine ligations. *Nucleic Acids Res.* **2013**, *41*, e148.

[8] Yu, Z.; Pan, Y.; Wang, Z.; Wang, J.; Lin, Q. Genetically encoded cyclopropene directs rapid, photoclick-chemistry-mediated protein labeling in mammalian cells. *Angew. Chem., Int. Ed.* **2012**, *51*, 10600-10604.

[9] Wiberg, K. B.; Bartley, W. J. J Cyclopropene. V. Some reactions of cyclopropene. *J. Am. Chem. Soc.* **1960**, *82*, 6375-6380.

[10] Lou, Y.; Horikawa, M.; Kloster, R. A.; Hawryluk, N. A.; Corey, E. J. A new chiral Rh(II) catalyst for enantioselective [2+1]-cycloaddition. Mechanistic implications and applications. *J. Am. Chem. Soc.* **2004**, *126*, 8916-8918.

[11] Cadogan, J. I. G.; Cameron, D. K.; Gosney, I.; Tinley, E. J.; Wyse, S. J.; Amaro, A. Applications of 3-oxabicyclo[3.2.0]hept-6-ene-2,4-dione (cyclobut-3-ene-1,2-dicarboxylic anhydride) as an acetylene equivalent in cycloadditions. *J. Chem. Soc., Perkin Trans. 1*, **1991**, 2081-2087.

[12] Brúson, H. A.; Riener, T. W. The chemistry of dicyclopentadiene. I. Hydration and rearrangement. *J. Am. Chem. Soc.* **1945**, *67*, 723-728.

[13] Thalhammer, F.; Wallfahrer, U.; Sauer, J. Reaktivität einfacher offenkettiger und cyclischer dienophile bei Diels-Alder-reaktionen mit inversem elektronenbedarf. *Tetrahedron Lett.* **1990**, *31*, 6851-6854.

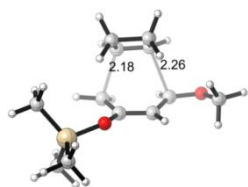
[14] Wolk, J. L.; Rozental, E.; Basch, H.; Hoz, S. Strain energy release and intrinsic barriers in internal nucleophilic reactions. *J. Org. Chem.* **2006**, *71*, 3876-3879.

[15] Roberts, J. D.; Caserio, M. C. *Basic Principles of Organic Chemistry*, 2nd ed.; W. A. Benjamin, Inc.: Menlo Park, CA, 1997.

[16] Schoenebeck, F.; Ess, D. H.; Jones, G. O.; Houk, K. N. Reactivity and regioselectivity in 1,3-dipolar cycloadditions of azides to strained alkynes and alkenes: a computational study. *J. Am. Chem. Soc.* **2009**, *131*, 8121-8133.

[17] Hayden, A. E.; Houk, K. N. Transition state distortion energies correlate with activation energies of 1,4-dihydrogenations and Diels-Alder cycloadditions of aromatic molecules. *J. Am. Chem. Soc.* **2009**, *131*, 4084-4089

[18] The calculated activation free energies for cycloadditions of 1,3-dimethoxybutadiene **2** and Danishefsky's diene **2'** with cyclobutene are 35.2 and 35.1 kcal/mol, respectively. The transition-state structure involving **2'** is shown below.



- [19] Frisch, M. J.; et al. *Gaussian 09*, revision C.01; Gaussian, Inc.: Wallingford, CT, 2010.
- [20] Zhao, Y.; Truhlar, D. G. The M06 suite of density functionals for main group thermochemistry, thermochemical kinetics, noncovalent interactions, excited states, and transition elements: two new functionals and systematic testing of four M06-class functionals and 12 other functionals. *Theor. Chem. Acc.* **2008**, *120*, 215-241.
- [21] Zhao, Y.; Truhlar, D. G. Density functionals with broad applicability in chemistry. *Acc. Chem. Res.* **2008**, *41*, 157-167.
- [22] Lan, Y.; Zou, L.; Cao, Y.; Houk, K. N. Computational methods to calculate accurate activation and reaction energies of 1,3-dipolar cycloadditions of 24 1,3-dipoles. *J. Phys. Chem. A* **2011**, *115*, 13906-13920.
- [23] Paton, R. S.; Mackey, J. L.; Kim, W. H.; Lee, J. H.; Danishefsky, S. J.; Houk, K. N. Origins of stereoselectivity in the *trans* Diels–Alder paradigm. *J. Am. Chem. Soc.* **2010**, *132*, 9335-9340.
- [24] Zhao, Y.; Truhlar, D. G. Computational characterization and modeling of buckyball tweezers: density functional study of concave–convex $\pi\cdots\pi$ interactions. *Phys. Chem. Chem. Phys.* **2008**, *10*, 2813-2818.
- [25] Ribeiro, R. F.; Marenich, A. V.; Cramer, C. J.; Truhlar, D. G. Use of solution-phase vibrational frequencies in continuum models for the free energy of solvation. *J. Phys. Chem. B* **2011**, *115*, 14556-14562.
- [26] Barone, V.; Cossi, M. Quantum calculation of molecular energies and energy gradients in solution by a conductor solvent model. *J. Phys. Chem. A* **1998**, *102*, 1995-2001.

- [27] Cossi, M.; Rega, N.; Scalmani, G.; Barone, V. Energies, structures, and electronic properties of molecules in solution with the C-PCM solvation model. *J. Comput. Chem.* **2003**, *24*, 669-681.
- [28] Glendening, E. D.; Reed, A. E.; Carpenter, J. E.; Weinhold, F. *NBO* version 3.1, 1996.
- [29] (a) Ringer, A. L.; Figgis, M. S.; Sinnokrot, M. O.; Sherrill, C. D. Aliphatic C-H/ π interaction: methane-benzene, methane-phenol, and methane-indole complexes. *J. Phys. Chem. A* **2006**, *110*, 10822-10828. (b) Maity, S.; Sedlak, R.; Hobza, P.; Patwari, G. N. Infrared-optical double resonance spectroscopic measurements and high level *ab initio* calculations on a binary complex between phenylacetylene and borane-trimethylamine. Understanding the role of C-H $\cdots\pi$ interactions. *Phys. Chem. Chem. Phys.*, **2009**, *11*, 9738-9743.
- [30] (a) Politzer, P.; Abu-Awwad, F. A comparative analysis of Hartree-Fock and Kohn-Sham orbital energies. *Theor. Chem. Acc.* **1998**, *99*, 83-87. (b) Kar, T.; Angyan, J. G.; Sannigrahi, A. B. Comparison of *ab initio* Hartree-Fock and Kohn-Sham orbitals in the calculation of atomic charge, bond index, and valence. *J. Phys. Chem. A* **2000**, *104*, 9953-9963. (c) Zhang, G.; Musgrave, C. B. Comparison of DFT methods for molecular orbital eigenvalue calculations. *J. Phys. Chem. A* **2007**, *111*, 1554-1561.
- [31] Rademacher, P. Photoelectron spectra of cyclopropane and cyclopropene compounds. *Chem. Rev.* **2003**, *103*, 933-976.
- [32] Staley, S. W.; Howard, A. E.; Strnad, J. T. Hyperconjugative effects on π^* negative-ion states. Electron transmission spectroscopy of cycloalkenes. *J. Org. Chem.* **1992**, *57*, 895-901.
- [33] Mitchell, R. W.; Dorko, E. A.; Merritt, J. A. Vibrational spectra of cyclopropene and cyclopropene-1,2-d₂. *J. Mol. Spectrosc.* **1968**, *26*, 197-212.

[34] Craig, N. C.; Borick, S. S.; Tucker, T. R.; Xiao, Y-Z. Vibrational spectra and assignments for 1-fluoro- and 1-chlorocyclobutenes: revised assignment for cyclobutene. *J. Phys. Chem.* **1991**, *95*, 3549-3558.

[35] Villarreal J. R.; Laane, J. Vibrational spectra and normal coordinate analysis for cyclopentene, cyclopentene-1-d₁, cyclopentene-1,2,3,3-d₄ and cyclopentene-d₈. *Spectrochim. Acta. A-M.* **1979**, *35*, 331-338.

[36] Neto, N.; Di Lauro, C. Vibrational spectra and molecular conformation of cyclenes-I
Vibrational assignment and valence force field of cyclohexene and cyclohexene-d₁₀. *Spectrochim. Acta. A-M.* **1967**, *23*, 1763-1774.